

Gabriel N. Gatica*, Cristian Inzunza, Ricardo Ruiz-Baier, and Felipe Sandoval

A posteriori error analysis of Banach spaces-based fully-mixed finite element methods for Boussinesq-type models

<https://doi.org/10.1515/jnma-2021-0101>

Received August 14, 2021; revised January 13, 2022; accepted April 01, 2022

Abstract: In this paper we consider Banach spaces-based fully-mixed variational formulations recently proposed for the Boussinesq and the Oberbeck–Boussinesq models, and develop reliable and efficient residual-based a posteriori error estimators for the 2D and 3D versions of the associated mixed finite element schemes. For the reliability analysis, we employ the global inf-sup condition for each sub-model, namely Navier–Stokes and heat equations in the case of Boussinesq, along with suitable Helmholtz decomposition in nonstandard Banach spaces, the approximation properties of the Raviart–Thomas and Clément interpolants, further regularity on the continuous solutions, and small data assumptions. In turn, the efficiency estimates follow from inverse inequalities and the localization technique through bubble functions in adequately defined local L^p spaces. Finally, several numerical results including natural convection in 3D differentially heated enclosures, are reported with the aim of confirming the theoretical properties of the estimators and illustrating the performance of the associated adaptive algorithm.

Keywords: Boussinesq–Oberbeck flows, Navier–Stokes equations, heat and mass transfer, fully-mixed finite element methods, a posteriori error analysis

Classification: 65N30, 65N12, 65N15, 35Q79, 80A20, 76R05, 76D07

1 Introduction

1.1 Scope

We have recently introduced in [17] and [18] new fully-mixed finite element methods for the stationary Boussinesq and Oberbeck–Boussinesq problems in \mathbb{R}^n , $n \in \{2, 3\}$, with temperature-dependent viscosities. The first model deals with the fluid motion generated by density differences due to temperature gradients, and it consists of the Navier–Stokes equations with a buoyancy term depending on the temperature, coupled to the heat equation with a convective term depending on the velocity of the fluid. The second one refers to natural convection in porous media when temperature and concentration differences occur simultaneously, and it is described by the incompressible Navier–Stokes/Brinkman equations nonlinearly coupled, via convective mass and heat transfer, to advection–diffusion equations for solute’s concentration and temperature.

The approach in [17] adapts an idea previously applied to the Navier–Stokes equations only (see, e.g., [19, 35]), where in addition to the velocity gradient, it introduces the Bernoulli stress (a part of the usual Cauchy stress whose divergence defines the momentum balance). The novelty in [17] consists in applying the very same idea to the energy equation. Instead of using classical primal, or dual-mixed methods, the tempera-

*Corresponding author: Gabriel N. Gatica, CI²MA and Departamento de Ingeniería Matemática, Universidad de Concepción, Casilla 160-C, Concepción, Chile. Email: ggatica@ci2ma.udec.cl

Cristian Inzunza, Felipe Sandoval, CI²MA and Departamento de Ingeniería Matemática, Universidad de Concepción, Casilla 160-C, Concepción, Chile.

Ricardo Ruiz-Baier, School of Mathematics, Monash University, 9 Rainforest Walk, Clayton 3800 VIC, Australia; Institute of Computer Science and Mathematical Modelling, Sechenov University, Moscow, Russian Federation; Universidad Adventista de Chile, Casilla 7-D, Chillán, Chile.

ture gradient and a vector-counterpart of the Bernoulli tensor are the new unknowns in the modified mixed formulation. As a consequence one eliminates the pressure (to later recover it via postprocessing) and the continuous formulation does not need augmentation terms as in, e.g., [14]. In this way, a Banach spaces-based variational formulation, showing exactly the same saddle-point structure in the flow and energy equations, is obtained, and hence the corresponding continuous and discrete analyses can be performed separately and very much in the same way for both sub-problems, which constitute appealing features from the theoretical and computational points of view. Possible finite element families include Raviart–Thomas spaces of order $k \geq n - 1$ for the Bernoulli tensor and its vector version, and piecewise polynomials of degree $\leq k$ for velocity, temperature, and both gradients.

In general, the use of a Banach spaces framework to analyze continuous and discrete formulations presents at least two important advantages. On one hand, it avoids the introduction of augmented formulations that increase the complexity of the problem. In fact, while the latter technique has shown to be very useful for the solvability analysis of a large class of nonlinear and coupled models posed in Hilbert spaces, in particular allowing corresponding Galerkin schemes with arbitrary finite element subspaces, it is no less true that the incorporation of further terms into the formulation, and the consequent extra computations that are required to set up the associated stiffness matrix and load vector, may lead to more expensive discrete systems. On the other hand, the spaces to which the unknowns belong arise naturally from Cauchy–Schwarz and Hölder inequalities when controlling diverse terms in the variational formulation. This approach yields formulations that are somewhat simpler and closer to the original physical model.

The theory from [17] was extended in [18] to the case of the Oberbeck–Boussinesq equations. There, besides the usual unknowns one has the temperature gradient, the concentration gradient, and a nonlinear flux combining advective and diffusive heat and concentration fluxes. Similarly as in [17], the weak formulation shows again a saddle-point structure on Banach spaces in both the Navier–Stokes/Brinkman and the thermal energy conservation equations. Consequently, the tools employed in [17], which include basically the Banach and Brouwer fixed-point theorems, along with the respective Babuška–Brezzi theory, are also utilized here for the continuous and discrete analyses. In this way, the same finite element subspaces from [17] can be used to obtain well-posed Galerkin schemes. Of note, while the approach employed in [17] and [18] could in principle seem very costly in terms of degrees of freedom, we stress that the increase in the number of unknowns is necessary to provide direct approximations to several other variables of physical interest as well (all them mentioned in the previous paragraphs). Moreover, they hold with the same rate of convergence of the remaining unknowns, whereas if one wanted to approximate those further variables by using only the velocity and pressure of the fluid, and the temperature or concentrations, then one would need to apply numerical differentiation formulae, which, as we know, lead to losses of accuracy of the respective computations. In addition, the methods are momentum and thermal energy conservative. These aspects are explored numerically in this paper. Further related contributions dealing with Banach spaces-based variational formulations have been addressed also in, e.g., [13, 27, 32] (see also the references therein).

Adaptive algorithms based on a posteriori error estimators are usually employed to recover optimal rates of convergence of finite element and mixed finite element methods that lose accuracy in highly nonlinear models or under the presence of singularities. In these cases, quasi uniform refinement quickly exhausts the computational capacity without obtaining satisfactory approximations of the solutions. A posteriori error analyses for Banach spaces-based mixed finite element methods are relatively recent. These include [12, 15]. In particular, the usual techniques employed within the Hilbertian framework are extended in [12] to the case of Banach spaces by deriving a reliable and efficient a posteriori error estimator for the steady-state Navier–Stokes problem. The above includes corresponding local estimates and new Helmholtz decompositions for the reliability, as well as respective inverse inequalities and local estimates of bubble functions for the efficiency. In turn, similar tools to those employed in [12] were previously applied in [15] to develop a residual-based a posteriori error analysis of primal-mixed finite element methods for the Navier–Stokes/Darcy–Forchheimer coupled problem. The amount of references is certainly much larger for Hilbert spaces-based variational formulations. Contributions addressing a posteriori error estimates for related problems as those studied herein can be found in [3–8, 11, 14, 20, 23, 25, 27, 36].

According to the above discussion, a main objective of this paper is, proceeding similarly to [12, 15], to derive reliable and efficient residual-based a posteriori error estimators in 2D and 3D for the fully-mixed finite element methods introduced in [17, 18]. Up to our knowledge, the present work provides the first a posteriori error analyses of non-augmented Banach spaces-based mixed finite element methods for the stationary Boussinesq and Oberbeck–Boussinesq systems. It is highlighted that the techniques to be developed here are not limited to the Boussinesq models. Indeed, in addition to the aforementioned works dealing with Navier–Stokes and Darcy–Forchheimer equations in which suitable modifications of them have been successfully applied, we announce in advance that the theory can be adapted to derive a posteriori error estimates of related models such as the coupled Brinkman–Forchheimer and double-diffusion equations studied in [13]. This subject constitutes undergoing work to be communicated in a forthcoming contribution.

The rest of the paper is organized as follows. In the remainder of this section we introduce some notations and definitions to be employed throughout the text. In Section 2 we recall from [17] the Boussinesq model, its fully-mixed variational formulation, and the associated mixed finite element scheme. Next, in Section 3 we derive in full details a reliable and efficient residual-based a posteriori error estimator for the 2D Boussinesq equations. We state preliminary results to be utilized in the reliability and efficiency analysis, and present in detail the proofs. Then, in Section 4 we establish the 3D version of the a posteriori error estimator provided in Section 3. In turn, the extension of the main results from Sections 3 and 4 to the Oberbeck–Boussinesq equations are summarized in Section 5. Finally, several numerical results illustrating the reliability and efficiency of the a posteriori error estimators, as well as the good performance of the adaptive algorithms induced by them, and confirming the recovery of optimal rates of convergence, are reported in Section 6.

1.2 Preliminary notations

Let $\Omega \subseteq \mathbb{R}^n$, $n \in \{2, 3\}$, be a given bounded domain with polyhedral boundary Γ , and let \mathbf{v} be the outward unit normal vector on Γ . Standard notation will be adopted for Lebesgue spaces $L^p(\Omega)$ and $L^p(\Gamma)$, and Sobolev spaces $W^{s,p}(\Omega)$ and $W^{s,p}(\Gamma)$, with $s \in \mathbb{R}$ and $p > 1$, whose corresponding norms, and semi-norms in the case of the latter, either for the scalar, vector, or tensor case, are denoted by $\|\cdot\|_{0,p;\Omega}$, $\|\cdot\|_{0,p;\Gamma}$, $\|\cdot\|_{s,p;\Omega}$, $|\cdot|_{s,p;\Omega}$, $\|\cdot\|_{s,p;\Gamma}$, and $|\cdot|_{s,p;\Gamma}$, respectively. In addition, $W^{s,2}(\Omega)$ and $W^{s,2}(\Gamma)$ are also denoted by $H^s(\Omega)$ and $H^s(\Gamma)$, and the notations of their norms and semi-norms are simplified to $\|\cdot\|_{s,\Omega}$, $|\cdot|_{s,\Omega}$, $\|\cdot\|_{s,\Gamma}$, and $|\cdot|_{s,\Gamma}$, respectively. In particular, $H^{1/2}(\Gamma)$ is the space of traces of functions of $H^1(\Omega)$, $H^{-1/2}(\Gamma)$ is its dual, and $\langle \cdot, \cdot \rangle_\Gamma$ stands for the duality pairing between $H^{-1/2}(\Gamma)$ and $H^{1/2}(\Gamma)$, and between its corresponding vector versions. On the other hand, given any generic scalar functional space M , we let \mathbf{M} and \mathbb{M} be the corresponding vectorial and tensorial counterparts, whereas $\|\cdot\|$, with no subscripts, will be employed for the norm of any element or operator whenever there is no confusion about the space to which they belong. Furthermore, as usual \mathbb{I} stands for the identity tensor in $\mathbb{R} := \mathbb{R}^{n \times n}$, and $|\cdot|$ denotes the Euclidean norm in $\mathbf{R} := \mathbb{R}^n$. Also, for any vector fields $\mathbf{v} = (v_i)_{i=1,n}$ and $\mathbf{w} = (w_i)_{i=1,n}$ we set the gradient, divergence, and tensor product operators, as

$$\nabla \mathbf{v} := \left(\frac{\partial v_i}{\partial x_j} \right)_{i,j=1,n}, \quad \operatorname{div}(\mathbf{v}) := \sum_{j=1}^n \frac{\partial v_j}{\partial x_j}, \quad \mathbf{v} \otimes \mathbf{w} := (v_i w_j)_{i,j=1,n}.$$

In turn, for any tensor fields $\boldsymbol{\tau} = (\tau_{ij})_{i,j=1,n}$ and $\boldsymbol{\zeta} = (\zeta_{ij})_{i,j=1,n}$, we let $\operatorname{div}(\boldsymbol{\tau})$ be the divergence operator div acting along the rows of $\boldsymbol{\tau}$, and define the transpose, the trace, the tensor inner product, and the deviatoric tensor, respectively, as

$$\boldsymbol{\tau}^t := (\tau_{ji})_{i,j=1,n}, \quad \operatorname{tr}(\boldsymbol{\tau}) := \sum_{i=1}^n \tau_{ii}, \quad \boldsymbol{\tau} : \boldsymbol{\zeta} := \sum_{i,j=1}^n \tau_{ij} \zeta_{ij}, \quad \boldsymbol{\tau}^d := \boldsymbol{\tau} - \frac{1}{n} \operatorname{tr}(\boldsymbol{\tau}) \mathbb{I}.$$

Next, given $p > 1$, we introduce the Banach spaces

$$\mathbf{H}(\operatorname{div}_p; \Omega) := \{\boldsymbol{\tau} \in \mathbf{L}^2(\Omega) : \operatorname{div}(\boldsymbol{\tau}) \in L^p(\Omega)\}, \quad \mathbb{H}(\operatorname{div}_p; \Omega) := \{\boldsymbol{\tau} \in \mathbb{L}^2(\Omega) : \operatorname{div}(\boldsymbol{\tau}) \in L^p(\Omega)\} \quad (1.1)$$

equipped with the natural norms

$$\begin{aligned}\|\boldsymbol{\tau}\|_{\text{div}_p; \Omega} &:= \|\boldsymbol{\tau}\|_{0,\Omega} + \|\text{div}(\boldsymbol{\tau})\|_{0,p;\Omega} \quad \forall \boldsymbol{\tau} \in \mathbf{H}(\text{div}_p; \Omega) \\ \|\boldsymbol{\tau}\|_{\mathbf{div}_p; \Omega} &:= \|\boldsymbol{\tau}\|_{0,\Omega} + \|\mathbf{div}(\boldsymbol{\tau})\|_{0,p;\Omega} \quad \forall \boldsymbol{\tau} \in \mathbb{H}(\mathbf{div}_p; \Omega).\end{aligned}$$

In addition, proceeding as in [17, Sect. 3.1], one can prove that for each $p \geq 2n/(n+2)$ there hold

$$\langle \boldsymbol{\tau} \cdot \mathbf{v}, v \rangle_{\Gamma} = \int_{\Omega} \left\{ \boldsymbol{\tau} \cdot \nabla v + v \text{div}(\boldsymbol{\tau}) \right\} \quad \forall (\boldsymbol{\tau}, v) \in \mathbf{H}(\text{div}_p; \Omega) \times \mathbf{H}^1(\Omega) \quad (1.2)$$

$$\langle \boldsymbol{\tau} \mathbf{v}, \mathbf{v} \rangle_{\Gamma} = \int_{\Omega} \left\{ \boldsymbol{\tau} : \nabla \mathbf{v} + \mathbf{v} \cdot \mathbf{div}(\boldsymbol{\tau}) \right\} \quad \forall (\boldsymbol{\tau}, \mathbf{v}) \in \mathbb{H}(\mathbf{div}_p; \Omega) \times \mathbf{H}^1(\Omega). \quad (1.3)$$

Also, given $p, q \in (1, +\infty)$, we say that they are conjugate to each other if $1/p + 1/q = 1$. Finally, we end this section by mentioning that, throughout the rest of the paper, we employ $\mathbf{0}$ to denote a generic null vector (or tensor), and use C and c , with or without subscripts, bars, tildes or hats, to denote generic constants independent of the discretization, which may take different values at different places.

2 The Boussinesq model

In this section we resort to [17] to introduce the Boussinesq model, its corresponding fully-mixed variational formulation, and the associated mixed finite element method.

2.1 The boundary value problem

The stationary Boussinesq problem consists of a system of equations in which the incompressible Navier–Stokes equation is coupled with the heat equation through a convective term and a buoyancy term typically acting in opposite direction to gravity. More precisely, given a fluid occupying the region Ω , an external force per unit mass $\mathbf{g} \in \mathbf{L}^\infty(\Omega)$, and data $\mathbf{u}_D \in \mathbf{H}^{1/2}(\Gamma)$ and $\varphi_D \in \mathbf{H}^{1/2}(\Gamma)$, the model of interest reads: Find a velocity field \mathbf{u} , a pressure field p and a temperature field φ such that

$$\begin{aligned}-\mathbf{div}(2\mu(\varphi)\mathbf{e}(\mathbf{u})) + (\nabla \mathbf{u})\mathbf{u} + \nabla p &= \varphi \mathbf{g} \quad \text{in } \Omega, \quad \text{div}(\mathbf{u}) = 0 \quad \text{in } \Omega \\ \int_{\Omega} p &= 0, \quad -\mathbf{div}(\mathbb{K}\nabla \varphi) + \mathbf{u} \cdot \nabla \varphi = 0 \quad \text{in } \Omega \\ \mathbf{u} &= \mathbf{u}_D \quad \text{on } \Gamma, \quad \varphi = \varphi_D \quad \text{on } \Gamma\end{aligned} \quad (2.1)$$

where $\mathbf{e}(\mathbf{u})$ is the symmetric part of the velocity gradient $\nabla \mathbf{u}$, also known as the strain rate tensor, and $\mathbb{K} \in \mathbf{L}^\infty(\Omega)$ is a uniformly positive tensor describing the thermal conductivity of the fluid, thus allowing the possibility of anisotropy. In turn, $\mu : \mathbb{R} \rightarrow \mathbb{R}^+$ is the temperature dependent viscosity, which is assumed to be a Lipschitz-continuous and bounded from above and below function, which means that there exist constants $L_\mu > 0$ and $\mu_1, \mu_2 > 0$, such that

$$|\mu(s) - \mu(t)| \leq L_\mu |s - t|, \quad \mu_1 \leq \mu(s) \leq \mu_2 \quad \forall s, t \geq 0. \quad (2.2)$$

We observe that, because of the incompressibility constraint (cf. second eq. of (2.1)) and the Dirichlet boundary condition (cf. fifth eq. of (2.1)), \mathbf{u}_D must satisfy the compatibility condition $\int_{\Gamma} \mathbf{u}_D \cdot \mathbf{v} = 0$.

2.2 The fully-mixed variational formulation

Following the approach from [17], we first introduce the velocity gradient \mathbf{t} , the Bernoulli stress tensor $\boldsymbol{\sigma}$, the temperature gradient $\tilde{\mathbf{t}}$, and the pseudoheat flux $\tilde{\boldsymbol{\sigma}}$ as auxiliary unknowns, that is

$$\mathbf{t} := \nabla \mathbf{u}, \quad \boldsymbol{\sigma} := 2\mu(\varphi)\mathbf{t}_{\text{sym}} - \frac{1}{2}(\mathbf{u} \otimes \mathbf{u}) - p\mathbf{I}, \quad \tilde{\mathbf{t}} := \nabla \varphi, \quad \tilde{\boldsymbol{\sigma}} := \mathbb{K}\tilde{\mathbf{t}} - \frac{1}{2}\varphi\mathbf{u}$$

where $\mathbf{t}_{\text{sym}} := \frac{1}{2}(\mathbf{t} + \mathbf{t}^t)$ is the symmetric part of \mathbf{t} . In this way, problem (2.1) can be rewritten as

$$\begin{aligned} \nabla \mathbf{u} &= \mathbf{t} && \text{in } \Omega \\ \text{tr}(\mathbf{t}) &= 0 && \text{in } \Omega \\ -\mathbf{div}(\boldsymbol{\sigma}) + \frac{1}{2}\mathbf{t}\mathbf{u} - \varphi \mathbf{g} &= \mathbf{0} && \text{in } \Omega \\ 2\mu(\varphi)\mathbf{t}_{\text{sym}} - \frac{1}{2}(\mathbf{u} \otimes \mathbf{u})^d &= \boldsymbol{\sigma}^d && \text{in } \Omega \\ \nabla \varphi &= \tilde{\mathbf{t}} && \text{in } \Omega \\ \mathbb{K}\tilde{\mathbf{t}} - \frac{1}{2}\varphi \mathbf{u} &= \tilde{\boldsymbol{\sigma}} && \text{in } \Omega \\ -\mathbf{div}(\tilde{\boldsymbol{\sigma}}) + \frac{1}{2}\mathbf{u} \cdot \tilde{\mathbf{t}} &= 0 && \text{in } \Omega \\ \mathbf{u} &= \mathbf{u}_D, \quad \varphi = \varphi_D && \text{on } \Gamma \\ \int_{\Omega} \text{tr}(2\boldsymbol{\sigma} + \mathbf{u} \otimes \mathbf{u}) &= 0 \end{aligned} \tag{2.3}$$

where p is eliminated and later recovered terms of $\boldsymbol{\sigma}$ and \mathbf{u} by using the identity

$$p = -\frac{1}{2n} \text{tr}(2\boldsymbol{\sigma} + \mathbf{u} \otimes \mathbf{u}). \tag{2.4}$$

In what follows we recall from [17] the variational formulation of (2.3). From its first two equations we note that, if \mathbf{u} is originally sought in $\mathbf{H}^1(\Omega)$, then \mathbf{t} must belong to the space

$$\mathbb{L}_{\text{tr}}^2(\Omega) := \{\mathbf{s} \in \mathbb{L}^2(\Omega) : \text{tr}(\mathbf{s}) = 0\}.$$

Now, testing the fourth equation of (2.3) against $\mathbf{s} \in \mathbb{L}_{\text{tr}}^2(\Omega)$, we formally obtain

$$2 \int_{\Omega} \mu(\varphi) \mathbf{t}_{\text{sym}} : \mathbf{s} - \frac{1}{2} \int_{\Omega} (\mathbf{u} \otimes \mathbf{u})^d : \mathbf{s} - \int_{\Omega} \boldsymbol{\sigma}^d : \mathbf{s} = 0 \tag{2.5}$$

from which we observe that the first term of (2.5) is well-defined thanks to the boundedness of μ (cf. (2.2)), whereas the third one is as well if $\boldsymbol{\sigma}$ is sought in $\mathbb{L}^2(\Omega)$. In turn, letting $\ell, j \in (1, +\infty)$ conjugate to each other, direct applications of the Cauchy–Schwarz and Hölder inequalities yield

$$\left| \int_{\Omega} (\mathbf{u} \otimes \mathbf{u})^d : \mathbf{s} \right| = \left| \int_{\Omega} (\mathbf{u} \otimes \mathbf{u}) : \mathbf{s} \right| \leq \| \mathbf{u} \|_{0,2\ell;\Omega} \| \mathbf{u} \|_{0,2j;\Omega} \| \mathbf{s} \|_{0,\Omega}$$

and hence the second term of (2.5) makes sense if one looks for \mathbf{u} in $\mathbf{L}^4(\Omega)$, which arises naturally by taking $\ell = j = 2$ in the foregoing inequality. In this way, knowing the spaces to which \mathbf{t} and \mathbf{u} should belong, we notice that the testing of the term $\frac{1}{2}\mathbf{t}\mathbf{u}$ in the third equation of (2.3) is possible only with a vector function $\mathbf{v} \in \mathbf{L}^4(\Omega)$ since, employing again the aforementioned inequalities, we find that

$$\left| \int_{\Omega} \mathbf{t}\mathbf{u} \cdot \mathbf{v} \right| \leq \| \mathbf{t} \|_{0,\Omega} \| \mathbf{u} \|_{0,4;\Omega} \| \mathbf{v} \|_{0,4;\Omega}.$$

As a consequence, the testing of the first term of the same equation against $\mathbf{v} \in \mathbf{L}^4(\Omega)$, along with Hölder's inequality, force $\mathbf{div}(\boldsymbol{\sigma})$ to belong to $\mathbf{L}^{4/3}(\Omega)$, and therefore $\boldsymbol{\sigma}$ is sought from now on in $\mathbb{H}(\mathbf{div}_{4/3}; \Omega)$ (cf. (1.1)). Applying a similar analysis to the sixth and seventh equations of (2.3), we deduce that $\mathbf{L}^2(\Omega)$, $\mathbf{L}^4(\Omega)$, and $\mathbb{H}(\mathbf{div}_{4/3}; \Omega)$ become the right spaces to look for $\tilde{\mathbf{t}}$, φ , and $\tilde{\boldsymbol{\sigma}}$, respectively. Note, in particular, that the space to which φ belongs is coherent with the testing of the term $\varphi \mathbf{g}$ in the third equation of (2.3) against $\mathbf{v} \in \mathbf{L}^4(\Omega)$.

Next, we consider the orthogonal decomposition

$$\mathbb{H}(\mathbf{div}_{4/3}; \Omega) = \mathbb{H}_0(\mathbf{div}_{4/3}; \Omega) \oplus R\mathbb{I} \tag{2.6}$$

where

$$\mathbb{H}_0(\mathbf{div}_{4/3}; \Omega) := \left\{ \boldsymbol{\tau} \in \mathbb{H}(\mathbf{div}_{4/3}; \Omega) : \int_{\Omega} \text{tr}(\boldsymbol{\tau}) = 0 \right\}$$

and observe, in particular, that the unknown σ can be uniquely decomposed, according to (2.6) and the condition $\int_{\Omega} \text{tr}(2\sigma + \mathbf{u} \otimes \mathbf{u}) = 0$, as

$$\sigma = \sigma_0 + c_0 \mathbb{I}, \quad \sigma_0 \in \mathbb{H}_0(\mathbf{div}_{4/3}; \Omega), \quad c_0 := -\frac{1}{2n|\Omega|} \int_{\Omega} \text{tr}(\mathbf{u} \otimes \mathbf{u}).$$

In this way, and similarly as for the pressure, the constant c_0 can be computed once the velocity is known, and hence it only remains to obtain σ_0 . In this regard, we now stress that the equations of (2.3) involving σ remain unchanged if σ is replaced by σ_0 , and hence from now on we denote σ_0 as simply $\sigma \in \mathbb{H}_0(\mathbf{div}_{4/3}; \Omega)$. In addition, thanks to the compatibility condition satisfied by the datum \mathbf{u}_D and the fact that \mathbf{t} is sought in $\mathbb{L}_{\text{tr}}^2(\Omega)$, we realize that testing the first equation of (2.3) against $\boldsymbol{\tau} \in \mathbb{H}(\mathbf{div}_{4/3}; \Omega)$ is equivalent to doing it against $\boldsymbol{\tau} \in \mathbb{H}_0(\mathbf{div}_{4/3}; \Omega)$. Regarding this fact, we point out that the formula (1.3) is employed to integrate the expression $\int_{\Omega} \nabla \varphi : \boldsymbol{\tau}$. Similarly, when testing the fifth equation of (2.3) against $\tilde{\boldsymbol{\tau}} \in \mathbf{H}(\text{div}_{4/3}; \Omega)$, the computation of $\int_{\Omega} \nabla \varphi \cdot \tilde{\boldsymbol{\tau}}$ makes use of (1.2).

Finally, in order to write the announced formulation in a simplified way, we now set the notations

$$\begin{aligned} (\varphi, \psi)_{\Omega} &:= \int_{\Omega} \varphi \psi, & (\mathbf{u}, \mathbf{v})_{\Omega} &:= \int_{\Omega} \mathbf{u} \cdot \mathbf{v}, & (\sigma, \boldsymbol{\tau})_{\Omega} &:= \int_{\Omega} \sigma : \boldsymbol{\tau} \\ \vec{\mathbf{u}} &:= (\mathbf{u}, \mathbf{t}), & \vec{\mathbf{v}} &:= (\mathbf{v}, \mathbf{s}) \in \mathbf{H} := \mathbf{L}^4(\Omega) \times \mathbb{L}_{\text{tr}}^2(\Omega), & \vec{\varphi} &:= (\varphi, \tilde{\mathbf{t}}), \vec{\psi} := (\psi, \tilde{\mathbf{s}}) \in \widetilde{\mathbf{H}} := \mathbf{L}^4(\Omega) \times \mathbf{L}^2(\Omega) \\ \|\vec{\mathbf{u}}\| &:= \|\mathbf{u}\|_{0,4;\Omega} + \|\mathbf{t}\|_{0,\Omega}, & \|\vec{\varphi}\| &:= \|\varphi\|_{0,4;\Omega} + \|\tilde{\mathbf{t}}\|_{0,\Omega} & \forall \vec{\mathbf{u}} &:= (\mathbf{u}, \mathbf{t}) \in \mathbf{H}, \quad \forall \vec{\varphi} &:= (\varphi, \tilde{\mathbf{t}}) \in \widetilde{\mathbf{H}}. \end{aligned}$$

In this way, the fully-mixed formulation of our stationary Boussinesq problem reduces to (see, [17, Sect. 3.1]): Find $(\vec{\mathbf{u}}, \sigma) \in \mathbf{H} \times \mathbb{H}_0(\mathbf{div}_{4/3}; \Omega)$ and $(\vec{\varphi}, \tilde{\sigma}) \in \widetilde{\mathbf{H}} \times \mathbf{H}(\text{div}_{4/3}; \Omega)$ such that

$$\begin{aligned} a_{\varphi}(\vec{\mathbf{u}}, \vec{\mathbf{v}}) + c(\mathbf{u}; \vec{\mathbf{u}}, \vec{\mathbf{v}}) + b(\vec{\mathbf{v}}, \sigma) &= F_{\varphi}(\vec{\mathbf{v}}) \quad \forall \vec{\mathbf{v}} \in \mathbf{H} \\ b(\vec{\mathbf{u}}, \boldsymbol{\tau}) &= G(\boldsymbol{\tau}) \quad \forall \boldsymbol{\tau} \in \mathbb{H}_0(\mathbf{div}_{4/3}; \Omega) \\ \tilde{a}(\vec{\varphi}, \vec{\psi}) + \tilde{c}_{\mathbf{u}}(\vec{\varphi}, \vec{\psi}) + \tilde{b}(\vec{\psi}, \tilde{\sigma}) &= 0 \quad \forall \vec{\psi} \in \widetilde{\mathbf{H}} \\ \tilde{b}(\vec{\varphi}, \tilde{\boldsymbol{\tau}}) &= \widetilde{G}(\tilde{\boldsymbol{\tau}}) \quad \forall \tilde{\boldsymbol{\tau}} \in \mathbf{H}(\text{div}_{4/3}; \Omega) \end{aligned} \tag{2.7}$$

where, given arbitrary $(\mathbf{w}, \varphi) \in \mathbf{L}^4(\Omega) \times \mathbf{L}^4(\Omega)$, the forms a_{φ} , b , $c(\mathbf{w}; \cdot, \cdot)$, \tilde{a} , \tilde{b} , and $\tilde{c}_{\mathbf{w}}$, the functionals F_{φ} , G , and \widetilde{G} , are defined by

$$a_{\varphi}(\vec{\mathbf{u}}, \vec{\mathbf{v}}) := (2\mu(\varphi)\mathbf{t}_{\text{sym}}, \mathbf{s})_{\Omega}, \quad b(\vec{\mathbf{v}}, \boldsymbol{\tau}) := -(\boldsymbol{\tau}, \mathbf{s})_{\Omega} - (\mathbf{v}, \mathbf{div}(\boldsymbol{\tau}))_{\Omega} \tag{2.8}$$

$$c(\mathbf{w}; \vec{\mathbf{u}}, \vec{\mathbf{v}}) := \frac{1}{2} \{ (\mathbf{t}\mathbf{w}, \mathbf{v})_{\Omega} - ((\mathbf{u} \otimes \mathbf{w})^d, \mathbf{s}^d)_{\Omega} \} \tag{2.9}$$

$$\tilde{a}(\vec{\varphi}, \vec{\psi}) := (\mathbf{K}\tilde{\mathbf{t}}, \tilde{\mathbf{s}})_{\Omega}, \quad \tilde{b}(\vec{\psi}, \tilde{\boldsymbol{\tau}}) := -(\tilde{\boldsymbol{\tau}}, \tilde{\mathbf{s}})_{\Omega} - (\psi, \text{div}(\tilde{\boldsymbol{\tau}}))_{\Omega} \tag{2.10}$$

$$\tilde{c}_{\mathbf{w}}(\vec{\varphi}, \vec{\psi}) := \frac{1}{2} \{ (\psi \mathbf{w}, \tilde{\mathbf{t}})_{\Omega} - (\varphi \mathbf{w}, \tilde{\mathbf{s}})_{\Omega} \} \tag{2.11}$$

$$F_{\varphi}(\vec{\mathbf{v}}) := (\varphi \mathbf{g}, \mathbf{v})_{\Omega}, \quad G(\boldsymbol{\tau}) := -\langle \boldsymbol{\tau} \mathbf{v}, \mathbf{u}_D \rangle_{\Gamma}, \quad \widetilde{G}(\tilde{\boldsymbol{\tau}}) := -\langle \tilde{\boldsymbol{\tau}} \cdot \mathbf{v}, \varphi_D \rangle_{\Gamma} \tag{2.12}$$

for all $\vec{\mathbf{u}} := (\mathbf{u}, \mathbf{t})$, $\vec{\mathbf{v}} := (\mathbf{v}, \mathbf{s}) \in \mathbf{H}$, $\boldsymbol{\tau} \in \mathbb{H}_0(\mathbf{div}_{4/3}; \Omega)$, $\tilde{\boldsymbol{\tau}} \in \mathbf{H}(\text{div}_{4/3}; \Omega)$, $\vec{\varphi} := (\varphi, \tilde{\mathbf{t}})$, $\vec{\psi} := (\psi, \tilde{\mathbf{s}}) \in \widetilde{\mathbf{H}}$. The well posedness of (2.7), which uses a fixed-point strategy along with the Babuška–Brezzi theory in Banach spaces, is established by [17, Th. 3.11]. The continuous and discrete analyses provided therein, as well as the one to be developed in what follows, are also valid if mixed boundary conditions are considered for the Navier–Stokes equations. Assuming, for instance $\mathbf{u} = \mathbf{u}_D$ on Γ_D and $\sigma \mathbf{v} = \mathbf{0}$ on Γ_N , where Γ_D and Γ_N are disjoint parts of Γ such that $\Gamma = \bar{\Gamma}_D \cup \bar{\Gamma}_N$, then just two minor changes are in order. The first one has to do with the space where σ is sought, which is given now by

$$\widetilde{\mathbb{H}}_0(\mathbf{div}_{4/3}; \Omega) := \left\{ \boldsymbol{\tau} \in \mathbf{H}(\mathbf{div}_{4/3}; \Omega) : \int_{\Omega} \text{tr}(\boldsymbol{\tau}) = 0, \quad \boldsymbol{\tau} \mathbf{v} = \mathbf{0} \text{ on } \Gamma_N \right\}.$$

In this case, it is easy to see that for each $\boldsymbol{\tau} \in \widetilde{\mathbb{H}}_0(\mathbf{div}_{4/3}; \Omega)$ there holds $\boldsymbol{\tau} \mathbf{v}|_{\Gamma_D} \in \mathbf{H}^{-1/2}(\Gamma_D)$, and hence the second change refers to the definition of the functional G , which becomes $G(\boldsymbol{\tau}) := -\langle \boldsymbol{\tau} \mathbf{v}, \mathbf{u}_D \rangle_{\Gamma_D}$, where $\langle \cdot, \cdot \rangle_{\Gamma_D}$ stands here for the duality pairing between $\mathbf{H}^{-1/2}(\Gamma_D)$ and $\mathbf{H}^{1/2}(\Gamma_D)$.

2.3 The finite element method

Let $\{\mathcal{T}_h\}_{h>0}$ be a family of regular triangulations \mathcal{T}_h of $\bar{\Omega}$ made of triangles K (when $n = 2$) or tetrahedra K (when $n = 3$). Then, given $h > 0$, we let \mathcal{T}_h^b be the corresponding barycentric refinement of \mathcal{T}_h , which originates from \mathcal{T}_h after joining the vertices of each element $K \in \mathcal{T}_h$ with its barycenter, and set its meshsize as $h := \max\{h_K : K \in \mathcal{T}_h^b\}$, where h_K denotes the diameter of K . In what follows, given an integer $\ell \geq 0$, $P_\ell(K)$ stands for the space of polynomials of degree $\leq \ell$ defined on K , with vector and tensor versions denoted by $\mathbf{P}_\ell(K) := [P_\ell(K)]^n$ and $\mathbb{P}_\ell(K) := [P_\ell(K)]^{n \times n}$, respectively. Then, given an integer $k \geq 0$, we set for each $K \in \mathcal{T}_h^b$ the local Raviart–Thomas space of order k as

$$\mathbf{RT}_k(K) := \mathbf{P}_k(K) \oplus P_k(K)\mathbf{x}$$

where $\mathbf{x} := (x_1, \dots, x_n)^t$ is a generic vector of \mathbb{R}^n . Next, following [17, Sect. 5], we assume from now on that $k+1 \geq n$, and introduce the following finite element subspaces approximating the unknowns \mathbf{u} , \mathbf{t} , $\boldsymbol{\sigma}$, φ , $\tilde{\mathbf{t}}$, and $\tilde{\boldsymbol{\sigma}}$, respectively,

$$\begin{aligned} \mathbf{H}_h^\mathbf{u} &:= \left\{ \mathbf{v}_h \in \mathbf{L}^4(\Omega) : \mathbf{v}_h|_K \in \mathbf{P}_k(K) \quad \forall K \in \mathcal{T}_h^b \right\} \\ \mathbb{H}_h^\mathbf{t} &:= \left\{ \mathbf{s}_h \in \mathbb{L}_{\text{tr}}^2(\Omega) : \mathbf{s}_h|_K \in \mathbb{P}_k(K) \quad \forall K \in \mathcal{T}_h^b \right\} \\ \mathbb{H}_h^\boldsymbol{\sigma} &:= \left\{ \boldsymbol{\tau}_h \in \mathbb{H}_0(\mathbf{div}_{4/3}; \Omega) : \mathbf{c}^t \boldsymbol{\tau}_h|_K \in \mathbf{RT}_k(K) \quad \forall \mathbf{c} \in \mathbf{R}, \quad \forall K \in \mathcal{T}_h^b \right\} \quad (2.13) \\ H_h^\varphi &:= \left\{ \psi_h \in \mathbf{L}^4(\Omega) : \psi_h|_K \in P_k(K) \quad \forall K \in \mathcal{T}_h^b \right\} \\ \mathbf{H}_h^{\tilde{\mathbf{t}}} &:= \left\{ \tilde{\mathbf{s}}_h \in \mathbf{L}^2(\Omega) : \tilde{\mathbf{s}}_h|_K \in \mathbf{P}_k(K) \quad \forall K \in \mathcal{T}_h^b \right\} \\ \mathbf{H}_h^{\tilde{\boldsymbol{\sigma}}} &:= \left\{ \tilde{\boldsymbol{\tau}}_h \in \mathbf{H}(\mathbf{div}_{4/3}; \Omega) : \tilde{\boldsymbol{\tau}}_h|_K \in \mathbf{RT}_k(K) \quad \forall K \in \mathcal{T}_h^b \right\}. \end{aligned}$$

In addition, and similarly to Section 2.1, we set the notations

$$\begin{aligned} \vec{\mathbf{u}}_h &:= (\mathbf{u}_h, \mathbf{t}_h), & \vec{\mathbf{v}}_h &:= (\mathbf{v}_h, \mathbf{s}_h) \in \mathbf{H}_h := \mathbf{H}_h^\mathbf{u} \times \mathbb{H}_h^\mathbf{t} \\ \vec{\varphi}_h &:= (\varphi_h, \tilde{\mathbf{t}}_h), & \vec{\psi}_h &:= (\psi_h, \tilde{\mathbf{s}}_h) \in \tilde{\mathbf{H}}_h := H_h^\varphi \times \mathbf{H}_h^{\tilde{\mathbf{t}}}. \end{aligned}$$

We remark that the use of the barycentric refinement \mathcal{T}_h^b instead of the original one \mathcal{T}_h , is motivated by the verification of one of the discrete stability conditions involving the subspaces $\mathbf{H}_h^\mathbf{u}$, $\mathbb{H}_h^\mathbf{t}$, and $\mathbb{H}_h^\boldsymbol{\sigma}$ (cf. [17, Eq. (5.15)]). Indeed, starting from an arbitrary pair of finite element subspaces U_h and Q_h of $\mathbf{H}_0^1(\Omega)$ and $L_0^2(\Omega)$ that yield a well-posed Galerkin scheme for the primal formulation of the Stokes problem, and proceeding similarly as in [10, 26], we derive in [17] sufficient conditions on $\mathbf{H}_h^\mathbf{u}$, $\mathbb{H}_h^\mathbf{t}$, and $\mathbb{H}_h^\boldsymbol{\sigma}$ (cf. [17, Eqs. (5.24) and (5.25)]), depending on U_h and Q_h , which guarantee the aforementioned stability. Then, taking in particular the Scott–Vogelius pair (U_h, Q_h) (cf. [37, 38]), which is given by continuous piecewise polynomials of degree $\leq k+1$, and discontinuous piecewise polynomials of degree $\leq k$, respectively, and which becomes stable only on the barycentric mesh \mathcal{T}_h^b , and under the assumption that $k+1 \geq n$, we are led to the finite element subspaces defined in (2.13). For further technical details on this issue, we refer to [17, Sect. 5.2].

Hence, the Galerkin scheme associated with (2.7) reads: Find $(\vec{\mathbf{u}}_h, \boldsymbol{\sigma}_h) \in \mathbf{H}_h \times \mathbb{H}_h^\boldsymbol{\sigma}$ and $(\vec{\varphi}_h, \tilde{\boldsymbol{\sigma}}_h) \in \tilde{\mathbf{H}}_h \times \mathbf{H}_h^{\tilde{\boldsymbol{\sigma}}}$ such that

$$\begin{aligned} a_{\varphi_h}(\vec{\mathbf{u}}_h, \vec{\mathbf{v}}_h) + c(\mathbf{u}_h, \vec{\mathbf{u}}_h, \vec{\mathbf{v}}_h) + b(\vec{\mathbf{v}}_h, \boldsymbol{\sigma}_h) &= F_{\varphi_h}(\vec{\mathbf{v}}_h) \quad \forall \vec{\mathbf{v}}_h \in \mathbf{H}_h \\ b(\vec{\mathbf{u}}_h, \boldsymbol{\tau}_h) &= G(\boldsymbol{\tau}_h) \quad \forall \boldsymbol{\tau}_h \in \mathbb{H}_h^\boldsymbol{\sigma} \\ \tilde{a}(\vec{\varphi}_h, \vec{\psi}_h) + \tilde{c}_{\mathbf{u}_h}(\vec{\varphi}_h, \vec{\psi}_h) + \tilde{b}(\vec{\psi}_h, \tilde{\boldsymbol{\sigma}}_h) &= 0 \quad \forall \vec{\psi}_h \in \tilde{\mathbf{H}}_h \\ \tilde{b}(\vec{\varphi}_h, \tilde{\boldsymbol{\tau}}_h) &= \tilde{G}(\tilde{\boldsymbol{\tau}}_h) \quad \forall \tilde{\boldsymbol{\tau}}_h \in \mathbf{H}_h^{\tilde{\boldsymbol{\sigma}}}. \end{aligned} \quad (2.14)$$

The solvability analysis and a priori error bounds for (2.14) employs a fixed-point strategy along with the discrete Babuška–Brezzi theory in Banach spaces (see [17, Theorems 4.11 and 6.2]).

3 A posteriori error analysis: the 2D case

In this section, we derive a reliable and efficient residual-based a posteriori error estimator for the two-dimensional version of (2.14). The 3D case, which follows from minor modifications of the one to be presented next, will be addressed in Section 4.

3.1 Preliminaries for reliability

Given $K \in \mathcal{T}_h^b$, we let $\mathcal{E}_h(K)$ be the set of its edges e , and let \mathcal{E}_h be the set of all the edges e of \mathcal{T}_h^b , with corresponding diameters denoted by h_e . Then, we set $\mathcal{E}_h = \mathcal{E}_h(\Omega) \cup \mathcal{E}_h(\Gamma)$, where $\mathcal{E}_h(\Omega) := \{e \in \mathcal{E}_h : e \subset \Omega\}$ and $\mathcal{E}_h(\Gamma) := \{e \in \mathcal{E}_h : e \subset \Gamma\}$. Also for each $e \in \mathcal{E}_h$ we fix unit normal and tangential vectors to e denoted by $\mathbf{v}_e := (v_1, v_2)^t$ and $\mathbf{s}_e := (-v_2, v_1)^t$, respectively. However, when no confusion arises, we simply write \mathbf{v} and \mathbf{s} instead of \mathbf{v}_e and \mathbf{s}_e , respectively. In addition, the usual jump operator $[\cdot]$ across an internal edge $e \in \mathcal{E}_h(\Omega)$ is defined for piecewise continuous tensor, vector, or scalar-valued functions ζ as simply $[\zeta] := \zeta|_K - \zeta|_{K'}$, where K and K' are the triangles of \mathcal{T}_h^b having e as a common edge. Furthermore, given scalar, vector, and matrix valued fields $\varphi, \mathbf{v} = (v_1, v_2)^t$, and $\boldsymbol{\tau} := (\tau_{ij})_{2 \times 2}$, respectively, we set

$$\underline{\operatorname{curl}}(\varphi) := \begin{pmatrix} \frac{\partial \varphi}{\partial x_2} \\ -\frac{\partial \varphi}{\partial x_1} \end{pmatrix}, \quad \underline{\operatorname{curl}}(\mathbf{v}) := \begin{pmatrix} \operatorname{curl}(v_1)^t \\ \operatorname{curl}(v_2)^t \end{pmatrix}, \quad \operatorname{rot}(\mathbf{v}) := \frac{\partial v_2}{\partial x_1} - \frac{\partial v_1}{\partial x_2}, \quad \operatorname{rot}(\boldsymbol{\tau}) := \begin{pmatrix} \operatorname{rot}(\tau_{11}, \tau_{12}) \\ \operatorname{rot}(\tau_{21}, \tau_{22}) \end{pmatrix}$$

where the derivatives involved are taken in the distributional sense.

Let us now recall the main properties of the Raviart–Thomas and Clément interpolation operators (cf. [16, 24]). We begin by defining for each $p \geq 2n/(n+2)$ the spaces

$$\mathbf{H}_p := \left\{ \boldsymbol{\tau} \in \mathbf{H}(\operatorname{div}_p; \Omega) : \boldsymbol{\tau}|_K \in \mathbf{W}^{1,p}(K) \quad \forall K \in \mathcal{T}_h^b \right\} \quad (3.1)$$

$$\widehat{\mathbf{H}}_h^\sigma := \left\{ \boldsymbol{\tau} \in \mathbf{H}(\operatorname{div}_p; \Omega) : \boldsymbol{\tau}|_K \in \mathbf{RT}_k(K) \quad \forall K \in \mathcal{T}_h^b \right\}. \quad (3.2)$$

In addition, we let $\Pi_h^k : \mathbf{H}_p \rightarrow \widehat{\mathbf{H}}_h^\sigma$ be the Raviart–Thomas interpolation operator, which is characterized for each $\boldsymbol{\tau} \in \mathbf{H}_p$ by the identities (see, e.g., [24, Sect. 1.2.7]):

$$\int_e (\Pi_h^k(\boldsymbol{\tau}) \cdot \mathbf{v}) \xi = \int_e (\boldsymbol{\tau} \cdot \mathbf{v}) \xi \quad \forall \xi \in \mathbf{P}_k(e), \quad \forall \text{ edge or face } e \text{ of } \mathcal{T}_h^b \quad (3.3)$$

when $k \geq 0$, and

$$\int_K \Pi_h^k(\boldsymbol{\tau}) \cdot \psi = \int_K \boldsymbol{\tau} \cdot \psi \quad \forall \psi \in \mathbf{P}_{k-1}(K), \quad \forall K \in \mathcal{T}_h^b$$

when $k \geq 1$. In turn, given $q > 1$ such that p and q are conjugate to each other, we let

$$\mathbf{H}_h^{\mathbf{u}} := \left\{ \mathbf{v} \in \mathbf{L}^q(\Omega) : \mathbf{v}|_K \in \mathbf{P}_k(K) \quad \forall K \in \mathcal{T}_h^b \right\} \quad (3.4)$$

and recall from [24, Lem. 1.41] that there holds

$$\operatorname{div}(\Pi_h^k(\boldsymbol{\tau})) = \mathcal{P}_h^k(\operatorname{div}(\boldsymbol{\tau})) \quad \forall \boldsymbol{\tau} \in \mathbf{H}_p$$

where $\mathcal{P}_h^k : \mathbf{L}^p(\Omega) \rightarrow \mathbf{H}_h^{\mathbf{u}}$ is the usual orthogonal projector with respect to the $\mathbf{L}^2(\Omega)$ -inner product, which satisfies the following error estimate (see [24, Prop. 1.135]): there exists a positive constant C_0 , independent of h , such that for $0 \leq l \leq k+1$ and $1 \leq p \leq \infty$ there holds

$$\|w - \mathcal{P}_h^k(w)\|_{0,p;\Omega} \leq C_0 h^l \|w\|_{l,p;\Omega} \quad \forall w \in \mathbf{W}^{l,p}(\Omega).$$

We stress that $\mathcal{P}_h^k(w)|_K = \mathcal{P}_K^k(w|_K) \quad \forall w \in \mathbf{L}^p(\Omega)$, where $\mathcal{P}_K^k : \mathbf{L}^p(K) \rightarrow \mathbf{P}_k(K)$ is the corresponding local orthogonal projector. In addition, denoting by $\mathbf{H}_h^{\mathbf{u}}$ the vector version of $\mathbf{H}_h^{\mathbf{u}}$ (cf. (3.4)), we let $\mathcal{P}_h^k : \mathbf{L}^p(\Omega) \rightarrow \mathbf{H}_h^{\mathbf{u}}$ be the vector version of \mathcal{P}_h^k .

Next, we collect some approximation properties of Π_h^k .

Lemma 3.1. *Given $p > 1$, there exist positive constants C_1 and C_2 , independent of h , such that for $0 \leq l \leq k$ and for each $K \in \mathcal{T}_h^b$ there holds*

$$\|\boldsymbol{\tau} - \Pi_h^k(\boldsymbol{\tau})\|_{0,p;K} \leq C_1 h_K^{l+1} |\boldsymbol{\tau}|_{l+1,p;K} \quad \forall \boldsymbol{\tau} \in \mathbf{W}^{l+1,p}(K). \quad (3.5)$$

and

$$\|\boldsymbol{\tau} \cdot v - \Pi_h^k(\boldsymbol{\tau}) \cdot v\|_{0,p;e} \leq C_2 h_e^{1-1/p} |\boldsymbol{\tau}|_{1,p;K} \quad \forall \boldsymbol{\tau} \in \mathbf{W}^{1,p}(K), \quad \forall e \in \mathcal{E}_h(K). \quad (3.6)$$

Proof. The estimate (3.5) follows straightforwardly from [24, Lem. B.67] and [24, Lem. 1.101] (see, e.g., [17, Lem. 5.3, Eq. (5.38)]), whereas for (3.6) we refer to [12, Lem. 4.2]. \square

Furthermore, denoting by \mathbb{H}_p and $\widehat{\mathbb{H}}_h^\sigma$ the tensor versions of \mathbf{H}_p (cf. (3.1)) and $\widehat{\mathbf{H}}_h^\sigma$ (cf. (3.2)), respectively, we let $\Pi_h^k : \mathbb{H}_p \rightarrow \widehat{\mathbb{H}}_h^\sigma$ be the operator Π_h^k acting row-wise. Then, according to the decomposition (2.6), for each $\boldsymbol{\tau} \in \mathbb{H}_p$ there holds

$$\Pi_h^k(\boldsymbol{\tau}) = \boldsymbol{\Pi}_{h,0}^k(\boldsymbol{\tau}) + d \mathbb{I}, \quad d := \frac{1}{n|\Omega|} \int_\Omega \text{tr}(\Pi_h^k(\boldsymbol{\tau})) \in \mathbb{R}, \quad \boldsymbol{\Pi}_{h,0}^k(\boldsymbol{\tau}) := \Pi_h^k(\boldsymbol{\tau}) - d \mathbb{I} \in \mathbb{H}_h^\sigma.$$

We next recall a stable Helmholtz decomposition for the Banach space $\mathbf{H}(\text{div}_p; \Omega)$, and select $p = 4/3$ for the forthcoming analysis. More precisely, we have the following result proven in [12, Lem. 4.4].

Lemma 3.2. *Given $p \in (1, +\infty)$, there exists a positive constant C_p such that for each $\boldsymbol{\tau} \in \mathbf{H}(\text{div}_p; \Omega)$ there exist $\boldsymbol{\eta} \in \mathbf{W}^{1,p}(\Omega)$ and $\boldsymbol{\xi} \in \mathbf{H}^1(\Omega)$ satisfying*

$$\boldsymbol{\tau} = \boldsymbol{\eta} + \underline{\text{curl}}(\boldsymbol{\xi}) \quad \text{in } \Omega, \quad \|\boldsymbol{\eta}\|_{1,p;\Omega} + \|\boldsymbol{\xi}\|_{1,\Omega} \leq C_p \|\boldsymbol{\tau}\|_{\text{div}_p;\Omega}.$$

We stress here that the foregoing result is certainly valid for the tensor version $\mathbb{H}(\text{div}_p; \Omega)$ of $\mathbf{H}(\text{div}_p; \Omega)$ as well, and hence in particular for $\mathbb{H}_0(\text{div}_p; \Omega)$. In other words, for each $\boldsymbol{\tau} \in \mathbb{H}_0(\text{div}_p; \Omega)$ there exist $\boldsymbol{\eta} \in \mathbf{W}^{1,p}(\Omega)$ and $\boldsymbol{\xi} \in \mathbf{H}^1(\Omega)$ such that

$$\boldsymbol{\tau} = \boldsymbol{\eta} + \underline{\text{curl}}(\boldsymbol{\xi}) \quad \text{in } \Omega, \quad \|\boldsymbol{\eta}\|_{1,p;\Omega} + \|\boldsymbol{\xi}\|_{1,\Omega} \leq C_p \|\boldsymbol{\tau}\|_{\text{div}_p;\Omega}. \quad (3.7)$$

On the other hand, defining $X_h := \{v_h \in C(\overline{\Omega}) : v_h|_K \in P_1(K) \ \forall K \in \mathcal{T}_h^b\}$ and denoting by \mathbf{X}_h its vector version, we let $I_h : H^1(\Omega) \rightarrow X_h$ and $\mathbf{I}_h : \mathbf{H}^1(\Omega) \rightarrow \mathbf{X}_h$ be the usual Clément interpolation operator and its vector version, respectively. Some local properties of I_h , and hence of \mathbf{I}_h , which correspond to the particular case of [24, Lem. 1.127] that arises by choosing there $m = 0$, $p = 2$, and $\ell = 1$, are established in the following lemma (for a proof, see [16]).

Lemma 3.3. *There exist positive constants C_1 and C_2 , such that for each $v \in H^1(\Omega)$:*

$$\|v - I_h v\|_{0,K} \leq C_1 h_K \|v\|_{1,\Delta(K)} \quad \forall K \in \mathcal{T}_h^b$$

and

$$\|v - I_h v\|_{0,e} \leq C_2 h_e^{1/2} \|v\|_{1,\Delta(e)} \quad \forall e \in \mathcal{E}_h$$

where $\Delta(K) := \bigcup \{K' \in \mathcal{T}_h^b : K' \cap K \neq \emptyset\}$ and $\Delta(e) := \bigcup \{K' \in \mathcal{T}_h^b : K' \cap e \neq \emptyset\}$.

3.2 Reliability

Recall that

$$\vec{\sigma} := ((\vec{\mathbf{u}}, \sigma), (\vec{\phi}, \tilde{\sigma})) \in \mathbb{X} := \mathbf{H} \times \mathbb{H}_0(\text{div}_{4/3}; \Omega) \times \widetilde{\mathbf{H}} \times \mathbf{H}(\text{div}_{4/3}; \Omega)$$

is the unique solution of problem (2.7), and that

$$\vec{\sigma}_h := ((\vec{\mathbf{u}}_h, \sigma_h), (\vec{\phi}_h, \tilde{\sigma}_h)) \in \mathbb{X}_h := \mathbf{H}_h \times \mathbb{H}_h^\sigma \times \widetilde{\mathbf{H}}_h \times \mathbf{H}_h^{\tilde{\sigma}}$$

is a solution of problem (2.14). Then, assuming from now on that $\mathbf{u}_D \in \mathbf{H}^{1+\delta}(\Gamma) \cap \mathbf{L}^4(\Gamma)$ and $\varphi_D \in \mathbf{H}^{1+\delta}(\Gamma) \cap \mathbf{L}^4(\Gamma)$, for some $\delta > 0$, which allows, in particular, to compute their tangential derivatives $\nabla \mathbf{u}_D \cdot \mathbf{s}$ and $\nabla \varphi_D \cdot \mathbf{s}$, we introduce for each $K \in \mathcal{T}_h^b$ the local error indicators

$$\tilde{\Theta}_K^{4/3} := \| -\mathbf{div}(\boldsymbol{\sigma}_h) + \frac{1}{2}\mathbf{t}_h \cdot \mathbf{u}_h - \varphi_h \mathbf{g} \|_{0,4/3;K}^{4/3} + \| -\mathbf{div}(\tilde{\boldsymbol{\sigma}}_h) + \frac{1}{2}\mathbf{u}_h \cdot \tilde{\mathbf{t}}_h \|_{0,4/3;K}^{4/3} \quad (3.8)$$

$$\begin{aligned} \bar{\Theta}_K^2 := & \| 2\mu(\varphi_h)\mathbf{t}_{h,\text{sym}} - \frac{1}{2}(\mathbf{u}_h \otimes \mathbf{u}_h)^d - \boldsymbol{\sigma}_h^d \|_{0,K}^2 + \| \mathbb{K}\tilde{\mathbf{t}}_h - \frac{1}{2}\varphi_h \mathbf{u}_h - \tilde{\boldsymbol{\sigma}}_h \|_{0,K}^2 \\ & + h_K^2 \|\mathbf{rot}(\mathbf{t}_h)\|_{0,K}^2 + h_K^2 \|\mathbf{rot}(\tilde{\mathbf{t}}_h)\|_{0,K}^2 + \sum_{e \in \mathcal{E}_h(K) \cap \mathcal{E}_h(\Omega)} h_e \left\{ \|[\mathbf{t}_h \cdot \mathbf{s}] \|_{0,e}^2 + \|[\tilde{\mathbf{t}}_h \cdot \mathbf{s}] \|_{0,e}^2 \right\} \\ & + \sum_{e \in \mathcal{E}_h(K) \cap \mathcal{E}_h(\Gamma)} h_e \left\{ \|\mathbf{t}_h \cdot \mathbf{s} - \nabla \mathbf{u}_D \cdot \mathbf{s} \|_{0,e}^2 + \|\tilde{\mathbf{t}}_h \cdot \mathbf{s} - \nabla \varphi_D \cdot \mathbf{s} \|_{0,e}^2 \right\} \end{aligned} \quad (3.9)$$

$$\begin{aligned} \hat{\Theta}_K^4 := & h_K^4 \|\mathbf{t}_h - \nabla \mathbf{u}_h\|_{0,4;K}^4 + h_K^4 \|\tilde{\mathbf{t}}_h - \nabla \varphi_h\|_{0,4;K}^4 \\ & + \sum_{e \in \mathcal{E}_h(K) \cap \mathcal{E}_h(\Gamma)} h_e \left\{ \|\mathbf{u}_D - \mathbf{u}_h\|_{0,4;e}^4 + \|\varphi_D - \varphi_h\|_{0,4;e}^4 \right\} \end{aligned} \quad (3.10)$$

so that the global a posteriori error estimator is defined as

$$\Theta = \left\{ \sum_{K \in \mathcal{T}_h^b} \tilde{\Theta}_K^{4/3} \right\}^{3/4} + \left\{ \sum_{K \in \mathcal{T}_h^b} \bar{\Theta}_K^2 \right\}^{1/2} + \left\{ \sum_{K \in \mathcal{T}_h^b} \hat{\Theta}_K^4 \right\}^{1/4}. \quad (3.11)$$

We recall here, according to the boundary integration by parts formula given in [21, Eq. (3.34), Lem. 3.5], which in turn follows by applying [34, Eq. (2.17) and Th. 2.11], that for each $\varphi_D \in \mathbf{H}^{1/2}(\Gamma)$ its tangential derivative $\nabla \varphi_D \cdot \mathbf{s}$ is the functional in $\mathbf{H}^{-1/2}(\Gamma)$ defined by

$$\langle \nabla \varphi_D \cdot \mathbf{s}, v \rangle_\Gamma := -\langle \mathbf{curl}(v) \cdot \mathbf{v}, \varphi_D \rangle_\Gamma \quad \forall v \in \mathbf{H}^1(\Omega).$$

Alternatively, if $\tilde{\varphi}_D$ is any function in $\mathbf{H}^1(\Omega)$ such that $\tilde{\varphi}_D|_\Gamma = \varphi_D$, then there holds

$$\langle \nabla \varphi_D \cdot \mathbf{s}, v \rangle_\Gamma = \langle \nabla \tilde{\varphi}_D \cdot \mathbf{s}, v \rangle_\Gamma = \int_\Omega \mathbf{curl} \tilde{\varphi}_D \cdot \nabla v \quad \forall v \in \mathbf{H}^1(\Omega).$$

The fact that $\nabla \tilde{\varphi}_D \in \mathbf{H}(\mathbf{rot}; \Omega) := \{\boldsymbol{\tau} \in \mathbf{L}^2(\Omega) : \mathbf{rot}(\boldsymbol{\tau}) \in \mathbf{L}^2(\Omega)\}$ guarantees that its tangential component is continuous across the edges of \mathcal{T}_h^b , and hence $\nabla \tilde{\varphi}_D \cdot \mathbf{s}$ is unambiguous on Γ . In particular, if $\varphi_D \in \mathbf{H}^{1+\delta}(\Gamma)$, for some $\delta > 0$, which means that $\tilde{\varphi}_D \in \mathbf{H}^{3/2+\delta}(\Omega)$, it follows that $\nabla \tilde{\varphi}_D \in \mathbf{H}^{1/2+\delta}(\Omega)$, and then $\nabla \varphi_D \cdot \mathbf{s}$ is identified to the function in $\mathbf{L}^2(\Gamma)$ given by $\nabla \tilde{\varphi}_D \cdot \mathbf{s}$. Analogue definitions and remarks hold for \mathbf{u}_D .

The residual character of each one of the terms defining the foregoing indicators becomes clear from a simple inspection of the strong problem (2.3) and thanks to the regularity of the continuous solution.

The main result of this section, which establishes the reliability of Θ , reads as follows.

Theorem 3.1. *Assume that the data are sufficiently small (as indicated below in Lemma 3.6). Then, there exists a positive constant C_{rel} , independent of h , such that*

$$\|\tilde{\boldsymbol{\sigma}} - \boldsymbol{\sigma}_h\|_{\mathbf{X}} \leq C_{\text{rel}} \Theta. \quad (3.12)$$

The proof of (3.12) is performed by means of several consecutive steps. We begin by recalling from [17, Sect. 3.2] the definitions of two suitable operators, namely $S : \mathbf{L}^4(\Omega) \times \mathbf{L}^4(\Omega) \rightarrow \mathbf{H}$ and $\tilde{S} : \mathbf{L}^4(\Omega) \rightarrow \widetilde{\mathbf{H}}$. In fact, for each $(\mathbf{w}, \varphi) \in \mathbf{L}^4(\Omega) \times \mathbf{L}^4(\Omega)$ we let $S(\mathbf{w}, \varphi) := \tilde{\mathbf{u}} = (\mathbf{u}, \mathbf{t}) \in \mathbf{H}$, where $(\tilde{\mathbf{u}}, \boldsymbol{\tau})$ is the solution of the problem arising from the first two equations of (2.7) after replacing a_φ and $c(\mathbf{u}; \cdot, \cdot)$ by a_φ and $c(\mathbf{w}; \cdot, \cdot)$, respectively, that is, $(\tilde{\mathbf{u}}, \boldsymbol{\tau}) \in \mathbf{H} \times \mathbf{H}_0(\mathbf{div}_{4/3}; \Omega)$ is such that

$$\begin{aligned} a_\varphi(\tilde{\mathbf{u}}, \tilde{\mathbf{v}}) + c(\mathbf{w}; \tilde{\mathbf{u}}, \tilde{\mathbf{v}}) + b(\tilde{\mathbf{v}}, \boldsymbol{\sigma}) &= F_\varphi(\tilde{\mathbf{v}}) \quad \forall \tilde{\mathbf{v}} \in \mathbf{H} \\ b(\tilde{\mathbf{u}}, \boldsymbol{\tau}) &= G(\boldsymbol{\tau}) \quad \forall \boldsymbol{\tau} \in \mathbf{H}_0(\mathbf{div}_{4/3}; \Omega). \end{aligned} \quad (3.13)$$

In turn, for each $\mathbf{w} \in \mathbf{L}^4(\Omega)$ we let $\tilde{S}(\mathbf{w}) := \tilde{\varphi} \in \widetilde{\mathbf{H}}$, where $(\tilde{\varphi}, \tilde{\boldsymbol{\sigma}})$ is the solution of the problem defined by the last two equations of (2.7) after replacing \mathbf{u} by \mathbf{w} , that is, $(\tilde{\varphi}, \tilde{\boldsymbol{\sigma}}) \in \widetilde{\mathbf{H}} \times \mathbf{H}(\mathbf{div}_{4/3}; \Omega)$ is such that

$$\begin{aligned} \tilde{a}(\tilde{\varphi}, \tilde{\psi}) + \tilde{c}_{\mathbf{w}}(\tilde{\varphi}, \tilde{\psi}) + \tilde{b}(\tilde{\psi}, \tilde{\boldsymbol{\sigma}}) &= 0 \quad \forall \tilde{\psi} \in \widetilde{\mathbf{H}} \\ \tilde{b}(\tilde{\varphi}, \tilde{\boldsymbol{\tau}}) &= \tilde{G}(\tilde{\boldsymbol{\tau}}) \quad \forall \tilde{\boldsymbol{\tau}} \in \mathbf{H}(\mathbf{div}_{4/3}; \Omega). \end{aligned} \quad (3.14)$$

We now recall from [17, Lemmas 3.5 and 3.6] that (3.13) and (3.14) are well-posed for each $(\mathbf{w}, \varphi) \in \mathbf{L}^4(\Omega) \times L^4(\Omega)$ and for each $\mathbf{w} \in \mathbf{L}^4(\Omega)$, respectively, which implies that the bilinear forms arising after adding the corresponding left-hand sides satisfy global inf-sup conditions uniformly. In other words, denoting from now on $\mathbf{W} := \mathbf{H} \times \mathbb{H}_0(\mathbf{div}_{4/3}; \Omega)$ and $\tilde{\mathbf{W}} := \tilde{\mathbf{H}} \times \mathbf{H}(\mathbf{div}_{4/3}; \Omega)$, there exist positive constants γ , and $\tilde{\gamma}$, independent of (\mathbf{w}, φ) and \mathbf{w} , respectively, such that

$$\gamma \|(\vec{\mathbf{z}}, \boldsymbol{\zeta})\|_{\mathbf{W}} \leq \sup_{\substack{(\vec{\mathbf{v}}, \boldsymbol{\tau}) \in \mathbf{W} \\ (\vec{\mathbf{v}}, \boldsymbol{\tau}) \neq \mathbf{0}}} \frac{a_\varphi(\vec{\mathbf{z}}, \vec{\mathbf{v}}) + c(\mathbf{w}; \vec{\mathbf{z}}, \vec{\mathbf{v}}) + b(\vec{\mathbf{v}}, \boldsymbol{\zeta}) + b(\vec{\mathbf{z}}, \boldsymbol{\tau})}{\|(\vec{\mathbf{v}}, \boldsymbol{\tau})\|_{\mathbf{W}}} \quad \forall (\vec{\mathbf{z}}, \boldsymbol{\zeta}) \in \mathbf{W} \quad (3.15)$$

$$\tilde{\gamma} \|(\vec{\varphi}, \tilde{\boldsymbol{\zeta}})\|_{\tilde{\mathbf{W}}} \leq \sup_{\substack{(\vec{\psi}, \tilde{\boldsymbol{\tau}}) \in \tilde{\mathbf{W}} \\ (\vec{\psi}, \tilde{\boldsymbol{\tau}}) \neq \mathbf{0}}} \frac{\tilde{a}(\vec{\varphi}, \vec{\psi}) + \tilde{c}_{\mathbf{w}}(\vec{\varphi}, \vec{\psi}) + \tilde{b}(\vec{\psi}, \tilde{\boldsymbol{\zeta}}) + \tilde{b}(\vec{\varphi}, \tilde{\boldsymbol{\tau}})}{\|(\vec{\psi}, \tilde{\boldsymbol{\tau}})\|_{\tilde{\mathbf{W}}}} \quad \forall (\vec{\varphi}, \tilde{\boldsymbol{\zeta}}) \in \tilde{\mathbf{W}}. \quad (3.16)$$

Next, proceeding as in [17, Sect. 3.4], we suppose further regularity on the solutions of the problem defining the operator S (cf. (3.13)). Indeed, we assume that $\mathbf{u}_D \in \mathbf{H}^{1/2+\varepsilon}(\Gamma)$ for some $\varepsilon \in [1/2, 1)$ (when $n = 2$) or $\varepsilon \in [3/4, 1)$ (when $n = 3$), and that for each $(\mathbf{w}, \varphi) \in \mathbf{L}^4(\Omega) \times L^4(\Omega)$ there holds

$$S(\mathbf{w}, \varphi) := \vec{\mathbf{u}} = (\mathbf{u}, \mathbf{t}) \in \mathbf{W}^{\varepsilon, 4}(\Omega) \times (\mathbb{L}_{\text{tr}}^2(\Omega) \cap \mathbb{H}^\varepsilon(\Omega)) \quad (3.17)$$

and (cf. [17, Eq. (3.62)]):

$$\|\mathbf{u}\|_{\varepsilon, 4; \Omega} + \|\mathbf{t}\|_{\varepsilon, \Omega} \leq c_S \{ \|\varphi\|_{0, 4; \Omega} \|\mathbf{g}\|_{0, \infty; \Omega} + (1 + \|\mathbf{w}\|_{0, 4; \Omega}) \|\mathbf{u}_D\|_{1/2+\varepsilon, \Gamma} \} \quad (3.18)$$

with a positive constant c_S independent of the given (\mathbf{w}, φ) . In particular, taking $\|(\mathbf{w}, \varphi)\| \leq r$, with $r > 0$ given, there holds

$$\|\mathbf{u}\|_{\varepsilon, 4; \Omega} + \|\mathbf{t}\|_{\varepsilon, \Omega} \leq c_S \{ r \|\mathbf{g}\|_{0, \infty; \Omega} + (1 + r) \|\mathbf{u}_D\|_{1/2+\varepsilon, \Gamma} \}. \quad (3.19)$$

Our first estimate aiming to prove (3.12) is established as follows.

Lemma 3.4. *There exists $C_1 > 0$, independent of h , such that*

$$\begin{aligned} \|(\vec{\mathbf{u}}, \boldsymbol{\sigma}) - (\vec{\mathbf{u}}_h, \boldsymbol{\sigma}_h)\|_{\mathbf{W}} &\leq C_1 \left\{ \| -\mathbf{div}(\boldsymbol{\sigma}_h) + \frac{1}{2} \mathbf{t}_h \mathbf{u}_h - \varphi_h \mathbf{g} \|_{0, 4/3; \Omega} + \|\vec{\mathbf{u}}_h\|_{\mathbf{H}} \|\mathbf{u} - \mathbf{u}_h\|_{0, 4; \Omega} \right. \\ &\quad \left. + \|2\mu(\varphi_h) \mathbf{t}_{h, \text{sym}} - \frac{1}{2} (\mathbf{u}_h \otimes \mathbf{u}_h)^d - \boldsymbol{\sigma}_h^d\|_{0, \Omega} + (\|\mathbf{g}\|_{0, \infty; \Omega} + \|\mathbf{t}\|_{\varepsilon, \Omega}) \|\varphi - \varphi_h\|_{0, 4; \Omega} + \|\mathcal{R}\| \right\} \end{aligned} \quad (3.20)$$

where $\mathcal{R} : \mathbb{H}_0(\mathbf{div}_{4/3}; \Omega) \rightarrow \mathbb{R}$ is the functional defined by

$$\mathcal{R}(\boldsymbol{\tau}) := (\mathbf{t}_h, \boldsymbol{\tau})_{\Omega} + (\mathbf{u}_h, \mathbf{div}(\boldsymbol{\tau}))_{\Omega} - \langle \boldsymbol{\tau} \mathbf{v}, \mathbf{u}_D \rangle_{\Gamma} \quad \forall \boldsymbol{\tau} \in \mathbb{H}_0(\mathbf{div}_{4/3}; \Omega). \quad (3.21)$$

Proof. We begin by applying (3.15) to $(\mathbf{w}, \varphi) = (\mathbf{u}, \varphi)$ and $(\vec{\mathbf{z}}, \boldsymbol{\zeta}) = (\vec{\mathbf{u}}, \boldsymbol{\sigma}) - (\vec{\mathbf{u}}_h, \boldsymbol{\sigma}_h)$. In this way, and additionally employing the first two equations of (2.7), we arrive at

$$\gamma \|(\vec{\mathbf{u}}, \boldsymbol{\sigma}) - (\vec{\mathbf{u}}_h, \boldsymbol{\sigma}_h)\|_{\mathbf{W}} \leq \sup_{\substack{(\vec{\mathbf{v}}, \boldsymbol{\tau}) \in \mathbf{W} \\ (\vec{\mathbf{v}}, \boldsymbol{\tau}) \neq \mathbf{0}}} \frac{\mathcal{Q}(\vec{\mathbf{v}}) + \mathcal{R}(\boldsymbol{\tau})}{\|(\vec{\mathbf{v}}, \boldsymbol{\tau})\|_{\mathbf{W}}} \quad (3.22)$$

where

$$\begin{aligned} \mathcal{Q}(\vec{\mathbf{v}}) &:= F_{\varphi}(\vec{\mathbf{v}}) - \{a_{\varphi}(\vec{\mathbf{u}}_h, \vec{\mathbf{v}}) + c(\mathbf{u}; \vec{\mathbf{u}}_h, \vec{\mathbf{v}}) + b(\vec{\mathbf{v}}, \boldsymbol{\sigma}_h)\} \quad \forall \vec{\mathbf{v}} \in \mathbf{H} \\ \mathcal{R}(\boldsymbol{\tau}) &:= G(\boldsymbol{\tau}) - b(\vec{\mathbf{u}}_h, \boldsymbol{\tau}) \quad \forall \boldsymbol{\tau} \in \mathbb{H}_0(\mathbf{div}_{4/3}; \Omega) \end{aligned}$$

which, according to the definitions of G (cf. (2.12)) and b (cf. (2.8)), yields (3.21). Next, adding and subtracting $F_{\varphi_h}(\vec{\mathbf{v}})$, $a_{\varphi_h}(\vec{\mathbf{u}}_h, \vec{\mathbf{v}})$, and $c(\mathbf{u}_h; \vec{\mathbf{u}}_h, \vec{\mathbf{v}})$, we obtain

$$\mathcal{Q}(\vec{\mathbf{v}}) := \mathcal{Q}_1(\vec{\mathbf{v}}) + F_{\varphi-\varphi_h}(\vec{\mathbf{v}}) + a_{\varphi_h}(\vec{\mathbf{u}}_h, \vec{\mathbf{v}}) - a_{\varphi}(\vec{\mathbf{u}}_h, \vec{\mathbf{v}}) + c(\mathbf{u}_h; \vec{\mathbf{u}}_h, \vec{\mathbf{v}}) - c(\mathbf{u}; \vec{\mathbf{u}}_h, \vec{\mathbf{v}}) \quad (3.23)$$

with

$$\mathcal{Q}_1(\vec{\mathbf{v}}) := F_{\varphi_h}(\vec{\mathbf{v}}) - a_{\varphi_h}(\vec{\mathbf{u}}_h, \vec{\mathbf{v}}) - c(\mathbf{u}_h; \vec{\mathbf{u}}_h, \vec{\mathbf{v}}) - b(\vec{\mathbf{v}}, \boldsymbol{\sigma}_h).$$

Then, bearing in mind the definitions of the forms and functionals involved (cf. (2.8), (2.9), and (2.12)), and applying the Hölder and Cauchy–Schwarz inequalities, we find that

$$|\Omega_1(\vec{\mathbf{v}})| \leq \left\{ \| -\operatorname{div}(\boldsymbol{\sigma}_h) + \frac{1}{2}\mathbf{t}_h \mathbf{u}_h - \varphi_h \mathbf{g} \|_{0,4/3;\Omega} + \| 2\mu(\varphi_h)\mathbf{t}_{h,\text{sym}} - \frac{1}{2}(\mathbf{u}_h \otimes \mathbf{u}_h)^d - \boldsymbol{\sigma}_h^d \|_{0,\Omega} \right\} \|\vec{\mathbf{v}}\|_{\mathbf{H}} \quad (3.24)$$

$$|F_{\varphi-\varphi_h}(\vec{\mathbf{v}})| \leq |\Omega|^{1/2} \|\mathbf{g}\|_{0,\infty;\Omega} \|\varphi - \varphi_h\|_{0,4;\Omega} \|\vec{\mathbf{v}}\|_{\mathbf{H}} \quad (3.25)$$

$$|c(\mathbf{u}_h; \vec{\mathbf{u}}_h, \vec{\mathbf{v}}) - c(\mathbf{u}; \vec{\mathbf{u}}_h, \vec{\mathbf{v}})| \leq \|\vec{\mathbf{u}}_h\|_{\mathbf{H}} \|\mathbf{u} - \mathbf{u}_h\|_{0,4;\Omega} \|\vec{\mathbf{v}}\|_{\mathbf{H}}. \quad (3.26)$$

In turn, proceeding as in the proof of [17, Lem. 3.8], that is using the Lipschitz-continuity of μ (cf. (2.2)), the Cauchy–Schwarz and Hölder inequalities again, and the regularity assumption on the operator S (cf. (3.17)), we obtain (cf. [17, Eqs. (3.67) and (3.68)]):

$$|\alpha_{\varphi_h}(\vec{\mathbf{u}}_h, \vec{\mathbf{v}}) - \alpha_{\varphi}(\vec{\mathbf{u}}_h, \vec{\mathbf{v}})| \leq 2L_{\mu} \|i_{\varepsilon}\| c(\varepsilon, n, |\Omega|) \|\mathbf{t}\|_{\varepsilon,\Omega} \|\varphi - \varphi_h\|_{0,4;\Omega} \|\vec{\mathbf{v}}\|_{\mathbf{H}} \quad (3.27)$$

where i_{ε} denotes the continuous injection of $\mathbb{H}^{\varepsilon}(\Omega)$ into $\mathbb{L}^{\varepsilon^*}(\Omega)$, with $\varepsilon^* := 2/(1 - \varepsilon)$, and $c(\varepsilon, n, |\Omega|)$ is a positive constant depending on ε , n , and $|\Omega|$. Hence, employing (3.24), (3.25), (3.26), and (3.27) to bound $|\Omega(\vec{\mathbf{v}})|$ (cf. (3.23)), and replacing the resulting estimate back into (3.22), we get (3.20) with $C_1 := \gamma^{-1} \max\{1, |\Omega|^{1/2}, 2L_{\mu} \|i_{\varepsilon}\| c(\varepsilon, n, |\Omega|)\}$, which completes the proof. \square

The bound for $\|(\vec{\varphi}, \vec{\boldsymbol{\sigma}}) - (\vec{\varphi}_h, \vec{\boldsymbol{\sigma}}_h)\|_{\bar{\mathbf{W}}}$ is provided next.

Lemma 3.5. *There exists $C_2 > 0$, independent of h , such that*

$$\|(\vec{\varphi}, \vec{\boldsymbol{\sigma}}) - (\vec{\varphi}_h, \vec{\boldsymbol{\sigma}}_h)\|_{\bar{\mathbf{W}}} \leq C_2 \left\{ \| -\operatorname{div}(\vec{\boldsymbol{\sigma}}_h) + \frac{1}{2}\mathbf{u}_h \cdot \tilde{\mathbf{t}}_h \|_{0,4/3;\Omega} + \|\mathbb{K}\tilde{\mathbf{t}}_h - \frac{1}{2}\varphi_h \mathbf{u}_h - \vec{\boldsymbol{\sigma}}_h \|_{0,\Omega} + \|\vec{\varphi}_h\|_{\bar{\mathbf{H}}} \|\mathbf{u} - \mathbf{u}_h\|_{0,4;\Omega} + \|\bar{\mathcal{R}}\| \right\} \quad (3.28)$$

where $\bar{\mathcal{R}} : \mathbf{H}(\operatorname{div}_{4/3}; \Omega) \rightarrow \mathbb{R}$ is the functional defined by

$$\bar{\mathcal{R}}(\tilde{\boldsymbol{\tau}}) := (\tilde{\mathbf{t}}_h, \tilde{\boldsymbol{\tau}})_{\Omega} + (\varphi_h, \operatorname{div}(\tilde{\boldsymbol{\tau}}))_{\Omega} - (\tilde{\boldsymbol{\tau}} \cdot \mathbf{v}, \varphi_D)_{\Gamma} \quad \forall \boldsymbol{\tau} \in \mathbf{H}(\operatorname{div}_{4/3}; \Omega). \quad (3.29)$$

Proof. It proceeds similarly to the proof of Lemma 3.4, but now applying the global inf-sup condition (3.16) to $\mathbf{w} = \mathbf{u}$ and $(\vec{\varphi}, \tilde{\boldsymbol{\zeta}}) = (\vec{\varphi}, \vec{\boldsymbol{\sigma}}) - (\vec{\varphi}_h, \vec{\boldsymbol{\sigma}}_h)$, and then employing the last two equations of (2.7), along with the definitions and boundedness properties of the forms and functionals involved (cf. (2.10), (2.11), and (2.12)). Further details are omitted. \square

Thanks to Lemmas 3.4 and 3.5, we are able to state now a preliminary estimate for the global error

$$\|\vec{\boldsymbol{\sigma}} - \vec{\boldsymbol{\sigma}}_h\|_{\mathbf{X}} = \|(\vec{\mathbf{u}}, \boldsymbol{\sigma}) - (\vec{\mathbf{u}}_h, \boldsymbol{\sigma}_h)\|_{\mathbf{W}} + \|(\vec{\varphi}, \vec{\boldsymbol{\sigma}}) - (\vec{\varphi}_h, \vec{\boldsymbol{\sigma}}_h)\|_{\bar{\mathbf{W}}}.$$

Indeed, it follows straightforwardly from (3.20) and (3.28) that

$$\begin{aligned} \|\vec{\boldsymbol{\sigma}} - \vec{\boldsymbol{\sigma}}_h\|_{\mathbf{X}} &\leq C_3 \left\{ \| -\operatorname{div}(\boldsymbol{\sigma}_h) + \frac{1}{2}\mathbf{t}_h \mathbf{u}_h - \varphi_h \mathbf{g} \|_{0,4/3;\Omega} + \| -\operatorname{div}(\vec{\boldsymbol{\sigma}}_h) + \frac{1}{2}\mathbf{u}_h \cdot \tilde{\mathbf{t}}_h \|_{0,4/3;\Omega} \right. \\ &\quad + \| 2\mu(\varphi_h)\mathbf{t}_{h,\text{sym}} - \frac{1}{2}(\mathbf{u}_h \otimes \mathbf{u}_h)^d - \boldsymbol{\sigma}_h^d \|_{0,\Omega} + \|\mathbb{K}\tilde{\mathbf{t}}_h - \frac{1}{2}\varphi_h \mathbf{u}_h - \vec{\boldsymbol{\sigma}}_h \|_{0,\Omega} \\ &\quad \left. + (\|\vec{\mathbf{u}}_h\|_{\mathbf{H}} + \|\vec{\varphi}_h\|_{\bar{\mathbf{H}}}) \|\mathbf{u} - \mathbf{u}_h\|_{0,4;\Omega} + (\|\mathbf{g}\|_{0,\infty;\Omega} + \|\mathbf{t}\|_{\varepsilon,\Omega}) \|\varphi - \varphi_h\|_{0,4;\Omega} + \|\mathcal{R}\| + \|\bar{\mathcal{R}}\| \right\} \end{aligned}$$

with $C_3 := \max\{C_1, C_2\}$. Then, according to the a priori estimates for $\|\vec{\mathbf{u}}_h\|_{\mathbf{H}}$ and $\|\vec{\varphi}_h\|_{\bar{\mathbf{H}}}$ provided by [17, Th. 4.11, Eqs. (4.24) and (4.25)], there exist positive constants $C_{S,d}$ and $C_{\bar{S},d}$, independent of h , such that

$$\|\vec{\mathbf{u}}_h\|_{\mathbf{H}} \leq C_{S,d} \{r \|\mathbf{g}\|_{0,\infty;\Omega} + (1+r) \|\mathbf{u}_D\|_{1/2,\Gamma}\} \quad (3.30)$$

and

$$\|\vec{\varphi}_h\|_{\bar{\mathbf{H}}} \leq C_{\bar{S},d} \{1 + \|\mathbb{K}\|_{0,\infty;\Omega} + r\} \|\varphi_D\|_{1/2,\Gamma}$$

whereas the regularity estimate (3.19) yields a corresponding bound for $\|\mathbf{t}\|_{\varepsilon,\Omega}$. Thus, it follows that

$$C_3 \{(\|\vec{\mathbf{u}}_h\|_{\mathbf{H}} + \|\vec{\varphi}_h\|_{\bar{\mathbf{H}}}) \|\mathbf{u} - \mathbf{u}_h\|_{0,4;\Omega} + (\|\mathbf{g}\|_{0,\infty;\Omega} + \|\mathbf{t}\|_{\varepsilon,\Omega}) \|\varphi - \varphi_h\|_{0,4;\Omega}\} \leq \max\{C(\text{data}), C_{\varepsilon}(\text{data})\} \|\vec{\boldsymbol{\sigma}} - \vec{\boldsymbol{\sigma}}_h\|_{\mathbf{X}}$$

where $C(\text{data})$ and $C_\varepsilon(\text{data})$ are the data-depending constants given by

$$\begin{aligned} C(\text{data}) &:= C_3 C_{S,\text{d}} \{r \|\mathbf{g}\|_{0,\infty;\Omega} + (1+r) \|\mathbf{u}_D\|_{1/2,\Gamma}\} + C_3 C_{\tilde{S},\text{d}} \{1 + \|\mathbb{K}\|_{0,\infty;\Omega} + r\} \|\varphi_D\|_{1/2,\Gamma} \\ C_\varepsilon(\text{data}) &:= C_3 \|\mathbf{g}\|_{0,\infty;\Omega} + C_3 c_S \{r \|\mathbf{g}\|_{0,\infty;\Omega} + (1+r) \|\mathbf{u}_D\|_{1/2+\varepsilon,\Gamma}\}. \end{aligned}$$

As a consequence, we readily deduce the following result.

Lemma 3.6. *Assume that*

$$\max \{C(\text{data}), C_\varepsilon(\text{data})\} \leq \frac{1}{2}$$

and let $\tilde{C} := 2C_3$. Then there holds

$$\begin{aligned} \|\tilde{\boldsymbol{\sigma}} - \boldsymbol{\sigma}_h\|_{\mathbb{X}} &\leq \tilde{C} \left\{ \|\mathbf{-div}(\boldsymbol{\sigma}_h) + \frac{1}{2} \mathbf{t}_h \mathbf{u}_h - \varphi_h \mathbf{g}\|_{0,4/3;\Omega} + \|-\mathbf{div}(\tilde{\boldsymbol{\sigma}}_h) + \frac{1}{2} \mathbf{u}_h \cdot \tilde{\mathbf{t}}_h\|_{0,4/3;\Omega} \right. \\ &\quad \left. + \|2\mu(\varphi_h)\mathbf{t}_{h,\text{sym}} - \frac{1}{2}(\mathbf{u}_h \otimes \mathbf{u}_h)^{\text{d}} - \boldsymbol{\sigma}_h^{\text{d}}\|_{0,\Omega} + \|\mathbb{K}\tilde{\mathbf{t}}_h - \frac{1}{2}\varphi_h \mathbf{u}_h - \tilde{\boldsymbol{\sigma}}_h\|_{0,\Omega} + \|\mathcal{R}\| + \|\tilde{\mathcal{R}}\| \right\}. \end{aligned} \quad (3.31)$$

According to (3.31), and in order to complete the derivation of our residual-based estimator, we need to bound the norms of the residual functionals \mathcal{R} and $\tilde{\mathcal{R}}$. In this regard, we now notice from the second and fourth equations of the Galerkin scheme (2.14) that $\mathcal{R}(\boldsymbol{\tau}_h) = 0$ for all $\boldsymbol{\tau}_h \in \mathbb{H}_h^\sigma$ and $\tilde{\mathcal{R}}(\tilde{\boldsymbol{\tau}}_h) = 0$ for all $\tilde{\boldsymbol{\tau}}_h \in \mathbf{H}_h^{\tilde{\sigma}}$, respectively, whence the aforementioned norms can be redefined as

$$\|\mathcal{R}\| := \sup_{\substack{\boldsymbol{\tau} \in \mathbb{H}_0(\mathbf{div}_{4/3};\Omega) \\ \boldsymbol{\tau} \neq 0}} \frac{\mathcal{R}(\boldsymbol{\tau} - \boldsymbol{\tau}_h)}{\|\boldsymbol{\tau}\|_{\mathbf{div}_{4/3};\Omega}} \quad \|\tilde{\mathcal{R}}\| := \sup_{\substack{\tilde{\boldsymbol{\tau}} \in \mathbf{H}(\mathbf{div}_{4/3};\Omega) \\ \tilde{\boldsymbol{\tau}} \neq 0}} \frac{\tilde{\mathcal{R}}(\tilde{\boldsymbol{\tau}} - \tilde{\boldsymbol{\tau}}_h)}{\|\tilde{\boldsymbol{\tau}}\|_{\mathbf{div}_{4/3};\Omega}} \quad (3.32)$$

where the functions $\boldsymbol{\tau}_h$ and $\tilde{\boldsymbol{\tau}}_h$ are chosen within the suprema of (3.32) so that they depend on the corresponding $\boldsymbol{\tau} \in \mathbb{H}_0(\mathbf{div}_{4/3};\Omega)$ and $\tilde{\boldsymbol{\tau}} \in \mathbf{H}(\mathbf{div}_{4/3};\Omega)$. More precisely, they are suitably defined in what follows by employing the Helmholtz decompositions provided by Lemma 3.2 and (3.7) with $p = 4/3$. Indeed, letting $\boldsymbol{\eta} \in \mathbb{W}^{1,4/3}(\Omega)$, $\boldsymbol{\xi} \in \mathbf{H}^1(\Omega)$, $\eta \in \mathbf{W}^{1,4/3}(\Omega)$, and $\xi \in \mathbf{H}^1(\Omega)$, such that

$$\boldsymbol{\tau} := \boldsymbol{\eta} + \underline{\mathbf{curl}}(\boldsymbol{\xi}), \quad \tilde{\boldsymbol{\tau}} := \eta + \mathbf{curl}(\xi) \quad \text{in } \Omega \quad (3.33)$$

with

$$\|\boldsymbol{\eta}\|_{1,4/3;\Omega} + \|\boldsymbol{\xi}\|_{1,\Omega} \leq C_{4/3} \|\boldsymbol{\tau}\|_{\mathbf{div}_{4/3};\Omega}, \quad \|\eta\|_{1,4/3;\Omega} + \|\xi\|_{1,\Omega} \leq C_{4/3} \|\tilde{\boldsymbol{\tau}}\|_{\mathbf{div}_{4/3};\Omega} \quad (3.34)$$

we set

$$\boldsymbol{\tau}_h := \Pi_h^k(\boldsymbol{\eta}) + \underline{\mathbf{curl}}(\mathbf{I}_h \boldsymbol{\xi}) + c \mathbb{I} \in \mathbb{H}_h^\sigma, \quad \tilde{\boldsymbol{\tau}}_h := \Pi_h^k(\eta) + \mathbf{curl}(\mathbf{I}_h \boldsymbol{\xi}) \in \mathbf{H}_h^{\tilde{\sigma}} \quad (3.35)$$

where the constant c is chosen so that $\text{tr}(\boldsymbol{\tau}_h)$ has a null mean value, and hence $\boldsymbol{\tau}_h$ does belong to \mathbb{H}_h^σ . Note that $\boldsymbol{\tau}_h$ and $\tilde{\boldsymbol{\tau}}_h$ can be seen as discrete Helmholtz decompositions of $\boldsymbol{\tau}$ and $\tilde{\boldsymbol{\tau}}$, respectively. In this way, using that $\mathcal{R}(c\mathbb{I}) = 0$, and denoting

$$\hat{\boldsymbol{\eta}} := \boldsymbol{\eta} - \Pi_h^k(\boldsymbol{\eta}), \quad \hat{\boldsymbol{\xi}} := \boldsymbol{\xi} - \mathbf{I}_h \boldsymbol{\xi}, \quad \hat{\eta} := \eta - \Pi_h^k(\eta), \quad \hat{\xi} := \xi - \mathbf{I}_h \boldsymbol{\xi}$$

it follows from (3.33) and (3.35) that

$$\mathcal{R}(\boldsymbol{\tau}) = \mathcal{R}(\boldsymbol{\tau} - \boldsymbol{\tau}_h) = \mathcal{R}(\hat{\boldsymbol{\eta}}) + \mathcal{R}(\underline{\mathbf{curl}}(\hat{\boldsymbol{\xi}})) \quad (3.36)$$

$$\tilde{\mathcal{R}}(\tilde{\boldsymbol{\tau}}) = \tilde{\mathcal{R}}(\tilde{\boldsymbol{\tau}} - \tilde{\boldsymbol{\tau}}_h) = \tilde{\mathcal{R}}(\hat{\eta}) + \tilde{\mathcal{R}}(\mathbf{curl}(\hat{\boldsymbol{\xi}})) \quad (3.37)$$

where, according to the definitions of \mathcal{R} and $\tilde{\mathcal{R}}$ (cf. (3.21) and (3.29)), we find that

$$\mathcal{R}(\hat{\boldsymbol{\eta}}) = (\mathbf{t}_h, \hat{\boldsymbol{\eta}})_\Omega + (\mathbf{u}_h, \mathbf{div}(\hat{\boldsymbol{\eta}}))_\Omega - \langle \hat{\boldsymbol{\eta}} \mathbf{v}, \mathbf{u}_D \rangle_\Gamma \quad (3.38)$$

$$\mathcal{R}(\underline{\mathbf{curl}}(\hat{\boldsymbol{\xi}})) = (\mathbf{t}_h, \underline{\mathbf{curl}}(\hat{\boldsymbol{\xi}}))_\Omega - \langle \underline{\mathbf{curl}}(\hat{\boldsymbol{\xi}}) \mathbf{v}, \mathbf{u}_D \rangle_\Gamma \quad (3.39)$$

$$\tilde{\mathcal{R}}(\hat{\eta}) = (\tilde{\mathbf{t}}_h, \hat{\eta})_\Omega + (\varphi_h, \mathbf{div}(\hat{\eta}))_\Omega - \langle \hat{\eta} \cdot \mathbf{v}, \varphi_D \rangle_\Gamma, \quad \tilde{\mathcal{R}}(\mathbf{curl}(\hat{\boldsymbol{\xi}})) = (\tilde{\mathbf{t}}_h, \mathbf{curl}(\hat{\boldsymbol{\xi}}))_\Omega - \langle \mathbf{curl}(\hat{\boldsymbol{\xi}}) \cdot \mathbf{v}, \varphi_D \rangle_\Gamma.$$

The following lemma establishes the residual upper bound for $\|\mathcal{R}\|$.

Lemma 3.7. *There exists a positive constant C , independent of h , such that*

$$\|\mathcal{R}\| \leq C \{\bar{\Phi} + \widehat{\Phi}\} \quad (3.40)$$

where

$$\bar{\Phi}^2 := \sum_{K \in \mathcal{T}_h^b} \bar{\Phi}_K^2, \quad \widehat{\Phi}^4 := \sum_{K \in \mathcal{T}_h^b} \widehat{\Phi}_K^4$$

with

$$\begin{aligned} \bar{\Phi}_K^2 &:= h_K^2 \|\mathbf{rot}(\mathbf{t}_h)\|_{0,K}^2 + \sum_{e \in \mathcal{E}_h(K) \cap \mathcal{E}_h(\Omega)} h_e \|[\mathbf{t}_h \mathbf{s}]\|_{0,e}^2 + \sum_{e \in \mathcal{E}_h(K) \cap \mathcal{E}_h(\Gamma)} h_e \|\mathbf{t}_h \mathbf{s} - \nabla \mathbf{u}_D \mathbf{s}\|_{0,e}^2 \\ \widehat{\Phi}_K^4 &:= h_K^4 \|\mathbf{t}_h - \nabla \mathbf{u}_h\|_{0,4;K}^4 + \sum_{e \in \mathcal{E}_h(K) \cap \mathcal{E}_h(\Gamma)} h_e \|\mathbf{u}_D - \mathbf{u}_h\|_{0,4;e}^4. \end{aligned}$$

Proof. According to (3.36), we begin by estimating $\mathcal{R}(\widehat{\boldsymbol{\eta}})$ (cf. (3.38)). Let us first observe that, for each $e \in \mathcal{E}_h$, the identity (3.3) and the fact that $\mathbf{u}_h|_e \in \mathbf{P}_k(e)$ yield $\int_e \widehat{\boldsymbol{\eta}} \mathbf{v} \cdot \mathbf{u}_h = 0$. Hence, locally integrating by parts the second term in (3.38), we readily obtain

$$\mathcal{R}(\widehat{\boldsymbol{\eta}}) = (\mathbf{t}_h - \nabla \mathbf{u}_h, \widehat{\boldsymbol{\eta}})_\Omega - \sum_{e \in \mathcal{E}_h(\Gamma)} \int_e \mathbf{u}_D \cdot \widehat{\boldsymbol{\eta}} \mathbf{v} = (\mathbf{t}_h - \nabla \mathbf{u}_h, \widehat{\boldsymbol{\eta}})_\Omega - \sum_{e \in \mathcal{E}_h(\Gamma)} \int_e (\mathbf{u}_D - \mathbf{u}_h) \cdot \widehat{\boldsymbol{\eta}} \mathbf{v}$$

from which, applying the Hölder inequality along with the approximation properties (3.5) and (3.6) (cf. Lemma 3.1) with $p = 4/3$ and $l = 0$, we find that

$$\begin{aligned} |\mathcal{R}(\widehat{\boldsymbol{\eta}})| &\leq \sum_{K \in \mathcal{T}_h^b} \|\mathbf{t}_h - \nabla \mathbf{u}_h\|_{0,4;K} \|\widehat{\boldsymbol{\eta}}\|_{0,4/3;K} + \sum_{e \in \mathcal{E}_h(\Gamma)} \|\mathbf{u}_D - \mathbf{u}_h\|_{0,4;e} \|\widehat{\boldsymbol{\eta}} \mathbf{v}\|_{0,4/3;e} \\ &\leq \widehat{C}_1 \left\{ \sum_{K \in \mathcal{T}_h^b} h_K \|\mathbf{t}_h - \nabla \mathbf{u}_h\|_{0,4;K} |\boldsymbol{\eta}|_{1,4/3;K} + \sum_{e \in \mathcal{E}_h(\Gamma)} h_e^{1/4} \|\mathbf{u}_D - \mathbf{u}_h\|_{0,4;e} |\boldsymbol{\eta}|_{1,4/3;K_e} \right\} \end{aligned}$$

where, given $e \in \mathcal{E}_h(\Gamma)$, K_e is the triangle of \mathcal{T}_h^b having e as an edge. Then, employing the discrete Hölder inequality in the above sums and then the first stability estimate of (3.34), we arrive at

$$|\mathcal{R}(\widehat{\boldsymbol{\eta}})| \leq \widehat{C}_2 \left\{ \sum_{K \in \mathcal{T}_h^b} h_K^4 \|\mathbf{t}_h - \nabla \mathbf{u}_h\|_{0,4;K}^4 + \sum_{e \in \mathcal{E}_h(\Gamma)} h_e \|\mathbf{u}_D - \mathbf{u}_h\|_{0,4;e}^4 \right\}^{1/4} \|\boldsymbol{\tau}\|_{\mathbf{div}_{4/3};\Omega}. \quad (3.41)$$

Next, we estimate $\mathcal{R}(\underline{\mathbf{curl}}(\widehat{\boldsymbol{\xi}}))$ (cf. (3.39)). In fact, regarding its second term, a suitable boundary integration by parts formula (cf. [21, Eq. (3.35), Lemma 3.5]) yields

$$\langle \underline{\mathbf{curl}}(\widehat{\boldsymbol{\xi}}) \mathbf{v}, \mathbf{u}_D \rangle_\Gamma = -\langle \nabla \mathbf{u}_D \mathbf{s}, \widehat{\boldsymbol{\xi}} \rangle_\Gamma. \quad (3.42)$$

In turn, locally integrating by parts the first term of $\mathcal{R}(\underline{\mathbf{curl}}(\widehat{\boldsymbol{\xi}}))$, we get

$$(\mathbf{t}_h, \underline{\mathbf{curl}}(\widehat{\boldsymbol{\xi}}))_\Omega = \sum_{K \in \mathcal{T}_h^b} \int_K \mathbf{rot}(\mathbf{t}_h) \cdot \widehat{\boldsymbol{\xi}} - \sum_{e \in \mathcal{E}_h(\Omega)} \int_e [\mathbf{t}_h \mathbf{s}] \cdot \widehat{\boldsymbol{\xi}} - \sum_{e \in \mathcal{E}_h(\Gamma)} \int_e \mathbf{t}_h \mathbf{s} \cdot \widehat{\boldsymbol{\xi}}$$

which, together with (3.42), imply

$$\mathcal{R}(\underline{\mathbf{curl}}(\widehat{\boldsymbol{\xi}})) = \sum_{K \in \mathcal{T}_h^b} \int_K \mathbf{rot}(\mathbf{t}_h) \cdot \widehat{\boldsymbol{\xi}} - \sum_{e \in \mathcal{E}_h(\Omega)} \int_e [\mathbf{t}_h \mathbf{s}] \cdot \widehat{\boldsymbol{\xi}} - \sum_{e \in \mathcal{E}_h(\Gamma)} \int_e (\mathbf{t}_h \mathbf{s} - \nabla \mathbf{u}_D \mathbf{s}) \cdot \widehat{\boldsymbol{\xi}}. \quad (3.43)$$

In this way, applying the Cauchy–Schwarz inequality, the approximation properties provided by Lemma 3.3, and again the first stability estimate of (3.34), we deduce from (3.43) that

$$|\mathcal{R}(\underline{\mathbf{curl}}(\widehat{\boldsymbol{\xi}}))| \leq \widehat{C}_3 \left\{ \sum_{K \in \mathcal{T}_h^b} h_K^2 \|\mathbf{rot}(\mathbf{t}_h)\|_{0,K}^2 + \sum_{e \in \mathcal{E}_h(\Omega)} h_e \|[\mathbf{t}_h \mathbf{s}]\|_{0,e}^2 + \sum_{e \in \mathcal{E}_h(\Gamma)} h_e \|\mathbf{t}_h \mathbf{s} - \nabla \mathbf{u}_D \mathbf{s}\|_{0,e}^2 \right\}^{1/2} \|\boldsymbol{\tau}\|_{\mathbf{div}_{4/3};\Omega}. \quad (3.44)$$

Finally, it is easy to see that (3.32), (3.36), (3.41), and (3.44) give (3.40), which ends the proof. \square

The derivation of the residual upper bound for $\|\tilde{\mathcal{R}}\|$ proceeds analogously to the proof of the previous lemma. We omit further details and state the corresponding result as follows.

Lemma 3.8. *There exists a positive constant C , independent of h , such that*

$$\|\tilde{\mathcal{R}}\| \leq C \{\bar{\Psi} + \widehat{\Psi}\}$$

where

$$\bar{\Psi}^2 := \sum_{K \in \mathcal{T}_h^b} \bar{\Psi}_K^2, \quad \widehat{\Psi}^4 := \sum_{K \in \mathcal{T}_h^b} \widehat{\Psi}_K^4$$

with

$$\begin{aligned} \bar{\Psi}_K^2 &:= h_K^2 \|\operatorname{rot}(\tilde{\mathbf{t}}_h)\|_{0,K}^2 + \sum_{e \in \mathcal{E}_h(K) \cap \mathcal{E}_h(\Gamma)} h_e \|[\tilde{\mathbf{t}}_h \cdot \mathbf{s}]\|_{0,e}^2 + \sum_{e \in \mathcal{E}_h(K) \cap \mathcal{E}_h(\Gamma)} h_e \|\tilde{\mathbf{t}}_h \cdot \mathbf{s} - \nabla \varphi_D \cdot \mathbf{s}\|_{0,e}^2 \\ \widehat{\Psi}_K^4 &:= h_K^4 \|\tilde{\mathbf{t}}_h - \nabla \varphi_h\|_{0,4;K}^4 + \sum_{e \in \mathcal{E}_h(K) \cap \mathcal{E}_h(\Gamma)} h_e \|\varphi_D - \varphi_h\|_{0,4;e}^4. \end{aligned}$$

We end this section by stressing that the reliability of the estimator Θ (cf. (3.11)), that is the proof of Theorem 3.1, is a direct consequence of Lemmas 3.6, 3.7, and 3.8. However, we observe that, while the resulting constant C_{rel} is independent of h , it is not explicitly computable since it depends on other constants, such as the ones arising from the interpolation errors and the regularity assumption on the operator S , which are not known explicitly. For the same reason, that is, dependence on unknown constants, the smallness assumptions on the data are not verifiable in practice. Unfortunately, improving these results has remained elusive. Nevertheless, the numerical examples reported in Section 6 illustrate the boundedness of C_{rel} and the good performance of the adaptive strategy suggested by the a posteriori error estimates.

3.3 Preliminaries for efficiency

For the efficiency analysis of Θ (cf. (3.11)) we proceed as in [6, 7, 15], and apply the localization technique based on bubble functions, and the inverse and discrete trace inequalities. For the former, given $K \in \mathcal{T}_h^b$, we let ψ_K be the usual element-bubble function (cf. [39, Eqs. (1.5) and (1.6)]), satisfying

$$\psi_K \in P_3(K), \quad \operatorname{supp}(\psi_K) \subseteq K, \quad \psi_K = 0 \quad \text{on } \partial T, \quad 0 \leq \psi_K \leq 1 \quad \text{in } K.$$

The specific properties of ψ_K to be employed in what follows, are collected in the following lemma, for whose proof we refer to [39, Lem. 3.3 and Rem. 3.2].

Lemma 3.9. *Let k be a non-negative integer, $p, q \in (1, +\infty)$ conjugate to each other, and $K \in \mathcal{T}_h^b$. Then, there exist positive constants c_1, c_2 , and c_3 , independent of h and K , but depending on the shape-regularity of the triangulations (minimum angle condition) and k , such that for each $u \in P_k(K)$ there hold*

$$c_1 \|u\|_{0,p;K} \leq \sup_{\substack{v \in P_k(K) \\ v \neq 0}} \frac{\int_K u \psi_K v}{\|v\|_{0,q;K}} \leq \|u\|_{0,p;K} \tag{3.45}$$

and

$$c_2 h_K^{-1} \|\psi_K u\|_{0,q;K} \leq \|\nabla(\psi_K u)\|_{0,q;K} \leq c_3 h_K^{-1} \|\psi_K u\|_{0,q;K}. \tag{3.46}$$

In turn, the aforementioned inverse inequality is stated as follows (cf. [24, Lem. 1.138]).

Lemma 3.10. *Let k, ℓ , and m be non-negative integers such that $m \leq \ell$, and let $r, s \in [1, +\infty]$, and $K \in \mathcal{T}_h^b$. Then, there exists $c > 0$, independent of h, K, r , and s , but depending on k, ℓ, m , and the shape regularity of the triangulations, such that*

$$\|v\|_{l,r;K} \leq c h_K^{m-\ell+n(1/r-1/s)} \|v\|_{m,s;K} \quad \forall v \in P_k(K). \tag{3.47}$$

Finally, proceeding as in [1, Th. 3.10], that is employing the usual scaling estimates with respect to a fixed reference element \widehat{K} , and applying the trace inequality in $W^{1,p}(\widehat{K})$, for a given $p \in (1, +\infty)$, one is able to establish the following discrete trace inequality.

Lemma 3.11. *Let $p \in (1, +\infty)$. Then, there exists $c > 0$, depending only on the shape regularity of the triangulations, such that for each $K \in \mathcal{T}_h^b$ and $e \in \mathcal{E}(K)$, there holds*

$$\|v\|_{0,p;e}^p \leq c \left\{ h_K^{-1} \|v\|_{0,p;K}^p + h_K^{p-1} |v|_{1,p;K}^p \right\} \quad \forall v \in W^{1,p}(K). \quad (3.48)$$

3.4 Efficiency

In this section we prove the efficiency of Θ (cf. (3.11)), which is stated as follows.

Theorem 3.2. *Assume, for simplicity, that \mathbf{u}_D and φ_D are piecewise polynomials. Then, there exists a positive constant C_{eff} , independent of h , such that*

$$C_{\text{eff}} \Theta + \text{h.o.t.} \leq \|\vec{\sigma} - \vec{\sigma}_h\|_X \quad (3.49)$$

where h.o.t. stands for one or several terms of higher order.

The rest of this section is devoted to the proof of (3.49). We begin with the following result.

Lemma 3.12. *There exist positive constants c , \tilde{c} , C , and \tilde{C} , independent of h , such that*

$$\begin{aligned} & \| -\mathbf{div}(\sigma_h) + \frac{1}{2} \mathbf{t}_h \mathbf{u}_h - \varphi_h \mathbf{g} \|_{0,4/3;\Omega} \\ & \leq c \left\{ \|\sigma - \sigma_h\|_{\mathbf{div}_{4/3};\Omega} + \|\mathbf{u} - \mathbf{u}_h\|_{0,4;\Omega} + \|\mathbf{t} - \mathbf{t}_h\|_{0,\Omega} + \|\varphi - \varphi_h\|_{0,4;\Omega} \right\} \end{aligned} \quad (3.50)$$

$$\begin{aligned} & \|2\mu(\varphi_h)\mathbf{t}_{h,\text{sym}} - \frac{1}{2}(\mathbf{u}_h \otimes \mathbf{u}_h)^d - \sigma_h^d\|_{0,\Omega} \\ & \leq C \left\{ \|\sigma - \sigma_h\|_{\mathbf{div}_{4/3};\Omega} + \|\mathbf{t} - \mathbf{t}_h\|_{0,\Omega} + \|\mathbf{u} - \mathbf{u}_h\|_{0,4;\Omega} + \|\varphi - \varphi_h\|_{0,4;\Omega} \right\} \end{aligned} \quad (3.51)$$

$$\| -\mathbf{div}(\tilde{\sigma}_h) + \frac{1}{2} \mathbf{u}_h \cdot \tilde{\mathbf{t}}_h \|_{0,4/3;\Omega} \leq \tilde{c} \left\{ \|\tilde{\sigma} - \tilde{\sigma}_h\|_{\mathbf{div}_{4/3};\Omega} + \|\tilde{\mathbf{t}} - \tilde{\mathbf{t}}_h\|_{0,\Omega} + \|\mathbf{u} - \mathbf{u}_h\|_{0,4;\Omega} \right\} \quad (3.52)$$

and

$$\|K\tilde{\mathbf{t}}_h - \frac{1}{2}\varphi_h \mathbf{u}_h - \tilde{\sigma}_h\|_{0,\Omega} \leq \tilde{C} \left\{ \|\tilde{\sigma} - \tilde{\sigma}_h\|_{\mathbf{div}_{4/3};\Omega} + \|\tilde{\mathbf{t}} - \tilde{\mathbf{t}}_h\|_{0,\Omega} + \|\mathbf{u} - \mathbf{u}_h\|_{0,4;\Omega} + \|\varphi - \varphi_h\|_{0,4;\Omega} \right\}. \quad (3.53)$$

Proof. Let us begin with the proof of (3.50). According to the third row of (2.3), and applying the triangle inequality and the continuous injection of $L^4(\Omega)$ into $L^{4/3}(\Omega)$, we readily find that

$$\begin{aligned} \| -\mathbf{div}(\sigma_h) + \frac{1}{2} \mathbf{t}_h \mathbf{u}_h - \varphi_h \mathbf{g} \|_{0,4/3;\Omega} &= \| \mathbf{div}(\sigma - \sigma_h) - \frac{1}{2}(\mathbf{t}\mathbf{u} - \mathbf{t}_h\mathbf{u}_h) + (\varphi - \varphi_h)\mathbf{g} \|_{0,4/3;\Omega} \\ &\leq \|\sigma - \sigma_h\|_{\mathbf{div}_{4/3};\Omega} + \frac{1}{2}\|\mathbf{t}\mathbf{u} - \mathbf{t}_h\mathbf{u}_h\|_{0,4/3;\Omega} + \|\mathbf{g}\|_{0,\infty;\Omega} \|\varphi - \varphi_h\|_{0,4;\Omega}. \end{aligned} \quad (3.54)$$

Then, subtracting and adding $\mathbf{t}\mathbf{u}_h$, and employing the triangle and Hölder inequalities, the latter with conjugate exponents given by $3/2$ and 3 , we obtain

$$\begin{aligned} \|\mathbf{t}\mathbf{u} - \mathbf{t}_h\mathbf{u}_h\|_{0,4/3;\Omega} &\leq \|\mathbf{t}(\mathbf{u} - \mathbf{u}_h)\|_{0,4/3;\Omega} + \|(\mathbf{t} - \mathbf{t}_h)\mathbf{u}_h\|_{0,4/3;\Omega} \\ &\leq \|\mathbf{t}\|_{0,\Omega} \|\mathbf{u} - \mathbf{u}_h\|_{0,4;\Omega} + \|\mathbf{t} - \mathbf{t}_h\|_{0,\Omega} \|\mathbf{u}_h\|_{0,4;\Omega}. \end{aligned} \quad (3.55)$$

Next, using the bounds for $\|\mathbf{t}\|_{0,\Omega}$ and $\|\mathbf{u}_h\|_{0,4;\Omega}$ provided by [17, Th. 3.11, Eq. (3.79)] and (3.30) (cf. [17, Th. 4.11, Eq. (4.24)]), respectively, we deduce from (3.55) the existence of a positive constant C , depending only on data, but independent of h , such that

$$\|\mathbf{t}\mathbf{u} - \mathbf{t}_h\mathbf{u}_h\|_{0,4/3;\Omega} \leq C \left\{ \|\mathbf{u} - \mathbf{u}_h\|_{0,4;\Omega} + \|\mathbf{t} - \mathbf{t}_h\|_{0,\Omega} \right\}$$

which, replaced back into (3.54), yields (3.50). In turn, for the proof of (3.51), we first make use of the fourth row of (2.3) and the triangle inequality to obtain

$$\begin{aligned} & \|2\mu(\varphi_h)\mathbf{t}_{h,\text{sym}} - \frac{1}{2}(\mathbf{u}_h \otimes \mathbf{u}_h)^d - \boldsymbol{\sigma}_h^d\|_{0,\Omega} \\ &= \|2\{\mu(\varphi_h)\mathbf{t}_{h,\text{sym}} - \mu(\varphi)\mathbf{t}_{\text{sym}}\} + \frac{1}{2}\{(\mathbf{u} \otimes \mathbf{u})^d - (\mathbf{u}_h \otimes \mathbf{u}_h)^d\} + \boldsymbol{\sigma}^d - \boldsymbol{\sigma}_h^d\|_{0,\Omega} \quad (3.56) \\ &\leq 2\left\{\|\mu(\varphi_h)\mathbf{t}_{h,\text{sym}} - \mu(\varphi)\mathbf{t}_{\text{sym}}\|_{0,\Omega} + \|(\mathbf{u} \otimes \mathbf{u}) - (\mathbf{u}_h \otimes \mathbf{u}_h)\|_{0,\Omega} + \|\boldsymbol{\sigma} - \boldsymbol{\sigma}_h\|_{0,\Omega}\right\}. \end{aligned}$$

Then, subtracting and adding $\mu(\varphi_h)\mathbf{t}_{\text{sym}}$, using the upper bound of μ (cf. (2.2)), proceeding as for the derivation of (3.27) (see also [17, Eq. (3.68)]), and employing the regularity estimate for $\|\mathbf{t}\|_{\varepsilon,\Omega}$ provided by (3.19), we find that

$$\begin{aligned} \|\mu(\varphi_h)\mathbf{t}_{h,\text{sym}} - \mu(\varphi)\mathbf{t}_{\text{sym}}\|_{0,\Omega} &\leq \|\mu(\varphi_h)(\mathbf{t}_{\text{sym}} - \mathbf{t}_{h,\text{sym}})\|_{0,\Omega} + \|(\mu(\varphi) - \mu(\varphi_h))\mathbf{t}_{\text{sym}}\|_{0,\Omega} \quad (3.57) \\ &\leq C\left\{\|\mathbf{t} - \mathbf{t}_h\|_{0,\Omega} + \|\varphi - \varphi_h\|_{0,4;\Omega}\right\} \end{aligned}$$

where C is a positive constant depending only on data and independent of h . Similarly, subtracting and adding \mathbf{u}_h in one factor of $\mathbf{u} \otimes \mathbf{u}$, and then applying Hölder's inequality, we get

$$\|(\mathbf{u} \otimes \mathbf{u}) - (\mathbf{u}_h \otimes \mathbf{u}_h)\|_{0,\Omega} \leq \|\mathbf{u}\|_{0,4;\Omega} \|\mathbf{u} - \mathbf{u}_h\|_{0,4;\Omega} + \|\mathbf{u}_h\|_{0,4;\Omega} \|\mathbf{u} - \mathbf{u}_h\|_{0,4;\Omega} \quad (3.58)$$

from which, making use of the bounds for $\|\mathbf{u}\|_{0,4;\Omega}$ and $\|\mathbf{u}_h\|_{0,4;\Omega}$ given by [17, Th. 3.11, Eq. (3.79)] and (3.30) (see also [17, Th. 4.11, Eq. (4.24)]), respectively, it follows that

$$\|(\mathbf{u} \otimes \mathbf{u}) - (\mathbf{u}_h \otimes \mathbf{u}_h)\|_{0,\Omega} \leq C \|\mathbf{u} - \mathbf{u}_h\|_{0,4;\Omega} \quad (3.59)$$

with another positive constant C depending only on data and independent of h as well. In this way, replacing the bounds from (3.57) and (3.59) in (3.56), we are lead to (3.51). The proofs of (3.52) and (3.53), being similar to those of (3.50) and (3.51), are omitted. \square

The local efficiency estimates to be stated by the next two lemmas have already been proved in the literature by using localization through bubble functions. We simply refer to their respective proofs.

Lemma 3.13. *There exist positive constants c , \tilde{c} , C , and \tilde{C} , such that*

$$\begin{aligned} h_K^2 \|\mathbf{rot}(\mathbf{t}_h)\|_{0,K}^2 &\leq c \|\mathbf{t} - \mathbf{t}_h\|_{0,K}^2, \quad h_K^2 \|\mathbf{rot}(\tilde{\mathbf{t}}_h)\|_{0,K}^2 \leq \tilde{c} \|\tilde{\mathbf{t}} - \tilde{\mathbf{t}}_h\|_{0,K}^2 \quad \forall K \in \mathcal{T}_h^b \\ h_e \|\llbracket \mathbf{t}_h \mathbf{s} \rrbracket\|_{0,e}^2 &\leq C \|\mathbf{t} - \mathbf{t}_h\|_{0,\omega_e}^2, \quad h_e \|\llbracket \tilde{\mathbf{t}}_h \cdot \mathbf{s} \rrbracket\|_{0,e}^2 \leq \tilde{C} \|\tilde{\mathbf{t}} - \tilde{\mathbf{t}}_h\|_{0,\omega_e}^2 \quad \forall e \in \mathcal{E}_h(\Omega) \end{aligned}$$

where ω_e is the union of the two elements of \mathcal{T}_h^b sharing the edge e .

Proof. See [9, Lemmas 4.3 and 4.4]. \square

Lemma 3.14. *Assume that \mathbf{u}_D and φ_D are piecewise polynomials. Then, there exist positive constants c and \tilde{c} , such that for each $e \in \mathcal{E}_h(\Gamma)$ there hold*

$$h_e \|\mathbf{t}_h \mathbf{s} - \nabla \mathbf{u}_D \mathbf{s}\|_{0,e}^2 \leq c \|\mathbf{t} - \mathbf{t}_h\|_{0,K_e}^2, \quad h_e \|\tilde{\mathbf{t}}_h \cdot \mathbf{s} - \nabla \varphi_D \cdot \mathbf{s}\|_{0,e}^2 \leq \tilde{c} \|\tilde{\mathbf{t}} - \tilde{\mathbf{t}}_h\|_{0,K_e}^2$$

where K_e is the triangle of \mathcal{T}_h^b having e as an edge.

Proof. See [31, Lem. 4.15]. \square

The inequalities supplied by Lemma 3.9 are invoked in the proof of the following lemma.

Lemma 3.15. *There exist positive constants c and \tilde{c} , independent of h , such that*

$$\begin{aligned} h_K^4 \|\mathbf{t}_h - \nabla \mathbf{u}_h\|_{0,4;K}^4 &\leq c \left\{ \|\mathbf{u} - \mathbf{u}_h\|_{0,4;K}^4 + h_K^2 \|\mathbf{t} - \mathbf{t}_h\|_{0,K}^4 \right\} \quad \forall K \in \mathcal{T}_h^b \\ h_K^4 \|\tilde{\mathbf{t}}_h - \nabla \varphi_h\|_{0,4;K}^4 &\leq \tilde{c} \left\{ \|\varphi - \varphi_h\|_{0,4;K}^4 + h_K^2 \|\tilde{\mathbf{t}} - \tilde{\mathbf{t}}_h\|_{0,K}^4 \right\} \quad \forall K \in \mathcal{T}_h^b. \end{aligned}$$

Proof. For the first inequality we proceed as in the proof of [15, Lem. 5.15]. In fact, given $K \in \mathcal{T}_h^b$, we begin by applying the vector version of the left hand side inequality of (3.45), with $p = 4$ and $q = 4/3$, to the local polynomial $\chi_K := \mathbf{t}_h - \nabla \mathbf{u}_h \in \mathbf{P}_k(K)$, which gives

$$c_1 \|\chi_K\|_{0,4;K} \leq \sup_{\substack{\mathbf{v} \in \mathbf{P}_k(K) \\ \mathbf{v} \neq 0}} \frac{\int_K \chi_K \cdot \psi_K \mathbf{v}}{\|\mathbf{v}\|_{0,4/3;K}}. \quad (3.60)$$

Then, using that $\mathbf{t} = \nabla \mathbf{u}$ in Ω , and integrating by parts, we find that

$$\int_K \chi_K \cdot \psi_K \mathbf{v} = \int_K \{ \nabla(\mathbf{u} - \mathbf{u}_h) - (\mathbf{t} - \mathbf{t}_h) \} \cdot \psi_K \mathbf{v} = - \int_K (\mathbf{u} - \mathbf{u}_h) \operatorname{div}(\psi_K \mathbf{v}) - \int_K (\mathbf{t} - \mathbf{t}_h) \cdot \psi_K \mathbf{v}$$

from which, employing the Hölder and Cauchy–Schwarz inequalities, noting that

$$\|\operatorname{div}(\psi_K \mathbf{v})\|_{0,4/3;\Omega} \leq \|\nabla(\psi_K \mathbf{v})\|_{0,4/3;\Omega}$$

and then applying the right-hand side inequality of (3.46), along with the fact that $0 \leq \psi_K \leq 1$, we obtain

$$\int_K \chi_K \cdot \psi_K \mathbf{v} \leq C \left\{ h_K^{-1} \|\mathbf{u} - \mathbf{u}_h\|_{0,4;K} \|\mathbf{v}\|_{0,4/3;K} + \|\mathbf{t} - \mathbf{t}_h\|_{0,K} \|\mathbf{v}\|_{0,K} \right\}. \quad (3.61)$$

In turn, according to the local inverse inequality (3.47) with $n = 2$, $\ell = m = 0$, $r = 2$, and $s = 4/3$, there holds $\|\mathbf{v}\|_{0,K} \leq c h_K^{-1/2} \|\mathbf{v}\|_{0,4/3;K}$, and thus (3.61) becomes

$$\int_K \chi_K \cdot \psi_K \mathbf{v} \leq C \left\{ h_K^{-1} \|\mathbf{u} - \mathbf{u}_h\|_{0,4;K} + h_K^{-1/2} \|\mathbf{t} - \mathbf{t}_h\|_{0,K} \right\} \|\mathbf{v}\|_{0,4/3;K}. \quad (3.62)$$

In this way, replacing (3.62) back into (3.60), and multiplying the resulting inequality by h_K , we get

$$h_K \|\mathbf{t}_h - \nabla \mathbf{u}_h\|_{0,4;K} \leq \|\mathbf{u} - \mathbf{u}_h\|_{0,4;K} + h_K^{1/2} \|\mathbf{t} - \mathbf{t}_h\|_{0,K}$$

so that taking the foregoing inequality to the power 4 the required bound is obtained. The second inequality is derived by an analogous reasoning, and hence we omit further details. \square

The remaining local efficiency estimates are established as follows.

Lemma 3.16. *Assume that \mathbf{u}_D and φ_D are piecewise polynomials. Then, there exist positive constants C and \tilde{C} , independent of h , such that*

$$\begin{aligned} h_e \|\mathbf{u}_D - \mathbf{u}_h\|_{0,4;e}^4 &\leq C \left\{ \|\mathbf{u} - \mathbf{u}_h\|_{0,4;K_e}^4 + h_{K_e}^2 \|\mathbf{t} - \mathbf{t}_h\|_{0,K_e}^4 \right\} \\ h_e \|\varphi_D - \varphi_h\|_{0,4;e}^4 &\leq \tilde{C} \left\{ \|\varphi - \varphi_h\|_{0,4;K_e}^4 + h_{K_e}^2 \|\tilde{\mathbf{t}} - \tilde{\mathbf{t}}_h\|_{0,K_e}^4 \right\} \end{aligned}$$

for all $e \in \mathcal{E}_h(\Gamma)$, and where K_e is the triangle of \mathcal{T}_h^b having e as an edge.

Proof. Being both inequalities proved in an analogous way, we only show the first one. In fact, given $e \in \mathcal{E}_h(\Gamma)$, we first observe that the local inverse inequality (3.47) with $n = 1$, $\ell = m = 0$, $r = 4$, and $s = 2$ yields $\|\mathbf{u}_D - \mathbf{u}_h\|_{0,4;e} \leq c h_e^{-1/4} \|\mathbf{u}_D - \mathbf{u}_h\|_{0,e}$. Hence, taking the above to the power 4, using that $\mathbf{u} = \mathbf{u}_D$ on Γ , applying the vector version of the discrete trace inequality (3.48) (cf. Lemma 3.11) with $p = 2$, recalling that $\mathbf{t} = \nabla \mathbf{u}$, and employing the triangle inequality, we find that

$$\begin{aligned} h_e \|\mathbf{u}_D - \mathbf{u}_h\|_{0,4;e}^4 &\leq C \|\mathbf{u} - \mathbf{u}_h\|_{0,e}^4 \leq C \left\{ h_{K_e}^{-1} \|\mathbf{u} - \mathbf{u}_h\|_{0,K_e}^2 + h_{K_e} \|\mathbf{t} - \nabla \mathbf{u}_h\|_{0,K_e}^2 \right\}^2 \\ &\leq C \left\{ h_{K_e}^{-1} \|\mathbf{u} - \mathbf{u}_h\|_{0,K_e}^2 + h_{K_e} \|\mathbf{t} - \mathbf{t}_h\|_{0,K_e}^2 + h_{K_e} \|\mathbf{t}_h - \nabla \mathbf{u}_h\|_{0,K_e}^2 \right\}^2. \end{aligned} \quad (3.63)$$

Next, and owing to the Cauchy–Schwarz inequality, we have that

$$\|\mathbf{w}\|_{0,K_e}^2 \leq |K_e|^{1/2} \|\mathbf{w}\|_{0,4;K_e}^2 \leq c h_{K_e} \|\mathbf{w}\|_{0,4;K_e}^2 \quad \forall \mathbf{w} \in \mathbf{L}^4(K_e)$$

and it follows from (3.63) that

$$\begin{aligned} h_e \|\mathbf{u}_D - \mathbf{u}_h\|_{0,4;e}^4 &\leq C \left\{ \|\mathbf{u} - \mathbf{u}_h\|_{0,4;K_e}^2 + h_{K_e} \|\mathbf{t} - \mathbf{t}_h\|_{0,K_e}^2 + h_{K_e}^2 \|\mathbf{t}_h - \nabla \mathbf{u}_h\|_{0,4;K_e}^2 \right\}^2 \\ &\leq c \left\{ \|\mathbf{u} - \mathbf{u}_h\|_{0,4;K_e}^4 + h_{K_e}^2 \|\mathbf{t} - \mathbf{t}_h\|_{0,K_e}^4 + h_{K_e}^4 \|\mathbf{t}_h - \nabla \mathbf{u}_h\|_{0,4;K_e}^4 \right\}. \end{aligned}$$

Finally, as a consequence of the first estimate from Lemma 3.15 we can bound the last term in the foregoing inequality, and this step concludes the proof. \square

At this point we stress that if \mathbf{u}_D and φ_D were not piecewise polynomials but sufficiently smooth, then higher order terms given by the errors arising from suitable polynomial approximations of these functions would appear in the efficiency estimates provided by Lemmas 3.14 and 3.16. This fact explains the eventual expression h.o.t. in the global efficiency estimate (3.49).

We end this section by remarking that the proof of (3.49) follows straightforwardly from Lemmas 3.12–3.16, and after summing up the local efficiency estimates over all $K \in \mathcal{T}_h^b$.

4 A posteriori error analysis: the 3D case

In this section we extend the results from Section 3 to the three-dimensional version of (2.14). Similarly as in the previous section, given a tetrahedron $K \in \mathcal{T}_h^b$, we let $\mathcal{E}(K)$ be the set of its faces, and let \mathcal{E}_h be the set of all faces of the triangulation \mathcal{T}_h^b . Then, we write $\mathcal{E}_h = \mathcal{E}_h(\Omega) \cup \mathcal{E}_h(\Gamma)$ with $\mathcal{E}_h(\Omega)$ and $\mathcal{E}_h(\Gamma)$ defined as in Section 3.1. Also, for each face $e \in \mathcal{E}_h$ we fix a unit normal \mathbf{v}_e to e . Now, let $\mathbf{v} \in \mathbf{L}^2(\Omega)$ such that $\mathbf{v}|_K \in \mathbf{C}(K)$ on each $K \in \mathcal{T}_h^b$. Then, given $e \in \mathcal{E}(K) \cap \mathcal{E}_h(\Omega)$, we denote by $[\![\mathbf{v} \times \mathbf{v}_e]\!]$ the tangential jump of \mathbf{v} across e , that is, $[\![\mathbf{v} \times \mathbf{v}_e]\!] := (\mathbf{v}|_K - \mathbf{v}|_{K'})|_e \times \mathbf{v}_e$, where K and K' are the tetrahedron of \mathcal{T}_h^b having e as a common face. In addition, for $\boldsymbol{\tau} \in \mathbb{L}^2(\Omega)$ such that $\boldsymbol{\tau}|_K \in \mathbb{C}(K)$, we let $[\![\boldsymbol{\tau} \times \mathbf{v}_e]\!]$ be the tangential jump of $\boldsymbol{\tau}$ across e , that is, $[\![\boldsymbol{\tau} \times \mathbf{v}_e]\!] := (\boldsymbol{\tau}|_K - \boldsymbol{\tau}|_{K'})|_e \times \mathbf{v}_e$. In what follows, when no confusion arises, we simply write \mathbf{v} instead of \mathbf{v}_e . On the other hand, we recall that the curl of a 3D vector $\mathbf{v} := (v_1, v_2, v_3)$ is the 3D vector

$$\mathbf{curl}(\mathbf{v}) = \nabla \times \mathbf{v} := \left(\frac{\partial v_3}{\partial x_2} - \frac{\partial v_2}{\partial x_3}, \frac{\partial v_1}{\partial x_3} - \frac{\partial v_3}{\partial x_1}, \frac{\partial v_2}{\partial x_1} - \frac{\partial v_1}{\partial x_2} \right)$$

and that, given a tensor function $\boldsymbol{\tau} := (\tau_{ij})_{3 \times 3}$, the operator $\underline{\mathbf{curl}}(\boldsymbol{\tau})$ is the 3×3 tensor whose rows are given by

$$\underline{\mathbf{curl}}(\boldsymbol{\tau}) := \begin{pmatrix} \mathbf{curl}(\tau_{11}, \tau_{12}, \tau_{13}) \\ \mathbf{curl}(\tau_{21}, \tau_{22}, \tau_{23}) \\ \mathbf{curl}(\tau_{31}, \tau_{32}, \tau_{33}) \end{pmatrix}.$$

In addition, $\boldsymbol{\tau} \times \mathbf{v}$ stands for the 3×3 tensor whose rows are given by the tangential components of each row of $\boldsymbol{\tau}$, that is,

$$\boldsymbol{\tau} \times \mathbf{v}_e := \begin{pmatrix} (\tau_{11}, \tau_{12}, \tau_{13}) \times \mathbf{v}_e \\ (\tau_{21}, \tau_{22}, \tau_{23}) \times \mathbf{v}_e \\ (\tau_{31}, \tau_{32}, \tau_{33}) \times \mathbf{v}_e \end{pmatrix}.$$

In turn, the tangential curl operator \mathbf{curl}_s and a tensor version of it, denoted $\underline{\mathbf{curl}}_s$, which is defined component-wise by \mathbf{curl}_s , will also be used.

Thus, for each $K \in \mathcal{T}_h^b$ we define

$$\begin{aligned} \bar{\Theta}_K^2 &:= \|2\mu(\varphi_h)\mathbf{t}_{h,\text{sym}} - \frac{1}{2}(\mathbf{u}_h \otimes \mathbf{u}_h)^d - \boldsymbol{\sigma}_h^d\|_{0,K}^2 + \|\mathbf{K}\tilde{\mathbf{t}}_h - \frac{1}{2}\varphi_h\mathbf{u}_h - \tilde{\boldsymbol{\sigma}}_h\|_{0,K}^2 \\ &\quad + h_K^2 \|\underline{\mathbf{curl}}(\mathbf{t}_h)\|_{0,K}^2 + h_K^2 \|\mathbf{curl}(\tilde{\mathbf{t}}_h)\|_{0,K}^2 + \sum_{e \in \mathcal{E}_h(\Omega)} h_e \left\{ \|\mathbf{t}_h \times \mathbf{v}\|_{0,e}^2 + \|[\![\tilde{\mathbf{t}}_h \times \mathbf{v}]\!]\|_{0,e}^2 \right\} \\ &\quad + \sum_{e \in \mathcal{E}_h(K) \cap \mathcal{E}_h(\Gamma)} h_e \left\{ \|\mathbf{t}_h \times \mathbf{v} - \underline{\mathbf{curl}}_s(\mathbf{u}_D)\|_{0,e}^2 + \|[\![\tilde{\mathbf{t}}_h \times \mathbf{v} - \mathbf{curl}_s(\varphi_D)]\!]\|_{0,e}^2 \right\}. \end{aligned} \tag{4.1}$$

Hence, bearing in mind the definitions of $\tilde{\Theta}_K^{4/3}$ (cf. (3.8)) and $\tilde{\Theta}_K^4$ (cf. (3.10)), which are also valid in the present 3D case, the associated global a posteriori error estimator is defined as

$$\Theta = \left\{ \sum_{K \in \mathcal{T}_h^b} \tilde{\Theta}_K^{4/3} \right\}^{3/4} + \left\{ \sum_{K \in \mathcal{T}_h^b} \tilde{\Theta}_K^2 \right\}^{1/2} + \left\{ \sum_{K \in \mathcal{T}_h^b} \tilde{\Theta}_K^4 \right\}^{1/4}. \quad (4.2)$$

In this way, the corresponding reliability and efficiency estimates, which constitute the analogue of Theorems 3.1 and 3.2, are stated as follows.

Theorem 4.1. *Assume that the data are sufficiently small (similarly as indicated in Lemma 3.6), and suppose that \mathbf{u}_D and φ_D are piecewise polynomials. Then, there exist positive constants C_{rel} and C_{eff} , independent of h , such that*

$$C_{\text{eff}} \Theta + \text{h.o.t.} \leq \| \vec{\sigma} - \vec{\sigma}_h \|_{\mathbb{X}} \leq C_{\text{rel}} \Theta.$$

The proof of Theorem 4.1 follows very closely the analysis of Section 3, except a few issues to be described throughout the following discussion. Indeed, we first observe that the general a posteriori error estimate given by Lemma 3.6 is also valid in 3D. Then, we follow [29, Th. 3.2] to derive a 3D version for arbitrary polyhedral domains of the Helmholtz decomposition provided by Lemma 3.2. Next, the associated discrete Helmholtz decomposition and the functionals \mathcal{R} and $\tilde{\mathcal{R}}$ are set and rewritten exactly as in (3.35), (3.36), and (3.37), respectively. Furthermore, in order to derive the new upper bounds of $\| \mathcal{R} \|$ and $\| \tilde{\mathcal{R}} \|$, we now need the 3D analogue of the integration by parts formula on the boundary given by (3.42). In fact, by applying the identities from [34, Ch. I, Eq. (2.17), and Th. 2.11], we deduce that in this case there holds

$$\langle \mathbf{curl} \boldsymbol{\xi} \cdot \mathbf{v}, \vartheta \rangle_{\Gamma} = -\langle \mathbf{curl}_s \vartheta, \boldsymbol{\xi} \rangle_{\Gamma} \quad \forall \boldsymbol{\xi} \in \mathbf{H}^1(\Omega), \quad \forall \vartheta \in \mathbf{H}^{1/2}(\Gamma).$$

In addition, the integration by parts formula on each tetrahedron $K \in \mathcal{T}_h^b$, which is used in the proof of the 3D analogue of Lemma 3.7, becomes (cf. [34, Ch. I, Th. 2.11])

$$\int_K \mathbf{curl} \mathbf{q} \cdot \boldsymbol{\xi} - \int_K \mathbf{q} \cdot \mathbf{curl} \boldsymbol{\xi} = \langle \mathbf{q} \times \mathbf{v}, \boldsymbol{\xi} \rangle_{\partial K} \quad \forall \mathbf{q} \in \mathbf{H}(\mathbf{curl}; \Omega), \quad \forall \boldsymbol{\xi} \in \mathbf{H}^1(\Omega)$$

where $\langle \cdot, \cdot \rangle_{\partial K}$ is the duality pairing between $\mathbf{H}^{-1/2}(\partial K)$ and $\mathbf{H}^{1/2}(\partial K)$, and, as usual, $\mathbf{H}(\mathbf{curl}, \Omega)$ is the space of vectors in $\mathbf{L}^2(\Omega)$ whose \mathbf{curl} lies also in $\mathbf{L}^2(\Omega)$. Note that, unlike the 2D case, it is not necessary for the reliability to assume that $\mathbf{u}_D \in \mathbf{H}^{1+\delta}(\Gamma)$ and $\varphi_D \in \mathbf{H}^{1+\delta}(\Gamma)$, for some $\delta > 0$, since the \mathbf{curl}_s is defined into $\mathbf{H}^{1/2}(\Gamma)$.

Finally, in order to prove the efficiency of Θ (cf. (4.2)), we first observe that the terms defining $\tilde{\Theta}_K^{4/3}$ (cf. (3.8)) and the first two defining $\tilde{\Theta}_K^2$ (cf. (4.1)) are estimated exactly as done for the 2D case in Lemma 3.12. For the remaining terms, we refer to [30, Lem. 4.2].

5 Extension to the Oberbeck–Boussinesq problem

The same tools and techniques employed in the previous sections can be applied for the a posteriori error analysis of the fully mixed scheme from [18] for the Oberbeck–Boussinesq model. The resulting a posteriori error estimators for the 2D and 3D cases are summarized in Sections 5.3 and 5.4.

5.1 The Oberbeck–Boussinesq problem

The stationary Oberbeck–Boussinesq problem consists of the incompressible Navier–Stokes–Brinkman equations coupled with the heat and mass transfer equations through a convective term and a buoyancy term acting in opposite direction to gravity. More precisely, given an external force per unit mass $\mathbf{g} \in \mathbf{L}^\infty(\Omega)$, and Dirichlet data $\mathbf{u}_D \in \mathbf{H}^{1/2}(\Gamma)$, and $\varphi_{1,D}, \varphi_{2,D} \in \mathbf{H}^{1/2}(\Gamma)$, the model reduces to: Find a velocity field \mathbf{u} , a pressure field p , a temperature field φ_1 , and a concentration field φ_2 , both defining a vector $\boldsymbol{\varphi} := (\varphi_1, \varphi_2)$, such

that

$$\begin{aligned} \gamma \mathbf{u} - \operatorname{div}(2\mu(\boldsymbol{\varphi})\mathbf{e}(\mathbf{u})) + (\nabla \mathbf{u})\mathbf{u} + \nabla p &= (\boldsymbol{\theta} \cdot \boldsymbol{\varphi})\mathbf{g} \quad \text{in } \Omega, \quad \operatorname{div}(\mathbf{u}) = 0 \quad \text{in } \Omega \\ -\operatorname{div}(\mathbb{K}_1 \nabla \varphi_1) + \mathbf{u} \cdot \nabla \varphi_1 &= 0 \quad \text{in } \Omega, \quad -\operatorname{div}(\mathbb{K}_2 \nabla \varphi_2) + \mathbf{u} \cdot \nabla \varphi_2 = 0 \quad \text{in } \Omega \\ \mathbf{u} = \mathbf{u}_D &\quad \text{on } \Gamma, \quad \varphi_1 = \varphi_{1,D} \quad \text{on } \Gamma, \quad \varphi_2 = \varphi_{2,D} \quad \text{on } \Gamma \end{aligned} \quad (5.1)$$

where γ is a positive constant inversely proportional to the reciprocal of the Darcy number Da , $\mu : \mathbb{R} \times \mathbb{R}^+ \rightarrow \mathbb{R}^+$ is the viscosity of the fluid, $\mathbf{e}(\mathbf{u})$ is the symmetric part of the velocity gradient $\nabla \mathbf{u}$, also known as the rate of strain tensor, $\boldsymbol{\theta} := (\theta_1, \theta_2)$ is a vector containing expansion coefficients, and $\mathbb{K}_j \in \mathbb{L}^\infty(\Omega)$, with $j \in \{1, 2\}$, are uniformly positive definite tensors describing the thermal conductivity of the fluid. In addition, μ is assumed bounded and Lipschitz continuous, which means that there exist constants $\mu_1, \mu_2, L_\mu > 0$, such that

$$\mu_1 \leq \mu(\boldsymbol{\varphi}) \leq \mu_2, \quad |\mu(\boldsymbol{\varphi}) - \mu(\boldsymbol{\psi})| \leq L_\mu |\boldsymbol{\varphi} - \boldsymbol{\psi}| \quad \forall \boldsymbol{\varphi}, \boldsymbol{\psi} \in \mathbb{R} \times \mathbb{R}^+$$

where $|\cdot|$ denotes from on the euclidean norm of \mathbb{R}^n , $n \in \{1, 2, 3\}$. The incompressibility of the fluid (cf. second eq. of (5.1)) and the Dirichlet boundary condition (cf. fifth eq. of (5.1)), imply that \mathbf{u}_D must satisfy the compatibility condition $\int_\Gamma \mathbf{u}_D \cdot \mathbf{v} = 0$. Then, using some of the auxiliary unknowns defined in Section 2.2, introducing the new ones that are set implicitly next, denoting $\boldsymbol{\varphi}_D := (\varphi_{1,D}, \varphi_{2,D})$, and eliminating the pressure p as before, the Oberbeck–Boussinesq problem (5.1) can be re-stated as follows: Find $(\mathbf{u}, \mathbf{t}, \boldsymbol{\sigma})$ and $(\varphi_j, \tilde{\mathbf{t}}_j, \tilde{\boldsymbol{\sigma}}_j)$, $j \in \{1, 2\}$, in suitable spaces to be indicated below such that

$$\begin{aligned} \nabla \mathbf{u} &= \mathbf{t} && \text{in } \Omega \\ \gamma \mathbf{u} - \operatorname{div} \boldsymbol{\sigma} + \frac{1}{2} \mathbf{t} \mathbf{u} - (\boldsymbol{\theta} \cdot \boldsymbol{\varphi})\mathbf{g} &= \mathbf{0} && \text{in } \Omega \\ 2\mu(\boldsymbol{\varphi})\mathbf{t}_{\text{sym}} - \frac{1}{2}(\mathbf{u} \otimes \mathbf{u})^d &= \boldsymbol{\sigma}^d && \text{in } \Omega \\ \nabla \varphi_j &= \tilde{\mathbf{t}}_j && \text{in } \Omega \\ \mathbb{K}_j \tilde{\mathbf{t}}_j - \frac{1}{2} \varphi_j \mathbf{u} &= \tilde{\boldsymbol{\sigma}}_j && \text{in } \Omega \\ -\operatorname{div} \tilde{\boldsymbol{\sigma}}_j + \frac{1}{2} \tilde{\mathbf{t}}_j \cdot \mathbf{u} &= 0 && \text{in } \Omega \\ \int_\Omega \operatorname{tr}(2\boldsymbol{\sigma} + \mathbf{u} \otimes \mathbf{u}) &= 0, \quad \mathbf{u} = \mathbf{u}_D \quad \boldsymbol{\varphi} = \boldsymbol{\varphi}_D && \text{on } \Gamma. \end{aligned} \quad (5.2)$$

5.2 The continuous and discrete formulations

Bearing in mind the definitions and notations from Section 2.2, and according to [18, Sect. 3.1], the fully-mixed variational formulation for (5.2) reads: Find $(\vec{\mathbf{u}}, \boldsymbol{\sigma}) \in \mathbf{H} \times \mathbb{H}_0(\operatorname{div}_{4/3}; \Omega)$ and $(\vec{\varphi}_j, \tilde{\boldsymbol{\sigma}}_j) \in \widetilde{\mathbf{H}} \times \mathbf{H}(\operatorname{div}_{4/3}; \Omega)$, $j \in \{1, 2\}$ such that

$$\begin{aligned} \hat{a}_{\boldsymbol{\varphi}}(\vec{\mathbf{u}}, \vec{\mathbf{v}}) + c(\mathbf{u}; \vec{\mathbf{u}}, \vec{\mathbf{v}}) + b(\vec{\mathbf{v}}, \boldsymbol{\sigma}) &= \hat{F}_{\boldsymbol{\varphi}}(\vec{\mathbf{v}}) \quad \forall \vec{\mathbf{v}} \in \mathbf{H} \\ b(\vec{\mathbf{u}}, \boldsymbol{\tau}) &= G(\boldsymbol{\tau}) \quad \forall \boldsymbol{\tau} \in \mathbb{H}_0(\operatorname{div}_{4/3}; \Omega) \\ \tilde{a}_j(\vec{\varphi}_j, \vec{\psi}_j) + \tilde{c}_{\mathbf{u}}(\vec{\varphi}_j, \vec{\psi}_j) + \tilde{b}(\vec{\psi}_j, \tilde{\boldsymbol{\sigma}}_j) &= 0 \quad \forall \vec{\psi}_j \in \widetilde{\mathbf{H}} \\ \tilde{b}(\vec{\varphi}_j, \tilde{\boldsymbol{\tau}}_j) &= \tilde{G}(\tilde{\boldsymbol{\tau}}_j) \quad \forall \tilde{\boldsymbol{\tau}}_j \in \mathbf{H}(\operatorname{div}_{4/3}; \Omega) \end{aligned} \quad (5.3)$$

where, given $\boldsymbol{\varphi} \in \mathbf{L}^4(\Omega)$, the forms $\hat{a}_{\boldsymbol{\varphi}}$ and \tilde{a}_j , and the functional $\hat{F}_{\boldsymbol{\varphi}}$, are defined by

$$\hat{a}_{\boldsymbol{\varphi}}(\vec{\mathbf{u}}, \vec{\mathbf{v}}) := (\gamma \mathbf{u}, \mathbf{v})_\Omega + (2\mu(\boldsymbol{\varphi})\mathbf{t}_{\text{sym}}, \mathbf{s})_\Omega, \quad \tilde{a}_j(\vec{\varphi}_j, \vec{\psi}_j) := (\mathbb{K}_j \tilde{\mathbf{t}}_j, \tilde{\mathbf{s}})_\Omega, \quad \hat{F}_{\boldsymbol{\varphi}}(\vec{\mathbf{v}}) := ((\boldsymbol{\theta} \cdot \boldsymbol{\varphi})\mathbf{g}, \mathbf{v})_\Omega$$

for all $\vec{\mathbf{u}} := (\mathbf{u}, \mathbf{t}), \vec{\mathbf{v}} := (\mathbf{v}, \mathbf{s}) \in \mathbf{H}$, for all $\boldsymbol{\tau} \in \mathbb{H}_0(\operatorname{div}_{4/3}; \Omega)$, for all $\vec{\varphi}_j := (\varphi_j, \tilde{\mathbf{t}}_j), \vec{\psi}_j := (\psi_j, \tilde{\mathbf{s}}_j) \in \widetilde{\mathbf{H}}$, and for all $\tilde{\boldsymbol{\tau}}_j \in \mathbf{H}(\operatorname{div}_{4/3}; \Omega)$. In turn, as stated at the beginning of this section, the forms b , c , \tilde{b} , and $\tilde{c}_{\mathbf{w}}$, the latter for a given $\mathbf{w} \in \mathbf{L}^4(\Omega)$, and the functionals G and \tilde{G} , are defined in Section 2.2.

In turn, using the same finite element subspaces from Section 2.3, the Galerkin scheme associated with (5.3) reads: Find $(\vec{\mathbf{u}}_h, \boldsymbol{\sigma}_h) \in \mathbf{H}_h \times \mathbb{H}_h^\sigma$ and $(\vec{\varphi}_{j,h}, \tilde{\boldsymbol{\sigma}}_{j,h}) \in \widetilde{\mathbf{H}}_h \times \mathbf{H}_h^{\tilde{\sigma}}, j \in \{1, 2\}$ such that

$$\begin{aligned} \tilde{a}(\boldsymbol{\varphi}_h(\vec{\mathbf{u}}_h, \vec{\mathbf{v}}_h) + c(\mathbf{u}_h; \vec{\mathbf{u}}_h, \vec{\mathbf{v}}_h) + b(\vec{\mathbf{v}}_h, \boldsymbol{\sigma}_h) = \hat{F}(\boldsymbol{\varphi}_h(\vec{\mathbf{v}}_h) &\quad \forall \vec{\mathbf{v}}_h \in \mathbf{H}_h \\ b(\vec{\mathbf{u}}_h, \boldsymbol{\tau}_h) = G(\boldsymbol{\tau}_h) &\quad \forall \boldsymbol{\tau}_h \in \mathbb{H}_h^\sigma \\ \tilde{a}_j(\vec{\varphi}_{j,h}, \vec{\psi}_{j,h}) + \tilde{c}_{\mathbf{u}_h}(\vec{\varphi}_{j,h}, \vec{\psi}_{j,h}) + \tilde{b}(\vec{\psi}_{j,h}, \tilde{\boldsymbol{\sigma}}_{j,h}) = 0 &\quad \forall \vec{\psi}_h \in \widetilde{\mathbf{H}}_h \\ \tilde{b}(\vec{\varphi}_{j,h}, \tilde{\boldsymbol{\tau}}_{j,h}) = \tilde{G}(\tilde{\boldsymbol{\tau}}_{j,h}) &\quad \forall \tilde{\boldsymbol{\tau}}_h \in \mathbf{H}_h^{\tilde{\sigma}}. \end{aligned} \quad (5.4)$$

For the well-posedness of (5.3) and (5.4) we refer to [18, Th. 3.9] and [18, Th. 4.7], respectively, whereas the a priori error estimates and corresponding rates of convergence are established in [18, Th. 5.1 and 5.2].

5.3 The a posteriori error estimator in 2D

Recall that

$$\tilde{\boldsymbol{\sigma}} = ((\vec{\mathbf{u}}, \boldsymbol{\sigma}), (\vec{\varphi}_1, \tilde{\boldsymbol{\sigma}}_1), (\vec{\varphi}_2, \tilde{\boldsymbol{\sigma}}_2)) \in \widehat{\mathbb{X}} := \mathbf{H} \times \mathbb{H}_0(\mathbf{div}_{4/3}; \Omega) \times \widetilde{\mathbf{H}} \times \mathbf{H}(\mathbf{div}_{4/3}; \Omega) \times \widetilde{\mathbf{H}} \times \mathbf{H}(\mathbf{div}_{4/3}; \Omega)$$

is the unique solution of problem (5.3), and that

$$\tilde{\boldsymbol{\sigma}}_h = ((\vec{\mathbf{u}}_h, \boldsymbol{\sigma}_h), (\vec{\varphi}_{1,h}, \tilde{\boldsymbol{\sigma}}_{1,h}), (\vec{\varphi}_{2,h}, \tilde{\boldsymbol{\sigma}}_{2,h})) \in \widehat{\mathbb{X}}_h := \mathbf{H}_h \times \mathbb{H}_h^\sigma \times \widetilde{\mathbf{H}}_h \times \mathbf{H}_h^{\tilde{\sigma}} \times \widetilde{\mathbf{H}}_h \times \mathbf{H}_h^{\tilde{\sigma}}$$

is a solution of (5.4). Then, assuming as in Section 3.2, that $\mathbf{u}_D \in \mathbf{H}^{1+\delta}(\Gamma) \cap \mathbf{L}^4(\Gamma)$ and $\varphi_{j,D} \in \mathbf{H}^{1+\delta}(\Gamma) \cap \mathbf{L}^4(\Gamma)$, for some $\delta > 0$, and for $j \in \{1, 2\}$, we define for $K \in \mathcal{T}_h^b$ the local error indicators

$$\begin{aligned} \tilde{\Psi}_K^{4/3} &:= \| \gamma \mathbf{u}_h - \mathbf{div}(\boldsymbol{\sigma}_h) + \frac{1}{2} \mathbf{t}_h \mathbf{u}_h - (\boldsymbol{\vartheta} \cdot \boldsymbol{\varphi}_h) \mathbf{g} \|_{0,4/3;K}^{4/3} + \sum_{j=1}^2 \| -\mathbf{div}(\tilde{\boldsymbol{\sigma}}_{j,h}) + \frac{1}{2} \mathbf{u}_h \cdot \tilde{\mathbf{t}}_{j,h} \|_{0,4/3;K}^{4/3} \quad (5.5) \\ \bar{\Psi}_K^2 &:= \| 2\mu(\boldsymbol{\varphi}_h) \mathbf{t}_h, \text{sym} - \frac{1}{2} (\mathbf{u}_h \otimes \mathbf{u}_h)^d - \boldsymbol{\sigma}_h^d \|_{0,K}^2 + \sum_{j=1}^2 \| \mathbb{K}_j \tilde{\mathbf{t}}_{j,h} - \frac{1}{2} \varphi_{j,h} \mathbf{u}_h - \tilde{\boldsymbol{\sigma}}_{j,h} \|_{0,K}^2 \\ &\quad + h_K^2 \| \mathbf{rot}(\mathbf{t}_h) \|_{0,K}^2 + \sum_{j=1}^2 h_K^2 \| \mathbf{rot}(\tilde{\mathbf{t}}_{j,h}) \|_{0,K}^2 + \sum_{e \in \mathcal{E}_h(K) \cap \mathcal{E}_h(\Omega)} h_e \| [\mathbf{t}_h \mathbf{s}] \|_{0,e}^2 \\ &\quad + \sum_{j=1}^2 \left\{ \sum_{e \in \mathcal{E}_h(K) \cap \mathcal{E}_h(\Omega)} h_e \| [\tilde{\mathbf{t}}_{j,h} \cdot \mathbf{s}] \|_{0,e}^2 + \sum_{e \in \mathcal{E}_h(K) \cap \mathcal{E}_h(\Gamma)} h_e \| \tilde{\mathbf{t}}_{j,h} \cdot \mathbf{s} - \nabla \varphi_{j,D} \cdot \mathbf{s} \|_{0,e}^2 \right\} \\ &\quad + \sum_{e \in \mathcal{E}_h(K) \cap \mathcal{E}_h(\Gamma)} h_e \| \mathbf{t}_h \mathbf{s} - \nabla \mathbf{u}_D \mathbf{s} \|_{0,e}^2 \quad (5.6) \end{aligned}$$

$$\begin{aligned} \widehat{\Psi}_K^4 &:= h_K^4 \| \mathbf{t}_h - \nabla \mathbf{u}_h \|_{0,4;K}^4 + \sum_{j=1}^2 h_K^4 \| \tilde{\mathbf{t}}_{j,h} - \nabla \varphi_{j,h} \|_{0,4;K}^4 \\ &\quad + \sum_{e \in \mathcal{E}_h(K) \cap \mathcal{E}_h(\Gamma)} h_e \| \mathbf{u}_D - \mathbf{u}_h \|_{0,4;e}^4 + \sum_{j=1}^2 \left\{ \sum_{e \in \mathcal{E}_h(K) \cap \mathcal{E}_h(\Gamma)} h_e \| \varphi_{j,D} - \varphi_{j,h} \|_{0,4;e}^4 \right\} \quad (5.7) \end{aligned}$$

so that the global a posteriori error estimator is given by

$$\Psi = \left\{ \sum_{K \in \mathcal{T}_h^b} \tilde{\Psi}_K^{4/3} \right\}^{3/4} + \left\{ \sum_{K \in \mathcal{T}_h^b} \bar{\Psi}_K^2 \right\}^{1/2} + \left\{ \sum_{K \in \mathcal{T}_h^b} \widehat{\Psi}_K^4 \right\}^{1/4}. \quad (5.8)$$

Then, the reliability and efficiency of Ψ , whose proofs follow very closely the analysis of Section 3, are established as follows.

Theorem 5.1. *Assume that the data are sufficiently small (similarly as indicated in Lemma 3.6), and suppose for simplicity that \mathbf{u}_D and $\varphi_{j,D}, j \in \{1, 2\}$, are piecewise polynomials. Then, there exist positive constants C_{rel} and C_{eff} , independent of h , such that*

$$C_{\text{eff}} \Psi + \text{h.o.t.} \leq \| \tilde{\boldsymbol{\sigma}} - \tilde{\boldsymbol{\sigma}}_h \|_{\mathbb{X}} \leq C_{\text{rel}} \Psi$$

where h.o.t. stands for one or several terms of higher order.

5.4 The a posteriori error estimator in 3D

In this case for each $K \in \mathcal{T}_h^b$ we define

$$\begin{aligned} \bar{\Psi}_K^2 := & \|2\mu(\boldsymbol{\varphi}_h)\mathbf{t}_{h,\text{sym}} - \frac{1}{2}(\mathbf{u}_h \otimes \mathbf{u}_h)^d - \boldsymbol{\sigma}_h^d\|_{0,K}^2 + \sum_{j=1}^2 \|\mathbb{K}_j \tilde{\mathbf{t}}_{j,h} - \frac{1}{2}\varphi_{j,h} \mathbf{u}_h - \tilde{\boldsymbol{\sigma}}_{j,h}\|_{0,K}^2 \\ & + h_K^2 \|\underline{\text{curl}}(\mathbf{t}_h)\|_{0,K}^2 + \sum_{j=1}^2 h_K^2 \|\underline{\text{curl}}(\tilde{\mathbf{t}}_{j,h})\|_{0,K}^2 + \sum_{e \in \mathcal{E}_h(K) \cap \mathcal{E}_h(\Omega)} h_e \|\llbracket \mathbf{t}_h \times \mathbf{v} \rrbracket\|_{0,e}^2 \\ & + \sum_{j=1}^2 \left\{ \sum_{e \in \mathcal{E}_h(K) \cap \mathcal{E}_h(\Omega)} h_e \|\llbracket \tilde{\mathbf{t}}_{j,h} \times \mathbf{v} \rrbracket\|_{0,e}^2 + \sum_{e \in \mathcal{E}_h(K) \cap \mathcal{E}_h(\Gamma)} h_e \|\tilde{\mathbf{t}}_{j,h} \times \mathbf{v} - \underline{\text{curl}}_s(\varphi_{j,D})\|_{0,e}^2 \right\} \\ & + \sum_{e \in \mathcal{E}_h(K) \cap \mathcal{E}_h(\Gamma)} h_e \|\mathbf{t}_h \times \mathbf{v} - \underline{\text{curl}}_s(\mathbf{u}_D)\|_{0,e}^2 \end{aligned}$$

so that, letting $\bar{\Psi}_K^{4/3}$ and $\bar{\Psi}_K^4$ as defined by (5.5) and (5.7), the global a posteriori error estimator is given by (5.8), while the reliability and efficiency results are stated analogously to Theorem 5.1.

6 Numerical results

This section presents three computational tests that illustrate the properties of the proposed family of methods. For each problem we provide a test with known closed-form solution that we use to quantify the robustness of the a posteriori error estimators (tests 1 and 3), while we consider in test 2 an application-driven problem without closed-form solutions. All computations use Alfeld splits (barycentric refined meshes) \mathcal{T}_h^b created from regular partitions \mathcal{T}_h of Ω , using the open-source mesh manipulator GMSH [33]. For the implementation of the numerical schemes we have used the open-source finite element library FEniCS [2]. A Newton–Raphson algorithm with null initial guess is used for the resolution of all nonlinear problems, whereas the solution of tangent systems resulting from the linearization is carried out with the multifrontal massively parallel sparse direct solver MUMPS. The condition of zero-average pressure (thanks to (2.4), translated in terms of the trace of the tensor quantity $2\boldsymbol{\sigma} + \mathbf{u} \otimes \mathbf{u}$) is imposed by means of a real Lagrange multiplier.

Errors between exact and approximate solutions are denoted as

$$\begin{aligned} e(\mathbf{u}) &:= \|\mathbf{u} - \mathbf{u}_h\|_{0,4;\Omega}, \quad e(\mathbf{t}) := \|\mathbf{t} - \mathbf{t}_h\|_{0,\Omega}, \quad e(\boldsymbol{\sigma}) := \|\boldsymbol{\sigma} - \boldsymbol{\sigma}_h\|_{\text{div}_{4/3};\Omega}, \quad e(p) := \|p - p_h\|_{0,\Omega} \\ e(\varphi) &:= \sum_{j=1}^2 \|\varphi_j - \varphi_{j,h}\|_{0,4;\Omega}, \quad e(\tilde{\mathbf{t}}) := \sum_{j=1}^2 \|\tilde{\mathbf{t}}_j - \tilde{\mathbf{t}}_{j,h}\|_{0,4;\Omega}, \quad e(\tilde{\boldsymbol{\sigma}}) := \sum_{j=1}^2 \|\tilde{\boldsymbol{\sigma}}_j - \tilde{\boldsymbol{\sigma}}_{j,h}\|_{\text{div}_{4/3};\Omega} \end{aligned}$$

while we let $r(\star)$ denote their corresponding rates of convergence, specified for the case of adaptive computations as

$$r(\star) := -2 \frac{\log(e(\star)/e'(\star))}{\log(\text{DoF}/\text{DoF}')} \quad \forall \star \in \{\mathbf{u}, \mathbf{t}, \boldsymbol{\sigma}, p, \varphi, \tilde{\mathbf{t}}, \tilde{\boldsymbol{\sigma}}\} \quad (6.1)$$

where DoF and DoF' denote the numbers of degrees of freedom associated with two consecutive meshes producing errors $e(\star)$ and $e'(\star)$, respectively. The local contributions of the residual-based a posteriori error estimators (3.11), (4.2), and (5.8), which come from the constitutive equations, the conservation equations, and the inter-element residuals, are used to steer the adaptive mesh-refining. We follow Algorithm 1, which, though explained below for (2.14) and Θ (cf. (3.11)), applies in the same way for (5.4) and Ψ (cf. (5.8)). It is designed based on the classical loop of

solving → estimating → marking → refining → solving → …

as specified in, e.g., [22, 39]. As in [18] we need to deal with the adaptive procedure associated with the initial triangular/tetrahedral mesh at each refinement step, and perform an additional step to treat its Alfeld split and to project the estimator on a macro (parent) mesh. The key user-defined parameter is N in step 12 of Algorithm 1.

Algorithm 1 – Adaptive refinement algorithm

```

1: for a given computation start with a coarse mesh  $\mathcal{T}_h$  made of triangles (or tetrahedra)  $\Delta$  and do
2:   generate the associated barycentric refinement  $\mathcal{T}_h^b$  made of triangles (or tetrahedra)  $K$ ;
3:   for the current mesh  $\mathcal{T}_h^b$  do
4:     solve the discrete problem (2.14) on the new barycentric mesh  $\mathcal{T}_h^b$ ;
5:   end for
6:   for each  $K \in \mathcal{T}_h^b$  do
7:     compute  $\tilde{\Theta}_K$ ,  $\bar{\Theta}_K$ , and  $\widehat{\Theta}_K$ , and then compute the local a posteriori error indicator  $\Theta_K := \tilde{\Theta}_K + \bar{\Theta}_K + \widehat{\Theta}_K$ ;
8:   end for
9:   for each  $\Delta \in \mathcal{T}_h$  do
10:    project the local a posteriori error indicator to the parent mesh  $\Theta_\Delta := \sum_{K \in \mathcal{T}_h^b, K \subseteq \Delta} \Theta_K$ ;
11:   end for
12:   if for an element in the parent mesh  $L \in \mathcal{T}_h$  (even for a boundary element) we have  $\Theta_L \geq N \max_{K \in \mathcal{T}_h^b} \Theta_K$  then
13:     mark  $L$  for refinement and mark further elements to guarantee that the triangulation remains
        regular;
14:   end if
15:   if sufficiently many elements in the parent mesh  $\mathcal{T}_h$  are marked so that they represent a given fraction
        of the total estimated error then
16:     stop
17:   else
18:     continue to the next step;
19:   end if
20:   generate an adapted parent mesh from  $\mathcal{T}_h$  through a variable metric/Delaunay automatic meshing
        algorithm using the local indicators  $\Theta_\Delta$ , targeting the equidistribution of the local error indicators in
        the updated parent mesh;
21:   define the resulting mesh as  $\mathcal{T}_h$  and go to step (2).
22: end for

```

6.1 Example 1: accuracy for the Boussinesq problem using uniform and adaptive mesh refinement

First we verify numerically the convergence of the mixed method applied to the Boussinesq equations by manufacturing exact solutions of (2.7) over the L-shaped domain $\Omega = (-1, 1)^2 \setminus (0, 1)^2$:

$$\mathbf{u} = \begin{pmatrix} \cos(\frac{\pi}{2}x_1) \sin(\frac{\pi}{2}x_2) \\ -\sin(\frac{\pi}{2}x_1) \cos(\frac{\pi}{2}x_2) \end{pmatrix}, \quad p = \frac{1 + \sin(x_1 x_2) \cos(x_1 + x_2)}{(x_1 - 0.01)^2 + (x_2 - 0.01)^2}$$

$$\varphi = \sin(x_1 x_2) + \cos(x_1 x_2) + e^{-100[(x_1 - 0.01)^2 + (x_2 - 0.01)^2]}$$

from which we can determine the exact strain rate, pseudostress, pseudo-heat, and heat flux. The values of the exact velocity and temperature are used for Dirichlet data \mathbf{u}_D and φ_D , and they are also used to generate matching right-hand side forcing term and heat source. We consider synthetic viscosity and conduction functions, as well as constant gravity acceleration as follows:

$$\mu(\varphi) = e^{-\varphi}, \quad \mathbb{K} = \begin{pmatrix} e^{-x_1} & \frac{1}{10}x_1 \\ \frac{1}{10}x_2 & e^{-x_2} \end{pmatrix}, \quad \mathbf{g} = \begin{pmatrix} 0 \\ -1 \end{pmatrix}.$$

Note that the order of convergence derived in [17] depends on both the polynomial degree and on the regularity of the exact solutions. As the manufactured pressure (and therefore the exact pseudostress) and the exact temperature have relatively high gradients near the reentrant corner, we expect the accuracy of the mixed finite element scheme to deteriorate upon using uniform mesh refinement.

Tab. 1: Example 1: Convergence history for the fully-mixed approximation with polynomial degree $k = 2$ and using uniform (top block) and adaptive mesh refinement guided by (3.11) (bottom block). DoF stands for the number of degrees of freedom associated with each barycentric refined mesh T_h^b , and Iter stands for the number of Newton–Raphson iterations required to reach the tolerance 10^{-8} .

With uniform mesh refinement

DoF	h	$e(\mathbf{u})$	$r(\mathbf{u})$	$e(\mathbf{t})$	$r(\mathbf{t})$	$e(\boldsymbol{\sigma})$	$r(\boldsymbol{\sigma})$	Iter
2899	1.0000	7.87e+00	—	1.47e+02	—	8.59e+02	—	15
11521	0.5000	5.61e+00	0.491	1.18e+02	0.319	5.47e+02	0.655	7
45937	0.2500	5.23e+00	0.130	1.05e+02	0.174	4.94e+02	0.312	5
183457	0.1250	3.10e+00	0.884	9.24e+01	0.445	3.60e+02	0.242	6
733249	0.0625	1.45e+00	0.679	7.05e+01	0.130	3.44e+02	0.164	7
$e(\varphi)$	$r(\varphi)$	$e(\tilde{\mathbf{t}})$	$r(\tilde{\mathbf{t}})$	$e(\tilde{\boldsymbol{\sigma}})$	$r(\tilde{\boldsymbol{\sigma}})$	$e(p)$	$r(p)$	$\text{eff}(\Theta)$
3.72e-01	—	2.89e+00	—	1.72e+01	—	2.61e+02	—	0.585
1.38e-01	1.439	2.13e+00	0.438	1.62e+01	0.081	2.20e+02	0.127	0.738
7.13e-02	0.953	1.24e+00	0.790	1.34e+01	0.272	5.19e+01	1.213	0.929
4.37e-02	0.708	9.61e-01	0.363	1.30e+01	0.045	4.39e+01	0.243	0.658
4.56e-03	3.261	7.95e-01	0.257	9.07e+00	0.362	2.80e+01	0.648	0.370

With adaptive mesh refinement

DoF	h	$e(\mathbf{u})$	$r(\mathbf{u})$	$e(\mathbf{t})$	$r(\mathbf{t})$	$e(\boldsymbol{\sigma})$	$r(\boldsymbol{\sigma})$	Iter
19405	0.5143	5.70e+00	—	2.57e+01	—	9.88e+02	—	6
30385	0.5144	3.90e+00	1.694	1.14e+01	0.958	1.17e+02	0.740	5
44236	0.5153	2.13e+00	3.573	7.02e+00	1.215	7.62e+01	2.270	4
57601	0.5146	5.57e-01	3.975	6.51e-01	3.580	3.30e+01	3.415	4
77653	0.5144	7.96e-02	3.933	3.67e-01	3.131	7.49e+00	3.165	3
111070	0.5146	9.73e-03	3.272	8.73e-02	3.036	3.01e+00	3.489	3
$e(\varphi)$	$r(\varphi)$	$e(\tilde{\mathbf{t}})$	$r(\tilde{\mathbf{t}})$	$e(\tilde{\boldsymbol{\sigma}})$	$r(\tilde{\boldsymbol{\sigma}})$	$e(p)$	$r(p)$	$\text{eff}(\Theta)$
6.92e-02	—	1.24e+00	—	1.31e+01	—	5.87e+01	—	0.642
4.97e-02	1.481	9.53e-01	1.155	1.13e+01	0.669	4.45e+01	1.236	0.643
2.11e-02	3.999	5.47e-01	2.954	6.97e+00	2.547	3.38e+01	2.470	0.634
9.65e-03	3.472	3.04e-01	3.572	4.29e-01	3.122	7.13e+00	3.778	0.634
2.10e-03	3.201	9.39e-02	3.484	3.13e-02	3.535	3.77e+00	3.323	0.634
7.08e-04	2.067	4.56e-02	3.229	7.10e-03	3.283	9.31e-01	3.892	0.635

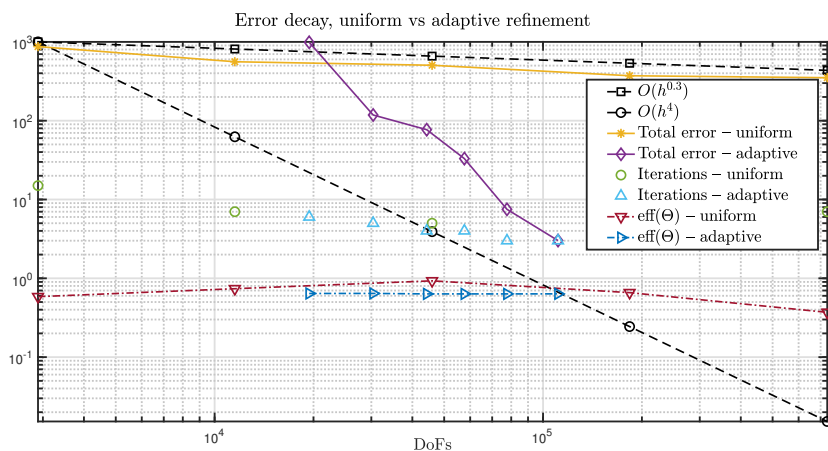


Fig. 1: Example 1: Total error decay obtained with a method with polynomial degree $k = 2$ and using uniform and adaptive mesh refinement.

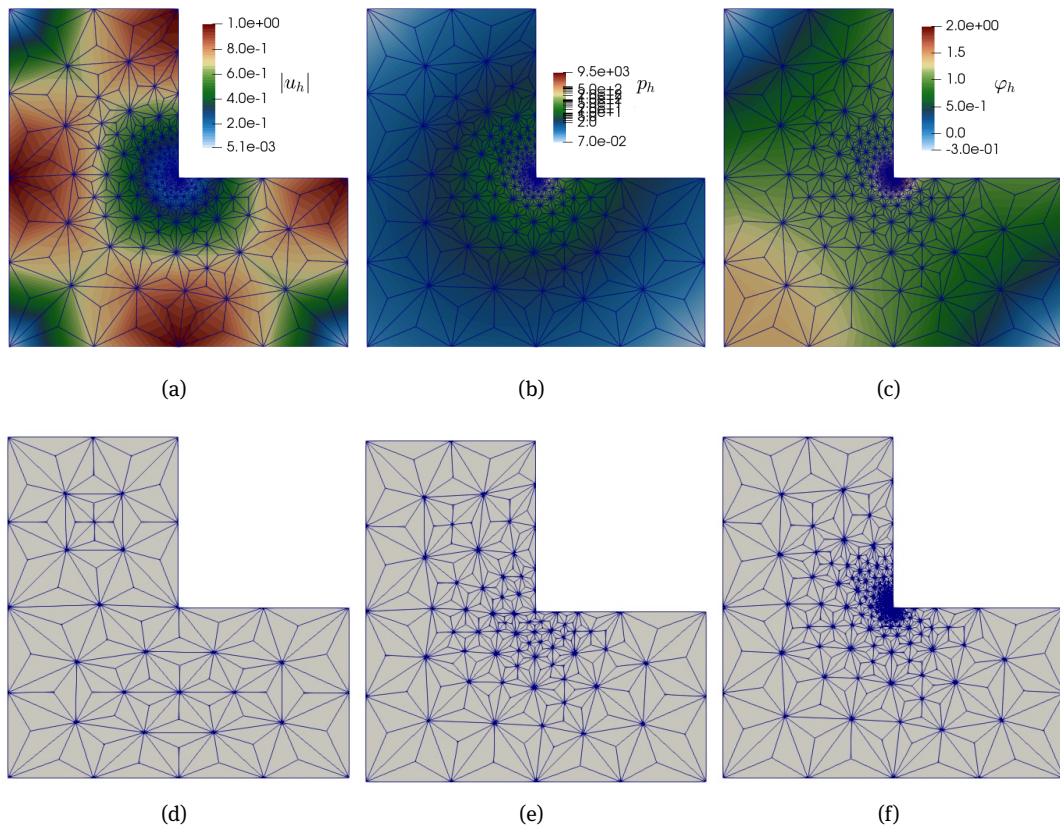


Fig. 2: Example 1: Approximate velocity magnitude (a), postprocessed pressure with colormap in log scale (b), and temperature distribution (c) obtained using a mixed method for the Boussinesq problem with $k = 2$ and after two steps of adaptive mesh refinement. Panels (d,e,f) show samples of adaptive meshes.

On each refinement level we compute approximate solutions, as well as errors and convergence rates defined as above. The error history for each field variable and the effectivity index for the estimator (3.11), $\text{eff}(\Theta) := e/\Theta$ (where e denotes the total error), are supplied in Table 1. There, we also list for each refinement step the iteration count for the Newton–Raphson algorithm (needed for the ℓ^2 -norm, either absolute or relative, of the incremental vector solution to be below the prescribed tolerance of 10^{-8}). These results tabulate the convergence of the method when following a uniform mesh refinement versus the adaptive case. In the uniform case we generate triangular meshes and refine them uniformly, then apply for each mesh a barycentric refinement, on which we compute numerical solutions and errors. In the adaptive case we use Algorithm 1. In all cases we see that the convergence is suboptimal for the uniform refinement whereas optimal and super-optimal rates are seen when we apply the adaptive algorithm. In addition, we observe that the effectivity index is much more stable in the adaptive case. We also see that the number of iterations is systematically lower in the adaptive case. Note that the asymptotic convergence and the fluctuation of the effectivity index can be easily tuned using step 12 in Algorithm 1. For example, using a refinement parameter $N = 0.05$ (instead of the value 0.01 used to generate Table 1) we get a slower convergence (but still super-optimal). Such behaviour is not surprising since the high gradients of pressure and temperature are concentrated only on a very small region near the reentrant corner. Once these gradients are resolved (which occurs after a couple of adaptive refinement steps), then the solution is relatively smooth, leading to superconvergence. Moreover, for this type of solutions, the experimental convergence computed as in (6.1) and used in the adaptive case, can be quite different compared to the usual rate computed using two consecutive meshsizes. For sake of completeness we also plot the total error decay vs the number of degrees of freedom in Fig. 1, that allows us

to infer an approximate fourth-order convergence for the adaptive scheme versus a rate of convergence of approximately 0.3 for the uniform case.

To further exemplify the performance of the scheme, we show in Fig. 2 approximate solutions (velocity magnitude, postprocessed pressure, and temperature) obtained by the adaptive method on relatively coarse meshes, together with examples of locally refined barycentric meshes indicating the expected refinement near the reentrant corner of the domain, located at the origin.

6.2 Example 2: adaptive computation for the 3D thermal cavity

Next we test the adaptive algorithm in a 3D problem consisting of the stationary Boussinesq equations on the unit cube $\Omega = (0, 1)^3$, where the distribution of temperature and flow patterns is driven by differentially heating the enclosure. The classical benchmark problem uses unity viscosity and thermal conductivity (see, e.g., [4, 28]), while here we use the nonlinear viscosity $\nu(\varphi) = 0.25 + \exp(-\varphi)$ together with $\mathbf{g} = (0, 0, \text{Ra})^t$ with a Rayleigh number of $\text{Ra} = 5 \cdot 10^4$. For the thermal energy conservation, the boundary is split into two regions: Γ_1 (top and bottom edges of the box) and Γ_2 (vertical walls) where temperature and heat flux are prescribed, respectively. The boundary temperature on Γ_1 is set to $\varphi_D = 0$ on the top surface and $\varphi_D = 1$ on the bottom. On Γ_2 we consider that the remainder squares of the boundary (that is, the cavity walls) are insulated, which translates in prescribing zero normal components for the heat flux $\tilde{\sigma}$, which is done as an essential boundary condition. Finally, no-slip velocities $\mathbf{u}_D = \mathbf{0}$ are prescribed everywhere on the boundary.

Starting with a coarse uniform tetrahedral mesh and its corresponding barycentric refinement, we compute numerical solutions using the mixed method with $k = 2$. The error estimator (4.2) guides the adaptive mesh refinement, which seems to focus the majority of the marking on the zone of higher temperature gradients. The performance of the scheme is exemplified in Fig. 3 where we display approximate temperature, heat flux, and velocity streamlines that exhibit a qualitative agreement with the expected flow recirculation. We also show in the bottom panels of the figure, some coarse adaptively refined grids.

For a more quantitative study, and in order to emphasize another advantage of the fully mixed scheme, we illustrate that the formulation is conservative in the momentum and thermal energy equations (cf. third and seventh equations of (2.3)). In Table 2 (top) we show, for each step of adaptive refinement, the number of degrees of freedom, the number of Newton–Raphson iterations required to reach convergence, the ℓ^∞ norm of the balanced momentum $-\mathbf{div}(\boldsymbol{\sigma}_h) + \frac{1}{2}\mathbf{t}_h \mathbf{u}_h - \varphi_h \mathbf{g}$, and the ℓ^∞ norm of the balanced thermal energy $-\mathbf{div}(\tilde{\sigma}_h) + \frac{1}{2}\mathbf{u}_h \cdot \tilde{\mathbf{t}}_h$. We can see that at every adaptive step these balances are indeed very close to zero. For sake of comparison, we compute the numerical solutions to the 3D thermal cavity problem using a classical (primal) finite element formulation in terms of velocity, pressure, and temperature, and discretized by a Taylor–Hood–P₁ scheme (and using a uniform, but not nested, refinement strategy). The secondary unknowns (velocity gradient, pseudostress, temperature gradient, and pseudo-flux) are postprocessed from the primary fields. Table 2 (bottom) displays the same quantities for this primal method, and we can clearly see a decay of the momentum and thermal energy errors, but in many orders of magnitude larger than those obtained with the fully mixed scheme, even for comparable number of degrees of freedom. In addition, the iteration count is also slightly lower in the adaptive case.

6.3 Example 3: accuracy for Oberbeck–Boussinesq in a truncated cube

We conclude our numerical tests with the verification of convergence of the mixed method and the adaptive mesh refinement applied to the Oberbeck–Boussinesq system. We use the non-convex domain $\Omega = (0, 1)^3 \setminus$

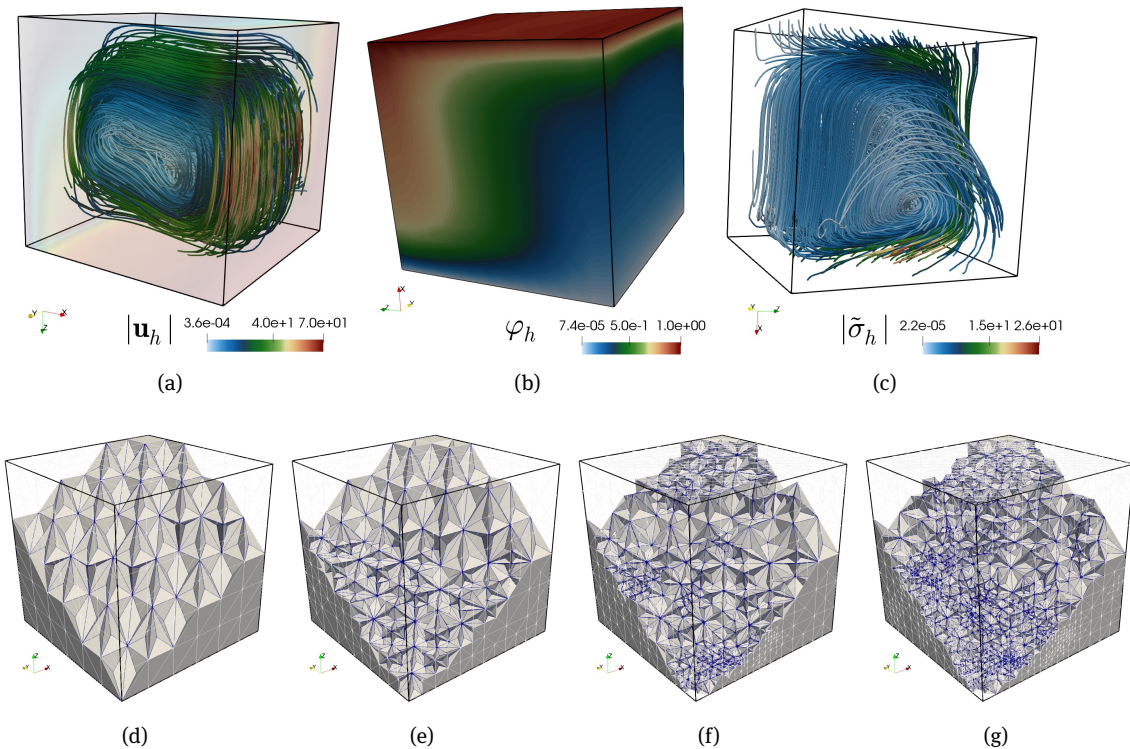


Fig. 3: Example 2: Different angle views for approximate velocity streamlines (a), temperature distribution (b), and heat flux streamlines (c) for the Boussinesq equations modeling the differentially heated cavity. Solutions computed with a method using $k = 2$ and a barycentric tetrahedral grid obtained after four steps of adaptive mesh refinement. Panels (d,e,f,g) show samples of adaptive meshes with a crinkle clip across the geometry.

Tab. 2: Example 2: Momentum and energy balance computed with the fully mixed scheme and adaptive mesh refinement (top) vs. a classical Taylor–Hood–Lagrange approximation of velocity–pressure–temperature and applying uniform mesh refinement (bottom).

Fully mixed method and adaptive mesh refinement

DoF	Iter	$\ \operatorname{div}(\sigma_h) - \frac{1}{2}\mathbf{t}_h \mathbf{u}_h + \varphi_h g\ _{\ell^\infty}$	$\ \operatorname{div}(\tilde{\sigma}_h) - \frac{1}{2}\mathbf{u}_h \cdot \tilde{\mathbf{t}}_h\ _{\ell^\infty}$
289801	6	7.761e-12	2.042e-12
372193	6	7.158e-12	5.527e-12
527365	5	9.263e-12	9.088e-12
620413	5	2.276e-11	1.823e-10
819805	6	6.733e-12	7.951e-12
1154365	5	8.537e-12	7.062e-12

Primal method and uniform mesh refinement

DoF	Iter	$\ \operatorname{div}(\sigma_h) - \frac{1}{2}\mathbf{t}_h \mathbf{u}_h + \varphi_h g\ _{\ell^\infty}$	$\ \operatorname{div}(\tilde{\sigma}_h) - \frac{1}{2}\mathbf{u}_h \cdot \tilde{\mathbf{t}}_h\ _{\ell^\infty}$
7278	7	304.885	70.143
22578	7	148.230	59.625
79918	7	64.109	48.614
259818	7	29.382	47.591
740526	6	19.171	46.900
1863538	7	14.245	45.812

Tab. 3: Example 3: Convergence history and Newton iteration count for the fully-mixed approximation of the Oberbeck–Boussinesq equations on a truncated cube.

With uniform mesh refinement

DoF	h	$e(\mathbf{u})$	$r(\mathbf{u})$	$e(t)$	$r(t)$	$e(\sigma)$	$r(\sigma)$	Iter
46251	1	0.5848	—	17.11	—	135.7	—	4
368921	0.5	0.1542	1.285	11.67	0.549	96.16	0.332	5
2947041	0.3056	0.1320	0.511	9.265	0.388	64.02	0.451	5
8655681	0.1528	0.0944	0.603	6.304	0.410	45.78	0.398	4
$e(\varphi)$	$r(\varphi)$	$e(\tilde{\mathbf{t}})$	$r(\tilde{\mathbf{t}})$	$e(\tilde{\sigma})$	$r(\tilde{\sigma})$	$e(p)$	$r(p)$	$\text{eff}(\psi)$
0.03211	—	0.6320	—	0.9353	—	6.432	—	0.767
0.02031	0.694	0.4377	0.467	0.6395	0.698	3.678	0.538	0.854
0.01276	0.766	0.1929	0.776	0.2684	0.819	2.353	0.692	0.612
0.00715	0.983	0.1307	0.462	0.2591	0.128	2.012	0.377	0.300

With adaptive mesh refinement

DoF	h	$e(\mathbf{u})$	$r(\mathbf{u})$	$e(t)$	$r(t)$	$e(\sigma)$	$r(\sigma)$	Iter
46251	1	0.5848	—	17.11	—	235.7	—	4
102181	1	0.3689	3.185	13.14	2.885	101.3	2.764	4
160002	0.7071	0.1952	2.838	9.246	2.233	60.17	2.552	4
334557	0.7071	0.0913	2.524	6.365	2.681	37.95	2.845	4
468940	0.7071	0.0532	2.487	4.032	2.528	22.79	2.709	3
667680	0.5719	0.0376	2.435	2.516	2.507	17.48	2.696	4
844490	0.5673	0.0193	2.617	1.254	2.791	11.89	2.391	3
$e(\varphi)$	$r(\varphi)$	$e(\tilde{\mathbf{t}})$	$r(\tilde{\mathbf{t}})$	$e(\tilde{\sigma})$	$r(\tilde{\sigma})$	$e(p)$	$r(p)$	$\text{eff}(\psi)$
0.03211	—	0.6325	—	0.9353	—	7.432	—	0.767
0.02371	2.474	0.3761	3.543	0.6802	2.497	5.457	1.954	0.654
0.01240	1.946	0.2189	2.413	0.3549	2.794	2.872	2.506	0.679
0.00628	2.666	0.1047	2.123	0.1985	2.342	1.916	2.126	0.670
0.00161	2.728	0.0722	2.401	0.1343	2.194	1.141	2.396	0.695
0.00092	2.729	0.0504	2.504	0.0865	2.946	0.753	2.560	0.695
0.00066	2.243	0.0299	2.538	0.0596	2.444	0.451	3.022	0.695

$[0.5, 1]^3$ (with a volume of $|\Omega| = 0.875$), and consider the following closed-form solutions

$$\mathbf{u} = \begin{pmatrix} \sin^2(\pi x_1) \sin(\pi x_2) \sin(2\pi x_3) \\ \sin(\pi x_1) \sin^2(\pi x_2) \sin(2\pi x_3) \\ -[\sin(2\pi x_1) \sin(\pi x_2) + \sin(\pi x_1) \sin(2\pi x_2)] \sin^2(\pi x_3) \end{pmatrix}$$

$$p = \frac{1 - x_1^2 - x_2^2 - x_3^2}{(x_1 - 0.55)^2 + (x_2 - 0.55)^2 + (x_3 - 0.55)^2}$$

$$\varphi_1 = 1 - \sin(\pi x_1) \cos(\pi x_2) \sin(\pi x_3), \quad \varphi_2 = \exp(-(x_1 - 0.55)^2 - (x_2 - 0.55)^2 - (x_3 - 0.55)^2).$$

The manufactured exact velocity, concentration, and temperature are used as Dirichlet data everywhere on the boundary. The pressure has a strong gradient near the reentrant corner of the domain and therefore we expect that adaptive mesh refinement outperforms the convergence of the method using meshes successively refined in a uniform way. We select the following parameter values

$$\mu(\varphi) = \exp(-\varphi_1), \quad \gamma = 1, \quad \alpha = (1, 0.5)^t, \quad \mathbb{K}_1 = \begin{pmatrix} \exp(-x_1) & 0 & 0 \\ 0 & \exp(-x_2) & 0 \\ 0 & 0 & \exp(-x_3) \end{pmatrix}, \quad \mathbb{K}_2 = \mathbb{I}.$$

The error history for each field variable (number of degrees of freedom associated with each mesh and experimental errors and convergence rates) and the effectivity index for the estimator (5.8) (its 3D version),

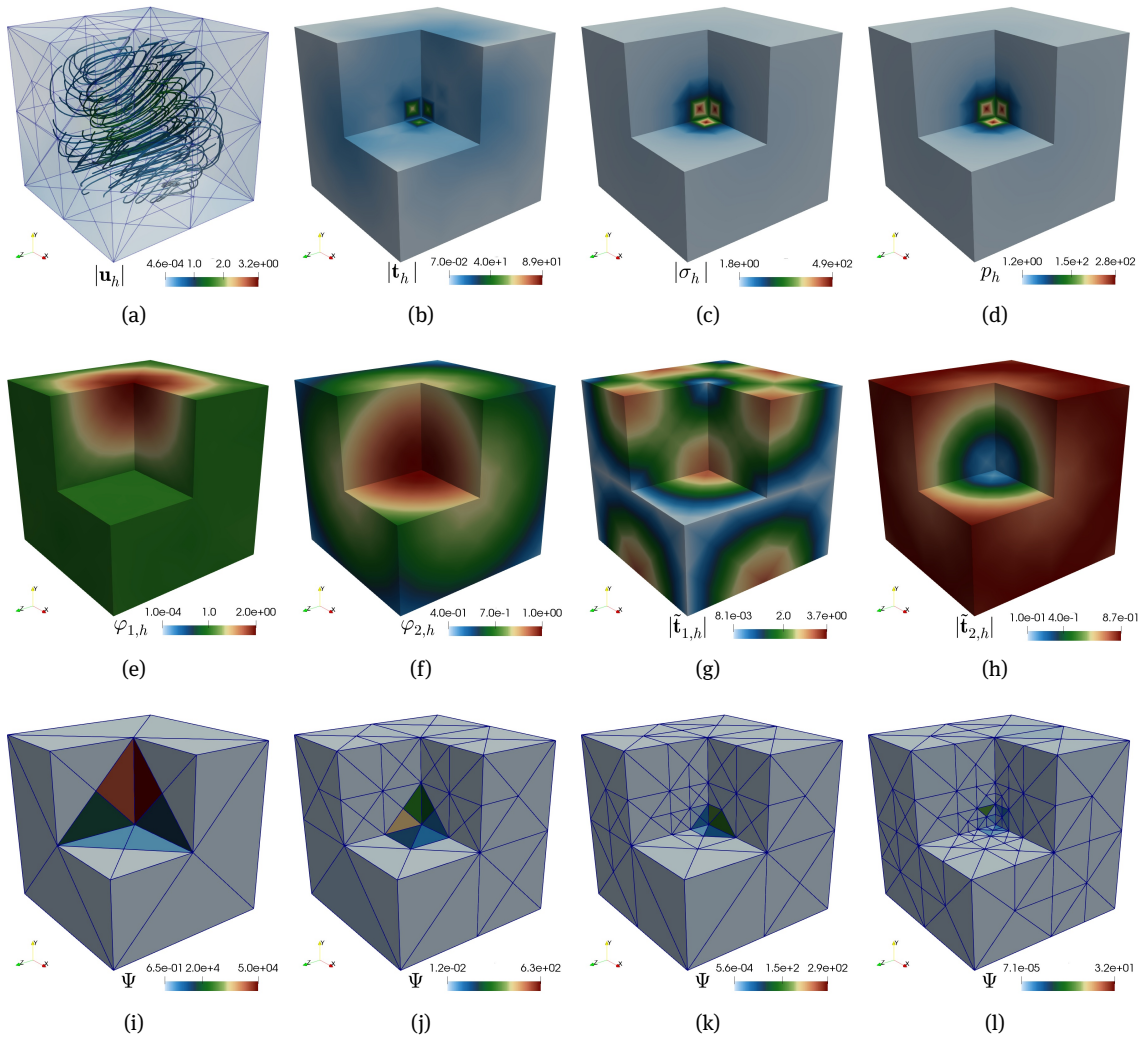


Fig. 4: Example 3: Approximate velocity magnitude and streamlines (a), velocity gradient (b), Bernoulli tensor (c), postprocessed pressure (d), temperature (e), concentration (f), temperature gradient (g), and concentration gradient (h), obtained using $k = 2$ and an adaptive barycentrically refined tetrahedral mesh. Panels (i,j,k,l) show the repartition of the indicator on coarse sample meshes.

$\text{eff}(\Psi) := e/\Psi$ (where e denotes the total error), are supplied in Table 3. As in the 2D Boussinesq case of Example 1, the lack of smoothness of the exact solution is reflected in the hindered convergence observed under uniform mesh refinement. Noticeably improved results are obtained for the case of adaptive mesh refinement. The overall mesh density is controlled through a refinement tolerance in order to produce adaptive meshes representing fewer degrees of freedom than in the uniform case. Even then the errors decay much faster for the adaptive case and the effectivity index remains in a neighborhood of 0.69, confirming the efficiency and reliability of the a posteriori error indicator. Approximate solutions are shown in Fig. 4.

Funding: This research was partially supported by ANID-Chile through the project Centro de Modelamiento Matemático (FB210005), and the Becas Chile Programme for national students; by Centro de Investigación en Ingeniería Matemática (CI²MA), Universidad de Concepción; by the Monash Mathematics Research Fund S05802-3951284; by the HPC-Europa3 Transnational Access programme through grant HPC175QA9K; by the Ministry of Science and Higher Education of the Russian Federation within the framework of state support for the creation and development of World-Class Research Centers ‘Digital biodesign and personalized health-

care' No. 075-15-2022-304; and by the Monash eResearch Centre and eSolutions-Research Support Services through the use of the MonARCH HPC Cluster.

References

- [1] S. Agmon, *Lectures on Elliptic Boundary Value Problems*, Van Nostrand, Princeton, NJ, 1965.
- [2] M. S. Alnæs, J. Blechta, J. Hake, A. Johansson, B. Kehlet, A. Logg, C. Richardson, J. Ring, M. E. Rognes, and G. N. Wells, The FEniCS project version 1.5, *Arch. Numer. Softw.*, **3** (2015), No. 100, 9–23.
- [3] K. Allali, A priori and a posteriori error estimates for Boussinesq equations, *Int. J. Numer. Anal. Model.*, **2** (2005), 179–196.
- [4] A. Allendes, C. Naranjo, and E. Otárola, Stabilized finite element approximations for a generalized Boussinesq problem: a posteriori error analysis, *Comput. Methods Appl. Mech. Engrg.*, **361** (2020), Art. 112703.
- [5] A. Allendes, E. Otárola, and A. J. Salgado, A posteriori error estimates for the stationary Navier–Stokes equations with Dirac measures, *SIAM J. Sci. Comput.*, **42** (2020), No. 3, A1860–A1884.
- [6] J. A. Almonacid, G. N. Gatica, and R. Oyarzúa, A posteriori error analysis of a mixed-primal finite element method for the Boussinesq problem with temperature-dependent viscosity, *J. Sci. Comput.*, **78** (2019), No. 2, 887–917.
- [7] M. Alvarez, G. N. Gatica, and R. Ruiz-Baier, A posteriori error estimation for an augmented mixed-primal method applied to sedimentation–consolidation systems, *J. Comput. Phys.*, **367** (2018), 322–346.
- [8] N. Assal, M. L. Hadji, and F. Z. Nouri, A posteriori error analysis for Navier–Stokes equations coupled with Darcy problem, *Calcolo*, **52** (2015), No. 4, 559–576.
- [9] T. P. Barrios, G. N. Gatica, M. González, and N. Heuer, A residual based a posteriori error estimator for an augmented mixed finite element method in linear elasticity, *M2AN Math. Model. Numer. Anal.*, **40** (2006), No. 5, 843–869.
- [10] D. Boffi, F. Brezzi, and M. Fortin, Reduced symmetry elements in linear elasticity, *Commun. Pure Appl. Anal.*, **8** (2009), No. 1, 95–121.
- [11] P. Burda, B. Sousedík, and K. Williamson, A posteriori error estimates and adaptive mesh refinement for the Stokes–Brinkman problem, *Math. Comput. Simul.*, **166** (2019), 266–282.
- [12] J. Camaño, S. Caucao, R. Oyarzúa, and S. Villa-Fuentes, A posteriori error analysis of a momentum conservative Banach-spaces based mixed-FEM for the Navier–Stokes problem, *Appl. Numer. Math.*, **176** (2022), 132–158.
- [13] S. Caucao, G. N. Gatica, and J. P. Ortega, A fully-mixed formulation in Banach spaces for the coupling of the steady Brinkman–Forchheimer and double-diffusion equations, *ESAIM Math. Model. Numer. Anal.*, **55** (2021), No. 6, 2725–2758.
- [14] S. Caucao, G. N. Gatica, and R. Oyarzúa, A posteriori analysis of an augmented fully mixed formulation for the nonisothermal Oldroyd–Stokes problem, *Numer. Methods Partial Differ. Equ.*, **35** (2019), No. 1, 295–324.
- [15] S. Caucao, G. N. Gatica, R. Oyarzúa, and F. Sandoval, Residual-based a posteriori error analysis for the coupling of the Navier–Stokes and Darcy–Forchheimer equations, *ESAIM Math. Model. Numer. Anal.*, **55** (2021), No. 2, 659–687.
- [16] P. Clément, Approximation by finite element functions using local regularisation, *RAIRO Modélisation Mathématique et Analyse Numérique*, **9** (1975), 77–84.
- [17] E. Colmenares, G. N. Gatica, and S. Moraga, A Banach spaces-based analysis of a new fully-mixed finite element method for the Boussinesq problem, *ESAIM Math. Model. Numer. Anal.*, **54** (2020), No. 5, 1525–1568.
- [18] E. Colmenares, G. N. Gatica, S. Moraga, and R. Ruiz-Baier, A fully-mixed finite element method for the steady state Oberbeck–Boussinesq system, *SMAI J. Comput. Math.*, **6** (2020), 125–157.
- [19] E. Colmenares and M. Neilan, Dual-mixed finite element methods for the stationary Boussinesq problem, *Comp. Math. Appl.*, **72** (2016), No. 7, 1828–1850.
- [20] J. de Frutos, B. García-Archilla, and J. Novo, Nonlinear convection–diffusion problems: fully discrete approximations and a posteriori error estimates, *IMA J. Numer. Anal.*, **31** (2011), No. 4, 1402–1430.
- [21] C. Domínguez, G. N. Gatica, and S. Meddahi, A posteriori error analysis of a fully-mixed finite element method for a two-dimensional fluid–solid interaction problem, *J. Comput. Math.*, **33** (2015), No. 6, 606–641.
- [22] W. Dörfler, A convergent adaptive algorithm for Poisson's equation, *SIAM J. Numer. Anal.*, **33** (1994), No. 3, 1106–1124.
- [23] F. Durango and J. Novo, A posteriori error estimations for mixed finite element approximations to the Navier–Stokes equations based on Newton-type linearization, *J. Comput. Appl. Math.*, **367** (2020), 112429.
- [24] A. Ern and J.-L. Guermond, *Theory and Practice of Finite Elements*, Applied Mathematical Sciences, Vol. 159, Springer-Verlag, New York, 2004.
- [25] A. Ern and M. Vohralík, Adaptive inexact Newton methods with a posteriori stopping criteria for nonlinear diffusion PDEs, *SIAM J. Sci. Comput.*, **35** (2013), No. 4, A1761–A1791.
- [26] M. Farhloul and M. Fortin, Dual hybrid methods for the elasticity and the Stokes problems: a unified approach, *Numer. Math.*, **76** (1997), No. 4, 419–440.
- [27] M. Farhloul, S. Niclaise, and L. Paquet, A priori and a posteriori error estimations for the dual mixed finite element method of the Navier–Stokes problem, *Numer. Methods Partial Differ. Equ.*, **25** (2009), No. 4, 843–869.

- [28] T. Fusegi and J. M. Hyun, A numerical study of 3D natural convection in a cube: effects of the horizontal thermal boundary conditions, *Fluid Dynam. Res.*, **8** (1991), No. 5-6, 221–230.
- [29] G. N. Gatica, A note on stable Helmholtz decompositions in 3D, *Appl. Anal.*, **99** (2020), No. 7, 1110–1121.
- [30] G. N. Gatica, C. Inzunza, R. Ruiz-Baier, and F. Sandoval, A posteriori error analysis of Banach spaces-based fully-mixed finite element methods for Boussinesq-type models, *Preprint 2021-20*, Centro de Investigación en Ingeniería Matemática (CIM), Universidad de Concepción, Chile, 2021.
- [31] G. N. Gatica, A. Márquez, and M. A. Sánchez, Analysis of a velocity–pressure–pseudostress formulation for the stationary Stokes equations, *Comput. Methods Appl. Mech. Engrg.*, **199** (2010), 1064–1079.
- [32] G. N. Gatica, R. Oyarzúa, R. Ruiz-Baier, and Y. D. Sobral, Banach spaces-based analysis of a fully-mixed finite element method for the steady-state model of fluidized beds, *Comput. Math. Appl.*, **84** (2021), 244–276.
- [33] C. Geuzaine and J.-F. Remacle, Gmsh: a three-dimensional finite element mesh generator with built-in pre- and post-processing facilities, *Int. J. Numer. Methods Engrg.*, **79** (2009), No. 11, 1309–1331.
- [34] V. Girault and P. A. Raviart, *Finite Element Methods for Navier–Stokes Equations. Theory and Algorithms*, Springer Series in Computational Mathematics, Vol. 5. Springer-Verlag, Berlin, 1986.
- [35] J. Howell and N. Walkington, Dual-mixed finite element methods for the Navier–Stokes equations, *ESAIM Math. Model. Numer. Anal.*, **47** (2013), No. 3, 789–805.
- [36] T. Sayah, A posteriori error estimates for the Brinkman–Darcy–Forchheimer problem, *Comput. Appl. Math.*, **40** (2021), No. 7, 256.
- [37] L. R. Scott and M. Vogelius, Conforming finite element methods for incompressible and nearly incompressible continua, *Lectures in Appl. Math.*, 22-2, Amer. Math. Soc., Providence, RI, 1985, pp. 221–244.
- [38] L. R. Scott and M. Vogelius, Norm estimates for a maximal right inverse of the divergence operator in spaces of piecewise polynomials, *RAIRO Modél. Math. Anal. Numér.*, **19** (1985), No. 1, 111–143.
- [39] R. Verfürth, *A Review of A-Posteriori Error Estimation and Adaptive Mesh-Refinement Techniques*, Wiley Teubner, Chichester, 1996.